No. 249
September 1982

IMPROVEMENT OF INLAND WATERWAY VESSEL AND BARGE TOW PERFORMANCE

Translated by
Dr. Robert Latorre
G. Luthra
K. Tang

THE UNIVERSITY OF MICHIGAN 1817

THE DEPARTMENT OF NAVAL ARCHITECTURE AND MARINE ENGINEERING

THE UNIVERSITY OF MICHIGAN
COLLEGE OF ENGINEERING

No. 249
September 1982

IMPROVEMENT OF INLAND WATERWAY VESSEL AND BARGE TOW PERFORMANCE: TRANSLATIONS OF SELECTED CHINESE, GERMAN AND RUSSIAN TECHNICAL ARTICLES

Translated by

Dr. R. Latorre

G. Luthra

K. Tang

Department of Naval Architecture
and Marine Engineering
College of Engineering
The University of Michigan
Ann Arbor, Michigan 48109

PREFACE

This report is part of a three year project to organize and translate foreign language articles on towed barges, inland waterway towboats, barge tows, and operations for teaching and use in design/research projects. In addition to this report, the project includes references [1]-[6]. The following topics are presented in this report:

a) Shallow water resistance and barge size selection;

b) Pushboat propeller design and matching with engine;

c) Design of rudders and steering nozzzles for towboats.

The extensive use of the inland waterways have resulted in a large number of Soviet investigations on improving inland waterway vessel design. These include articles on estimating shallow water resistance, trimaran resistance, empirical formulas for wake and thrust deduction for vessels with tunnel sterns, as well as the evaluation of over twelve steering arrangements for inland waterway vessels.

Mr. Tang, Kezhang, visiting scholar from Dalian Marine College, translated the Chinese articles on the selection of the barge size and towboat horsepower and the influence of the design margin on the propeller diameter and pitch/diameter ratio. Finally Mr. G. Luthra, Versuchsanstalt fur Binnenschiffbau, Duisburg, W. Germany, kindly translated his article on the influence of flanking rudders on propeller thrust.

Robert Latorre

1] "Improvement of Barge Towing," NA&ME Dept. Report No. 226, May, 1980, 51 pp.

2] "Recent Developments in Barge Design, Towing and Pushing," MARINE TECHNOLOGY, Vol. 18, No. 1, January, 1981, pp. 10-21.

3] "Improvement of River Towboat Propulsion," NA&ME Dept. Report No. 243, November, 1981, 69 pp.

4] "River Towboat Hull and Propulsion," SNAME Great Lakes/Great Rivers Section Meeting, January 28, 1982. (To appear in MARINE TECHNOLOGY)

5] "River Towboat Tunnel Stern," INTERNATIONAL SHIPBUILDING PROGRESS, Vol. 29, No. 338, October, 1982, pp. 252-259.

6] "Influence of Starting Acceleration and Towrope Length on Towed Barge Trajectory," INTERNATIONAL SHIPBUILDING PROGRESS, Vol. 28, No. 325, September, 1981, pp 200-206.

CONTENTS

ON THE TREND TOWARDS THE DEVELOPMENT OF PUSH-TRAIN OF THE LOWER CHANGJIANG (YANGTSE) RIVER IN NEAR FUTURE[1]

BY

C. WANG[2], J. WANG[2], G. LI[2]
Y. YAN[2], B. WANG[3], Y. XU[3]

ABSTRACT

This paper describes a technical and economical analysis of pushboat-barge-trains for the lower Changjiang (Yangtse) River conducted by the authors with the aid of a computer.

The comprehensive economic index E is used to assess the economic effect of the push-train scheme while the resistance of the push-train is estimated using a new method developed by the authors. The influence of the structure of the transportation cost on the economy of the push-train is analyzed in terms of the optimum matching functional relationship among the pushboat power, crew wage, the number of barges, and fuel cost per ton, for a large number of examples. It is indicated that the structure of the transportation cost of push-train is one of the decisive factors determining both the pushboat power and the push-train size.

Based on the results of calculations and analysis of more than twenty thousand schemes, the paper points out that at the present time and in the foreseeable future according to the structure of the transportation cost and the annual freight transportation on the lower Changjiang (Yangste) River an optimum economic effect can be obtained by developing 2 x 4 barge trains (2000 t. barges) pushed by a 1200-1800 horsepower towboat and 2 x 2 barge-trains (2000 t. barges) pushed by a 540-1200 horsepower towboat for present and near future operation on the lower Changjiang River.

TRANSLATION[4]

Since adopting multiple barge being pushed by pushboats (push train) transportation in the Changjiang River system in 1974, several barge types (300 tonnes, 1000 tonnes, and 5000 tonnes) and numerous pushboats have been used on the main river routes. The results have proved that the push-train is the most effective transport baseline for the Changjiang River. Therefore, it will be further developed along with the industrial and agricultural development of China.

Recently in countries where river transport flourishes, such as the United States, the freight rate of the river transport is lower than the railroad and highway transport freight rates. (Assigning the river transport freight rate a value of 1, then the railroad freight rate is 5 and the highway freight rate is 22). With development of this transport system, the push-train size increases, ie. the pushboat power, the barge size and deadweight, as well as the barge train's deadweight all increase. Presently the towboat horsepower exceeds 10,000 HP, while in the upper Mississippi River the barge train deadweight is 20,000 tons and in the lower Mississippi River the barge train deadweight is about 40,000-50,000 tons. The larger pushtrains consisting of 40-60 barges have a 60,000-80,000 ton deadweight.

Considering the trend to increase the barge train size in foreign countries, what is a reasonable trend for the push-train development in the river transport of China especially for the lower Changjian River? The authors hold that the utilization of large push-trains on the lower Changjian River can only occur when the annual freight transported will be suitable for the transport and cost structure. With the present situation and long range future projections of the annual freight levels, it appears best to develop small barge trains pushed by small power pushboats on the lower Changjiang River to obtain the most economic impact in the present and near future.

I) Assumptions used in the Scheme for Technical and Economic Analysis

1. Analysis Scheme Assumptions

In accordance with the transportation conditions on the Changjiang River, the following assumptions were adopted in setting up the analysis scheme.

---

[1] Transactions of the Chinese Society of Naval Architecture and Marine Engineering No. 74, July, 1981, pp. 34-45.

[2] Changjiang Ship Design Institute

[3] Wu Han Institute of Water Transportation Engineering

[4] Translated by Tang Kezhang, Associate Professor, Dalian Marine College, Visiting Scholar from P.R. China

a) Three transport routes:

Hanshen route (Wuhan-Shanghai): 1,125 km long
Yubao route (Yuxikuo-Baoshan): 450 km long
Pujian route (Pukuo-Jian): 105 km long

b) Five annual freight transport levels:

2×10^6 tonnes/year
4×10^6 tonnes/year
6×10^6 tonnes/year
8×10^6 tonnes/year
12×10^6 tonnes/year

c) Five barge deadweights:

1000 tonnes	3000 tonnes
1500 tonnes	5000 tonnes
2000 tonnes	

d) Eight pushboat horsepowers (metric)

370 HP	1800 HP
540 HP	2700 HP
800 HP	4000 HP
1200 HP	6000 HP

e) Eighteen barge train formations mxn (m: number of columns wide, n: number of rows long)

1 x 2	3 x 2	5 x 2
1 x 4	3 x 4	5 x 4
1 x 6	3 x 6	5 x 6
2 x 2	4 x 2	6 x 2
2 x 4	4 x 4	6 x 4
2 x 6	4 x 6	6 x 6

From the combination of a-e it is possible to obtain 3 x 5 x 5 x 8 x 18 = 10800 schemes. Additional changes in port time, barge building costs, crew wages, and fuel price resulted in over 20,000 schemes to be studied in the analysis.

2. Technical-Economic Analysis

The technical economic analysis were made with the DJS-6 computer. According to actual service conditions on the lower Changjiang River, the push-train maximum speed is between 8 km/hr and 19km/hr. The flow chart of the calculation is shown in Fig. 1.

The technical economic analysis consists of three parts:

2-A. The technical index calculation for the push-train

The formula for the barge resistance (effective horsepower EHP) is as follows [1]:

$$EHP_B + 4.5\times10^{-4} C_1 C_2 C_3 \frac{m^{0.9} n^{0.58}}{(1.05-0.25n)^{4.5}} \times \frac{\Delta^{0.523} b^{0.477}}{T^{0.151}} \times V^{2.95} \qquad (1)$$

where:

Δ: Barge displacement, tonnes
b: Beam of barge, m
T: Draft of barges, m
V: Barge train speed
C_1: Transverse formation correction coefficient:

$$C_1 = 1 + \frac{m^2+m-2}{m^{1.9}} \left(43.2 - 55.8 \frac{V}{\sqrt{L_B}}\right) \times 10^{-3} \qquad (2)$$

C_2: Longitudinal formation correction coefficient:

$$C_2 = 1 + (43.41 - 1.75^n)\left(\frac{V}{\sqrt{L}} - 1.38\right) \times 10^{-3} \qquad (3)$$

C_3: Barge C_B influence coefficient

$$C_3 = 1 + 2.65\,(C_B - 0.9118)\left(\frac{V}{\sqrt{L_B}}\right)^{2.5} \qquad (4)$$

C_B: Barge Block Coefficient
L_B: Length of barge train

$$L_B = (n-2)L_{OA} + 2L \text{ , m} \qquad (5)$$

L_{OA}: Length overall of barge, m
L: waterline length of barge, m

The push-train resistance formula for effective horsepower is as follows [1]:

$$EHP_F = EHP_B \left(1 + \frac{\Delta_T}{m \cdot n \cdot \Delta}\right) \qquad (6)$$

where:

Δ_T: Pushboat displacement, tonnes

In order to make comparisons, the basic assumptions for calculating the pushboat thrust are as follows:

a) Draft limitations: The pushboat draft for powers of 800 HP or less is 3.2m. The pushboat draft for powers of 1200 HP or greater is 3.4m.

b) Propeller diameter limitations: Propeller diameter is taken as 80% of pushboat draft. (Translator's Note: The propeller diameter on U.S. towboats is 1.0 or 1.1 the draft using tunnel sterns).

c) Propellers are designed at the optimal operating rpm and highest possible propulsive efficiency.

d) The pushboats are twin engined and the engine rated power is used for the power in the thrust calculation.

e) Two types of propeller design are used. The choice of K_a 4-70 propeller with

Type	Market Cost (10^4 Yuan/vessel) 1 Yuan = $0.50*
540 HP Pushboat	90
800 HP Pushboat	120
2640 HP Pushboat	280
4000 HP Pushboat	327
1000 Ton Barge	53
5000 Ton Barge	146

TABLE 1

*Note: Exchange based on present PRC Currency to $1.00 US 8/82

the Chinese JP7704 simplified nozzle design, or the Troust B4-70 propeller is based on the design with higher efficiency.

f) Required barge-trains are calculated for the designated route and the annual freight transport level on the route assuming the average current velocity in the lower Changjiang River (assumed 4 km/hr in this study), operating cycle, service factor and the still water speeds of the barge trains formations (computer results). In order to increase the utilization of the pushboats, a turn around tow is assumed available at the terminal ports, so the actual required number of barge trains is the actual number plus two.

2-B Economic Analysis

a) Cost Estimates for Pushboats and Barges

Recent costs of barges and pushboats vary between shipyards as well as in the method used in estimating the costs. Therefore, the current market price shown in Table 1 are used in estimating the costs.

b) The Approased Pushboat Cost

In order to compare different schemes, it is assumed that all the pushboats already used in service. The building costs of other barges can be estimated on the basis of the costs of these two barges. (Since the hull structure of the 5,000 ton barges has a lower strength, the weight of the steel structure used in the cost estimation was increased by 20%).

The expression used to estimate the barge cost is:

$$C = C_g + C_s \tag{7}$$

where

C: cost of the barge, 10^4 Yuan

Type of Pushboat HP	Appraised Cost 10^4 Yuan 1 Yuan = $ 0.50
370	100
540	110
800	144
1200	180
1800	235
2700	310
4000	392
6000	482

TABLE 2 Cost of Pushboats used in Analysis

C_g: steel hull cost of the barge, 10^4 Yuan
C_s: outfitting cost of the barge, 10^4 Yuan

The expression used to estimate the empty barge weight is:

$$P = P_g + P_s \tag{8}$$

where

P_g: steel hull weight of barge, tonnes
P_s: outfit weight of barge, tonnes

From the above expressions (7) and (8) the barge steel hull weight coefficient K_g and the barge price coefficient K_c were then obtained:

$$K_g = \frac{P_g}{L_{OA}BD}\ , \text{ tons/m}^3 \tag{9}$$

$$K_c = \frac{C_g}{P_g}\ , \text{ Yuan/Ton} \tag{10}$$

where

L_{OA}: length overall, m
B: moulded beam, m
D: moulded depth, m

The values of K_c and K_g can be calculated from the 1000 and 5000 ton barge data. These values were used to plate K_c - $L_{OA}BD$ line and K_g - $L_{OA}BD$ line. For other barge sizes, the values of K_c and K_g can be obtained from these lines and the values of P_g and C_g can then be obtained. The appraised cost of barges with different tonnages could be estimated by adding the outfitting cost (Table 3).

d) Transportation Cost Calculation

The transport costs include depreciation, repair charges, wages and substance costs, fuel and lubricating oil costs, port charges, and overhead. The depreciation and repair charges are

Tonnage	1000	1500	2000	3000	5000
Appraised Cost 10^4 Yuan	53	82	83	133	174

TABLE 3 Appraised Cost of Barges

assumed equal to 7.07% of the building cost. Overhead and port charges are taken as 3.5% of direct costs (the direct costs is the total cost of fuel, lubricating oil, wages, subsistance, depreciation, and repairs). The average crew wage was assumed as 1,500 Yuan/year per person. The engine fuel rate was taken as 175 gr/HP-HR with the lubricating oil consumption 1.2% of the fuel consumption. The fuel price was taken as 174.25 Yuan/ton and the lubricating oil price was taken as 1,500 Yuan/ton. The operation is taken as 340 days per year with a serive rate of 96.5% for barges and 80.5% for the pushboats. Following current data, the Yubao route has a freight rate 1.09 times that of the Hanshen route and the freight rate of the Pujian route is 2.682 times that of the Hanshen route. The tax is taken as 3% of the total income. Port time of the push boats is 24 hours for the Hanshen route, 12 hours for the Yubao route and 4 hours for the Pujian route.

3. Calculation of Economic Effectiveness Index

To indicate the overall economic effectiveness of push train, the following index E was used:

$$E = \frac{(\text{Transportation Cost} + 0.1 \times (\text{Total Construction Cost of Pusher-Barge Train}))}{\text{Annual Freight Flow} \times \text{Transport Distance}}$$

The barge trains with lower E values are more economically effective. Using E to indicate the river tow's economic effectiveness is reasonable, simple as well as reliable. The detailed analysis is given in reference [2].

II. RESULTS OF ANALYSIS

1. Reasonable barge types for use on the lower Changjian River

There are 144 combinations which can be formed from matching the 8 types of pushboats and the 18 barge train arrangements (144 = 8 x 18) for any specified barge size. From these schemes we can work out the practical scheme based on minimum E. Then a E-Q-P graph can be plotted as in Fig. 2 where Q is the annual freight flow and P is the barge deadweight.

The comparative economic effectiveness of the barge train can be determined from Fig. 2 which indicates that 1500 and 2000 tonne barges are the worse. The economic effectiveness of using 3000 tonne barges is similar to that with 2000 tonne barge except over a short route with a small annual freight flow. The economic effectiveness of the 5000 tonne barges is better than that of the 3000 and 2000 tonne barges. From the overall economic effectiveness of the entire transport system, it is clear that the 2000 tonne barges are better than the 3000 tonne barges for transporting bulk cargo such as staples giving consideration to the port's cargo handling equipment and the service charger of the harbor tugs. With the current port situation along the Changjiang River, it is also considered best to develop 2000 tonne barges. With the exception of a few ports and shipping enterprizes where large barges will have benefits, it is not suitable to develop 5000 tonne bulk cargo barges. In crude oil transport, the 5000 tonne barges are profitable.

As indicated above, it is recommended that initially 2000 tonne tank barges should be developed for the lower Changjian River. The barge size can be selected as 67.5 x 10.8 (L x B) from the river vessel profile outline album. These dimensions are suitable for navigation in the locks connecting the branch lines.

2. Recent Trends in the Development of the Barge Tow and Pushboat Power

The plot of E-BHP-Q is shown in Fig. 3, BHP is the pushboat power, and Q is the annual freight level based on the computer calculations. The circles on the curves represent the point where the index E is the smallest for a given pushboat HP. These represent the optimum combination of the pushboat and barge tow arrangement. It is possible to plot 9 groups of curves, but in this figure only 3 are shown. Each group is plotted for a specified route distance, and barge type. The three groups presented in this article represent push-trains of 2000 tonne barges operating on the 105 km and 1125 km routes.

It is shown in Fig. 3 that there exists an optimal scheme which has a minimum index E for a specified route distance, annual freight flow and barge size. When the annual freight flow on the Hanshen route (Fig. 3a) exceeds 4 x 10^6 tonnes/year, the optimal pushboat power is between 1220-1900 horsepower, with an optimal tow arrangement of 2 x 4. When the annual freight flow is below 4 x 10^6 tonnes/year then the optimum is a 2 x 2 barge formation pushed by pushboats from 540 to 1200 horsepower.

When the annual freight flow is more than 8 x 10^6 tonnes/year, on the Yubao route (Fig. 3b) the optimum barge arrangement is 2 x 4 using 2000 tonne barges with a optimal pushboat power of 1200 HP. For annual freight flows less than 8 x 10^6 tonnes/year, the lowest value of the index E is obtained

Item	Wages	Fuel Costs	Depreciation & Repairs	Port & Overhead
Percentage Annual Cost	3.6	18.8	51.6	26

TABLE 5 Proportion of Total Costs for Example C, at Initial Conditions

Item	Wages	Fuel Costs	Depreciation & Repairs	Port & Overhead
Percentage Annual Cost	17	22	35	26

TABLE 6 Proportion of Total Costs for Example C, at Revised Conditions

necessary to include additional factors i.e. shallow water, fast currents, etc. which were neglected.

REFERENCES

1. Wang, Bao-lin, Xu, Yong-sui, Wang, Cai-dong, Wang, Jin-sheng, Li, Guo-heng, and Yan, Yong-yao, "A New Method for Estimating the Resistance of River Push-trains," Journal of Wuhan Institute of Water Transportation Engineering, Vol. 4, 1980.

2. Wang, Bao-lin, Xu, Yong-sui, Wang, Cai-dong, Wang, Jin-sheng, Li, Guo-heng, and Yan, Yong-yao, "The Overall Economical Index of River Push-Trains," Journal of Wuhan Institue of Water Transportation Engineering, Vol 3, 1980.

3. Wang, Bao-lin, Xu, Yong-sui, Wang, Cai-dong, Wang, Jin-sheng, Li, Guo-heng, and Yan, Yong-yao, "The Influence of the Cost Structure on the Effectiveness of Push-Trains Operating on the Lower Changjiang River." Report of the Sumposium on Technical and Economical Analysis of Shipbuilding of China in 1980.

Additional references can be found on the U.S. Inland Waterway analysis is:

4. Howe, C.W. etal, "Inland Waterway Transportation," John Hopkins Press, Baltimore, Maryland 21218, 1969 ($5.00).

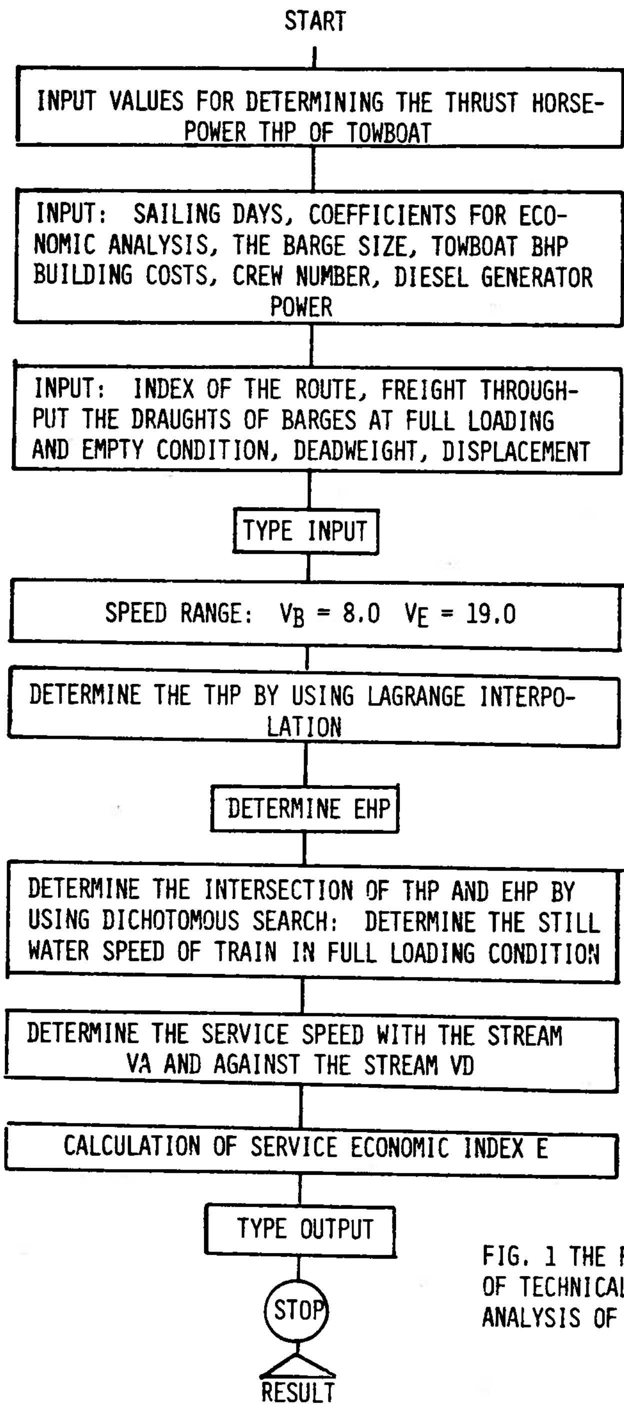

FIG. 1 THE FLOWCHART OF TECHNICAL ECONOMIC ANALYSIS OF THE SCHEME

FIG. 2 E vs Q

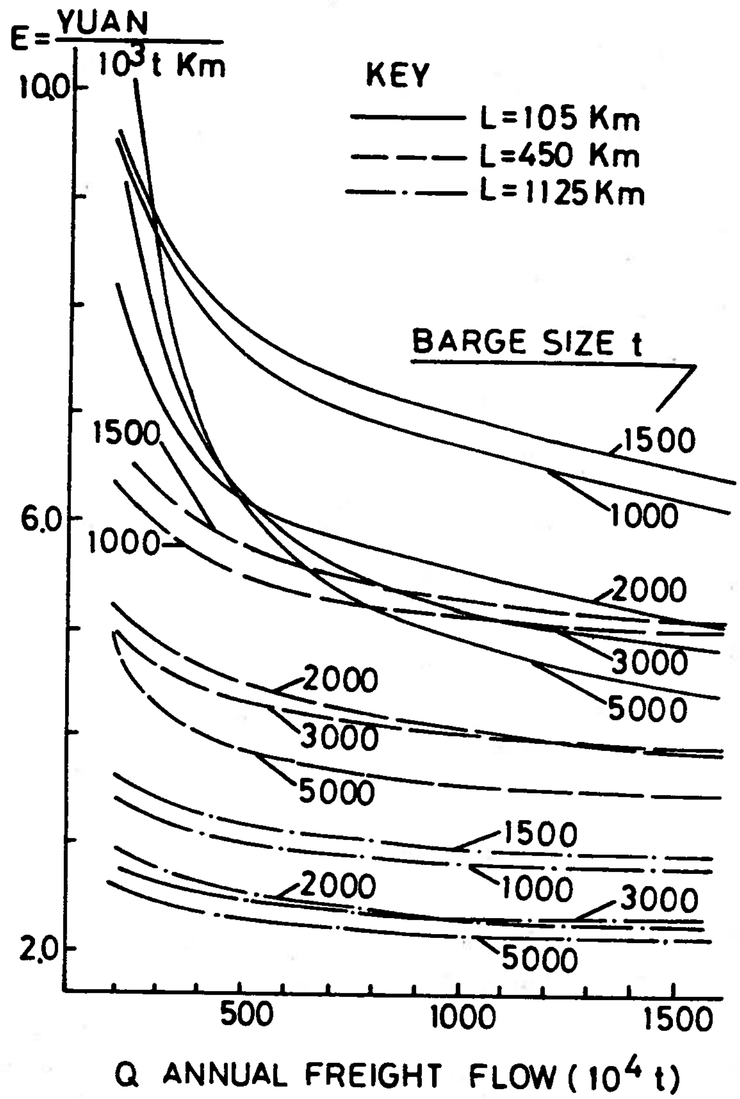

FIG. 3-a E vs TOWBOAT BHP
L = 1125 Km ; 2000 t BARGES

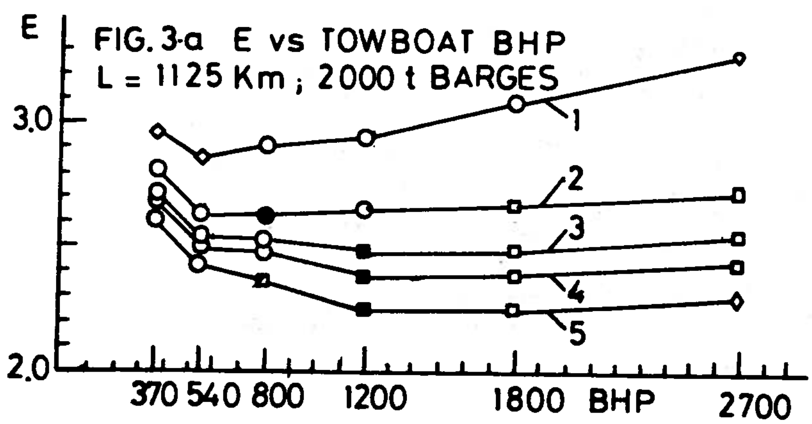

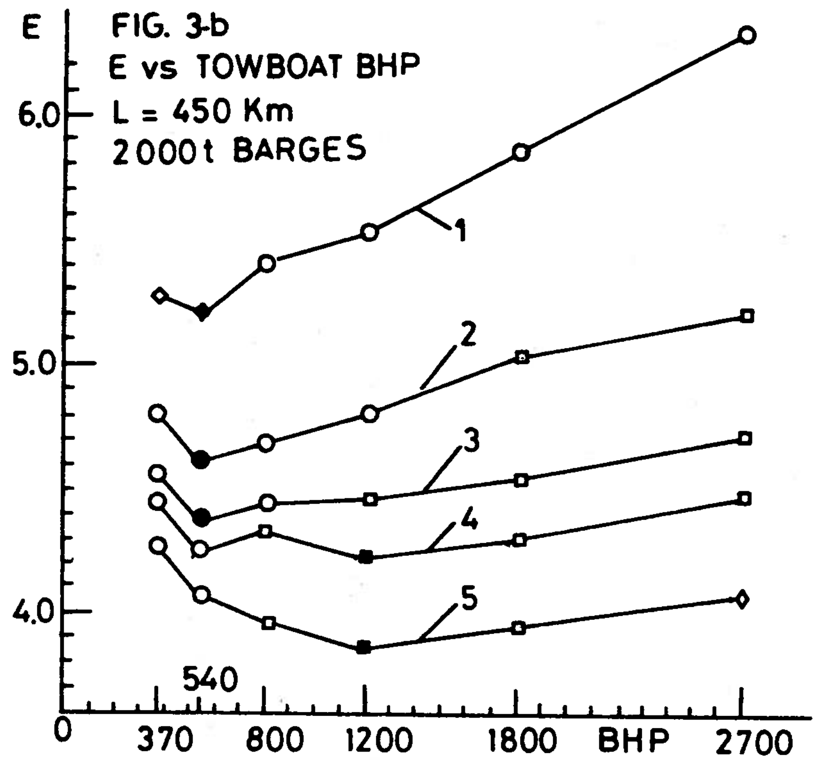
E
FIG. 3-b
E vs TOWBOAT BHP
L = 450 Km
2000t BARGES
6.0
5.0
4.0
540
0
370
800
1200
1800
BHP
2700
1
2
3
4
5

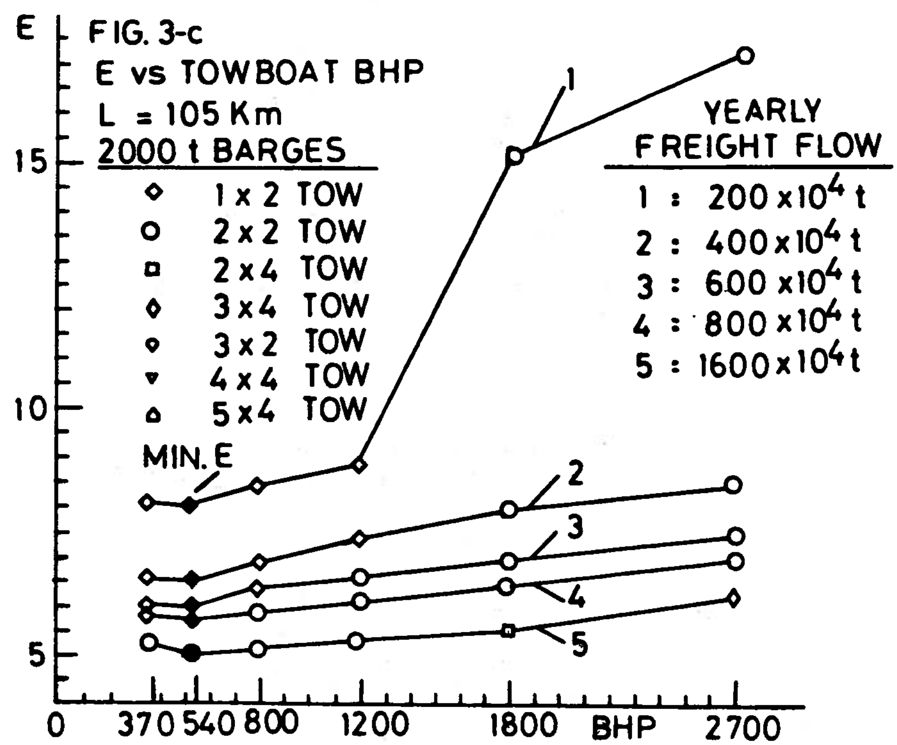
E
FIG. 3-c
E vs TOWBOAT BHP
L = 105 Km
2000 t BARGES
1 x 2 TOW
2 x 2 TOW
2 x 4 TOW
3 x 4 TOW
3 x 2 TOW
4 x 4 TOW
5 x 4 TOW
YEARLY
FREIGHT FLOW
1 : 200 x10⁴ t
2 : 400 x10⁴ t
3 : 600 x10⁴ t
4 : 800 x10⁴ t
5 : 1600 x10⁴ t
MIN. E
15
10
5
0
370
540
800
1200
1800
BHP
2700
1
2
3
4
5

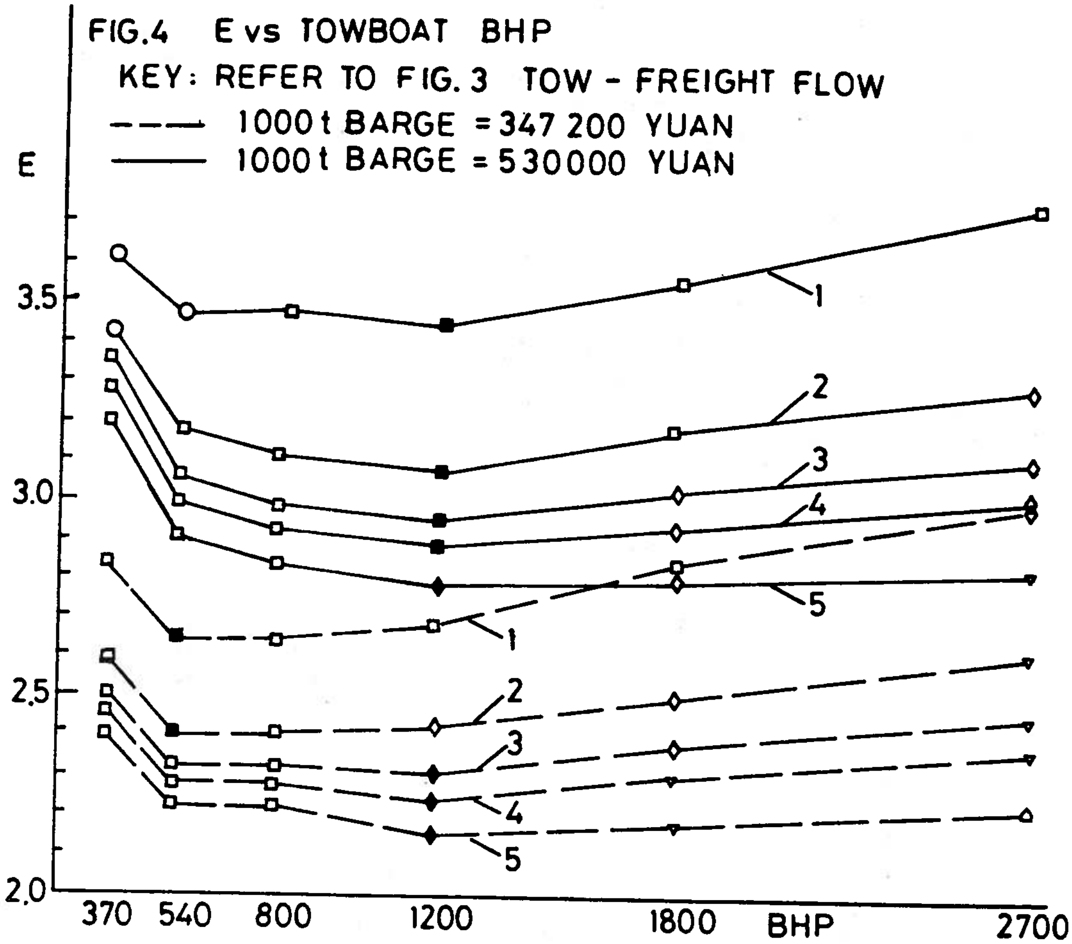

FIG.4 E vs TOWBOAT BHP

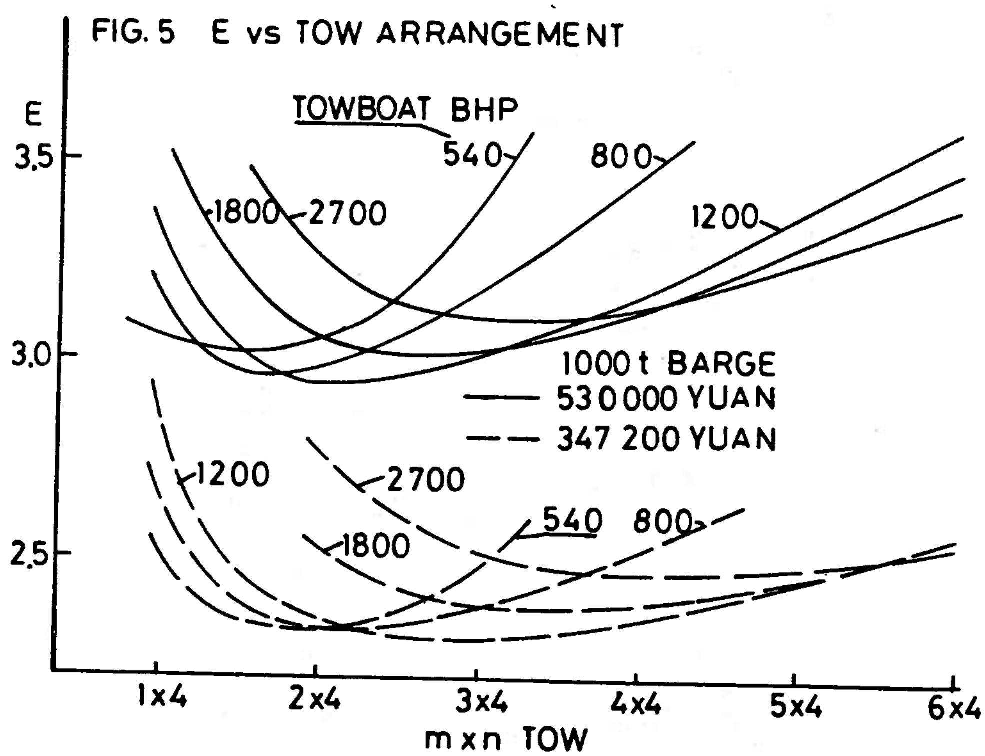

FIG. 5 E vs TOW ARRANGEMENT

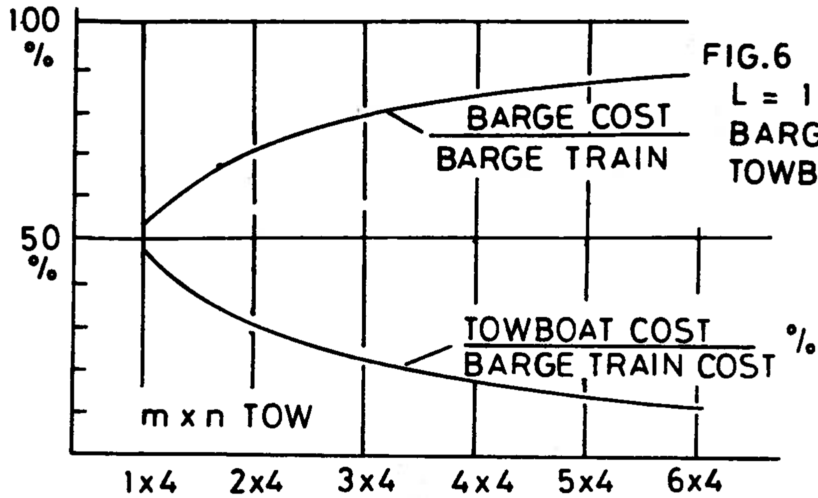

FIG.6 COST BREAKDOWN
L = 1125 Km Q = 600 x 10^4 t/year
BARGE 1000 t
TOWBOAT 1200 BHP

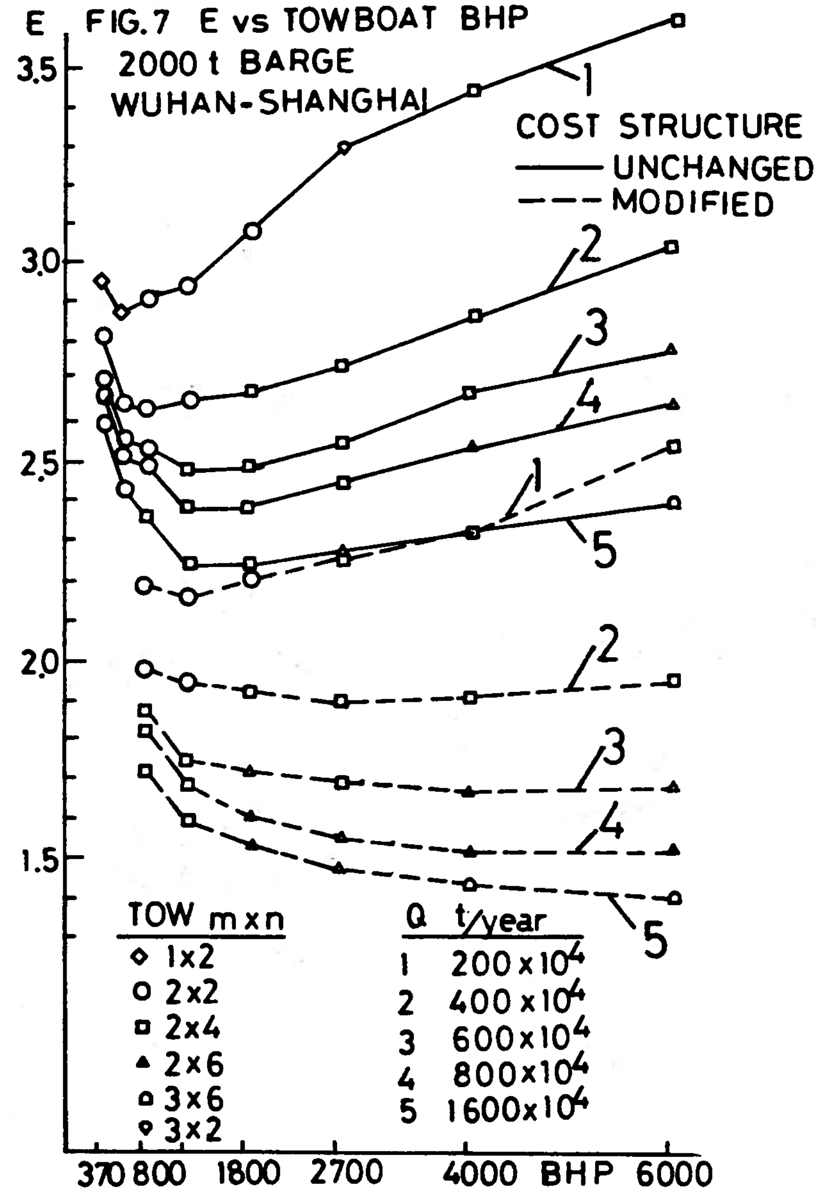

FIG.7 E vs TOWBOAT BHP

DETERMINATION OF RESISTANCE OF DISPLACEMENT SHIPS IN SHALLOW WATER[1]

BY

I.O. VELEDNITSKY[2]

ABSTRACT

This article is taken from the Soviet book: SHIP HYDRODYNAMICS IN SHALLOW WATER[1]. It reviews the methods developed in the west and Soviet Union for correcting ship resistance measured in deep, unrestricted water for the influences of limited water depth h and channel width B_C. The Froude Hypothesis is used so

$$R_T = R_R + R_f$$

where $R_T = \xi_T \cdot 1/2\rho V_0^2 S$: Total Resistance

$R_R = \xi_0 \cdot 1/2\rho V_0^2 S$: Residual Resistance

$R_f = \xi_f \cdot 1/2\rho V_0^2 S$: Frictional Resistance

ρ : fluid density

S : wetted surface of ship

In these methods corrections are made for the loss of speed V_0 and the increase in residual resistance coefficient ξ_0 for the effects of shallow water depth and limited channel width. [TRANSLATOR]

TRANSLATION[3]

For carrying out the practical calculation of resistance of vessels moving in shallow water, displacement ships can be conditionally divided into two groups:

ships in subcritical ($F_n = \frac{V}{\sqrt{gh}} < 1.0$); and

ships in supercritical ($Fn = \frac{V}{\sqrt{gh}} > 1.0$,

h = water depth) speed zones. For designs in the supercritical speed zone, the resistance calculation can be made with simplifications (Section 39).

The resistance of ships in shallow water has been determined from series tests conducted in an attempt to obtain results generalizing the ship or model resistance in conditions of restricted channel depth h.

The numerous past tests of Taylor and the record used for the basis of his records series diagrams permit the evaluation of the ship resistance increase in regions of subcritical and critical speed relative to the ship resistance in deep water, as well as the ship resistance decrease in regions of supercritical speeds. Comparisons using these diagrams show that for a reduction in speed not exceeding 10%, the increase in displacement ship resistance can reach 300% to 500%.

The Taylor diagrams refer to warships and are available in [125].

In 1934, Schlichting [212] used past studies to develop a method for calculating the influence of shallow water. In principle this method uses previous assumptions following theoretical reasoning. Schlicting did not use a magnification of the resistance for a vessel operating at a constant speed. He determined the reduction in the deep water speed when the vessel passes in to shallow water. From this approach the speed reduction can be introduced in the form of two parts: speed reduction due to the reduced speed of wave propagation in shallow water and the appearance of reversed flow. Schlichting's ideas were followed in the method developed by I.V. Girs and Yu.V. Afanasyev [64].

In the Girs and Afanasyev approach the speed is determined as a percentage of the vessel speed in deep water V_0 (Fig. 7.1). Assuming that the residual resistance R_0 corresponds to this deep water speed V_0, then the R_0 value will occur in shallow water at a speed $V_\Delta - \Delta V_1$. The correction ΔV_R takes into account the influence of reversed flow. All additional differences based on the results of the authors' experimental investigations are not included. The value of the correction ΔV_2 is determined from Fig. 7.2 where the abcissa is the

Froude number $F_n = \frac{V}{\sqrt{gh}}$ and the ordinate

is $\Delta V_2/V$ in percent. The desired corrections $\Delta V_2/v$ is presented in the form of curves, each corresponding to a fixed value

[1]Basin, A.M., Velednitsky, I.O., Lyakhovitsky, A.G., SHIP HYDRODYNAMICS IN SHALLOW WATER, Sudostroeniye, Leningrad, 1976, Sec. 37. pp. 266-275.

[2]Assistant Professor, River Transport Institute, Leningrad.

[3]Translated by R. Latorre, Dept. of Naval Architecture and Marine Engineering, The University of Michigan.

of h/T draft T relative to the channel depth h.

The use of this method is illustrated by the following example. (Refer to Table 7.1 and Fig. 7.3). The calculation gives results for a ship having the following dimensions and form coefficients: L = 36m, B = 4.2m, T = 0.65m, C_B = 0.63. The deep water speed-resistance curve and the construction of the resistance curve in shallow water is shown in Fig. 7.3.

Table 7.1 Determination of Corrections ΔV_1 and ΔV_2 using method of I.V. Girs and Yu.V. Afanasyev [64]

Item	Value		
Ship Speed, V_0 , m/s	2	4	6
$F_h = V\sqrt{gh}$, (h = 1.3m)	0.56	1.12	1.68
$\Delta V_1/V_0$ (Fig. 7.1)	0	0.16	0.40
ΔV_1 m/s	0	0.64	2.4
$\Delta V_2/V_0$ (Fig. 7.2)	0.08	0.12	0.0
ΔV_2 m/s	0.16	0.48	0.0

The diagram in Fig. 7.2 for the ΔV_2 correction supplements the earlier study of Yu.V. Afanasyev and extends the results to the supercritical speed regime. This supplementary diagram indicates the increase in ship speed in the supercritical speed is 50%. This large speed increase has not been confirmed by experimental data. In a later discussion recommendations will be made for the practical use of the Girs-Afanasyev diagrams (Fig. 7.2).

From the results of a series of model investigations of high speed ships P.A. Apukhtin [12],[13], worked out a diagram which can be used to estimate the speed loss of a ship in shallow water (Fig. 7.4). In the graph the x axis has the relative speed given by F_n and the $\Delta V/V_0$ are constructed for constant values of h/T. Using P.A. Apukhtin's diagram is simple and is illustrated in Fig. 7.5.

Basic ideas are used in the approach of A.B. Karpov [78]. He represents the shallow water phenomena by substituting for a given speed V_0, the effective speeds V_1 and V_2 for the calculations of residual and frictional resistance. The ship resistance R operating in shallow water with a channel depth h is

$$R = 1/2\rho S\ [(\xi_f + \Delta\xi)V_1^2 + \xi_0\ V_2^2] \qquad (7.1)$$

where:

ρ : water density

S : wetted surface of vessel also noted by Ω

ξ_f : coefficient of friction at Reynolds No. $R_N = \frac{V_1 L}{\nu}$

$\Delta\xi$: correlation allowance also noted by C_A = 0.0004

ξ_0 : coefficient of residual resistance measured in deep water at $F_n = V_2/\sqrt{gL}$

The value of the speeds V_1 and V_2 are determined form the following formulae:

$$V_1 = \frac{V_0}{\alpha_*} \quad \text{and} \quad V_2 = \frac{V_0}{\alpha_{**}} \qquad (7.2)$$

Here the coefficients α_{**} are determined from the diagrams proposed by A.V. Karpov [78] (Fig. 7.6). These coefficients depend on the values of h/T and F_n. The frictional resistance coefficient ξ_f is determined by friction line (ATTC or ITTC line) based on the Reynolds number calculated at speed V_1. The coefficient of residual resistance ξ_0 is based on data for the residual resistance coefficient in deep water conditions taken at Froude number $F_n = V_2/\sqrt{gL}$.

In a later publication there is another method for determining ship resistance in shallow water for subcritical speeds [11]. This method, however, is overly complicated in its calculation procedure and does not increase the accuracy of the calculation.

Approximate values for the speed lost in shallow water for subcritical speeds can be determined with the assistance of Lackenby's diagram [204] presented in Fig. 7.7.

In this diagram constant curves of speed reduction in shallow water $\delta V/V_0$ in percent. The speed reduction is based on the value of depth Froude number F_n and a parameter characterizing the channel depth in the form of $\sqrt{\Omega_0}/h$ (where Ω_0 is the submerged cross sectional area at midships).

Some of the developed calculation methods for resistance in shallow water permit constructing resistance curves in regions of subcritical and supercritical speeds. If at the subcritical speeds these methods appear to be acceptable for practical purposes, at the critical speed there is a large difference compared with the actual value. This explains why when experiments are performed in towing tanks the resistance value can correspond to critical speeds especially in the study of transient phenomenon accompanying the motion of the

Table 7.2 Relationship of Change in Coefficient of Residual Resistance $\Delta\xi_0$ for different channel widths B_C

Notation: h: channel depth; T: vessel draft B_C: channel width; B: vessel beam

	B/B_C						
h/T	0.04	0.08	0.12	0.16	0.20	0.25	0.30
1.5	0.040	0.097	0.161	0.247	0.348	0.482	-
2.0	0.034	0.081	0.137	0.203	0.279	0.386	0.570
2.5	0.028	0.067	0.112	0.162	0.218	0.300	0.418
3.0	0.023	0.054	0.089	0.127	0.166	0.225	0.302
3.5	0.018	0.041	0.068	0.096	0.125	0.168	0.223
4.0	0.013	0.030	0.050	0.072	0.094	0.126	0.172
5.0	0.008	0.016	0.028	0.042	0.057	0.082	0.115
6.0	0.005	0.011	0.020	0.032	0.043	0.062	0.089
8.0	0.003	0.007	0.011	0.019	0.028	0.045	0.066
10.0	0.003	0.007	0.011	0.018	0.026	0.038	0.055

Table 7.3 Relationship of ratio V'/V_0 for vessel moving in channel with width B_C and depth h to vessel moving in water depth h and unlimited width

Notation: h: channel depth; T: vessel draft; B_C: channel width; B: vessel beam

	B/B_C						
h/T	0.04	0.08	0.12	0.16	0.20	0.25	0.30
1.5	0.968	0.933	0.894	0.849	0.795	0.699	-
2.0	0.978	0.950	0.921	0.886	0.843	0.780	0.685
2.5	0.982	0.962	0.938	0.913	0.885	0.846	0.796
3.0	0.986	0.970	0.952	0.934	0.915	0.889	0.859
3.5	0.989	0.977	0.965	0.952	0.938	0.918	0.895
4.0	0.992	0.983	0.974	0.964	0.953	0.937	0.916
5.0	0.996	0.990	0.983	0.976	0.968	0.957	0.941
6.0	0.997	0.993	0.989	0.983	0.977	0.967	0.954
8.0	0.999	0.996	0.994	0.989	0.985	0.977	0.965
10.0	0.999	0.996	0.994	0.990	0.987	0.980	0.971

model at the same speed.

Most reliable methods used to determine the resistance of ship motion in the presence of shallow water appear to be methods which correlate full scale and model test results.

Studies using typical test methods include results with errors caused by limited water depth h and further increased by the influence of the towing tank walls.

In [182] a convenient method for practical use is presented. It is based on the assumption that identical resistance values R can be obtained for deep and restricted water at different speeds. Examination of regions of subcritical speeds shows for identical resistance values the speed in shallow water is smaller than the speed in deep water.

The total resistance in deep and shallow water is represented in the form of two components: frictional resistance and residual resistance. In addition to assuming the frictional resistance component in deep and shallow water is based on the schoenherr friction line, it is also assumed that the influence of shallow water on the frictional resistance can be included with the change in the residual resistance.

Borrowing from [182] the formula for the coefficient of residual resistance ξ_0 in unrestricted water is given by:

$$\xi_0 = (\xi_0' - \Delta\xi_0)\left(\frac{V'}{V_0}\right)^2 \qquad (7.3)$$

where: ξ_0 : coefficient of residual resistance at a channel depth h with unlimited channel width B_C.

ξ_0' : coefficient of residual resistance at a channel depth h with restricted width B_C.

$\Delta\xi_0$: change in coefficient of residual resistance due to the influence of limited channel width

V_0 : speed corresponding to channel depth h with unlimited width B_C

V' : speed corresponding to channel depth h with limited width B_C

The value of $\Delta\xi_0$ can be obtained from Table 7.2 and the speed relationships can be obtained from Table 7.3.

More detailed analysis of the data presented in the previously mentioned tables showed that it is permissible to establish the relationship within sufficient accuracy for practical work, the speed in the restricted channel width to the speed in unrestricted water using Fig. 7.8 where V'/V_0 depends on the condition of constriction $\frac{B}{B_C} \cdot \frac{T}{h} = bt$. The relationship of the difference in the coefficient of residual resistance $\Delta\xi_0/\xi_0'$ is summarized in Fig. 7.5.

The coefficient of residual resistance of ship at a given depth h of shallow water and in a channel in its scaling is illustrated in Fig. 7.10 taken from [182].

REFERENCES CITED

11. Anfimov, V.N., Vaganov, G.I., Pavlenko, V.G., "Ship Draft Calculations," TRANSPORT, Moscow, 1970 (In Russian)

12. Apukhtin, P.A., "Influence of Shallow Water on Resistance of Passenger Vessels," Sudostroeniye, No. 4, April 1947, (In Russian).

13. Apukhtin, P.A., Voytkunskii, Ya.I., "Water Resistance to Ship Motion," MASHGIZ, Moscow, 1953, (In Russian).

64. Girs, I.V., "Investigation of Effects of Shallow Water on Ship Resistance," TURDY VNITOSS, T. III, 1938 Vol. 1. (In Russian).

78. Karpov, A.B., "Calculation of Ship Resistance in Restricted Waters," TRUDY GII. T. IV, Vol. 2, 1946, (In Russian)

125. Pavlenko, G.E., "Water Resistance to Ship Motion" MORSKII TRANSPORT, Moscow, 1956 (In Russian).

182. Artjushkov, L.S., "Wall Effect Correction for Shallow Water Model Tests," N.E. Coast Institution of Engineers and Shipbuilders, 1968.

204. Lackenby, H., "The Effect of Shallow Water on Ship Speed," Shipbuilder and Marine Engine Builder, September 1963.

212. Schlichting, O., "Schiffswiderstand auf beschranktem wassertiefe, STG. 1934.

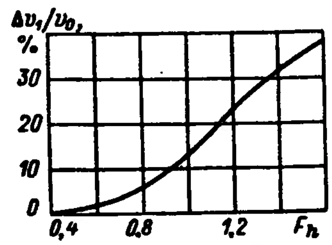

Fig. 7.1 Graph for determining correction Δv_1.

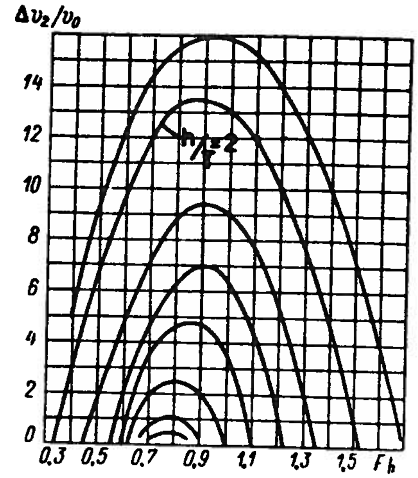

Fig. 7.2 Graph for determining correction Δv_2.

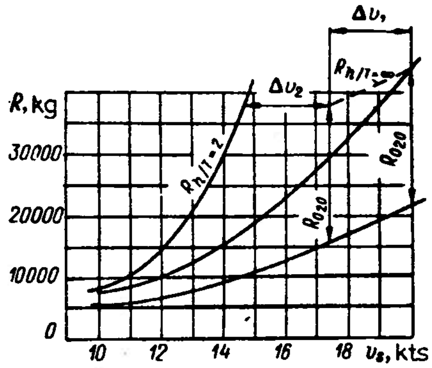

Fig. 7.3 Construction of Ship Resistance Curve for motion in shallow water using corrections Δv_1 and Δv_2.

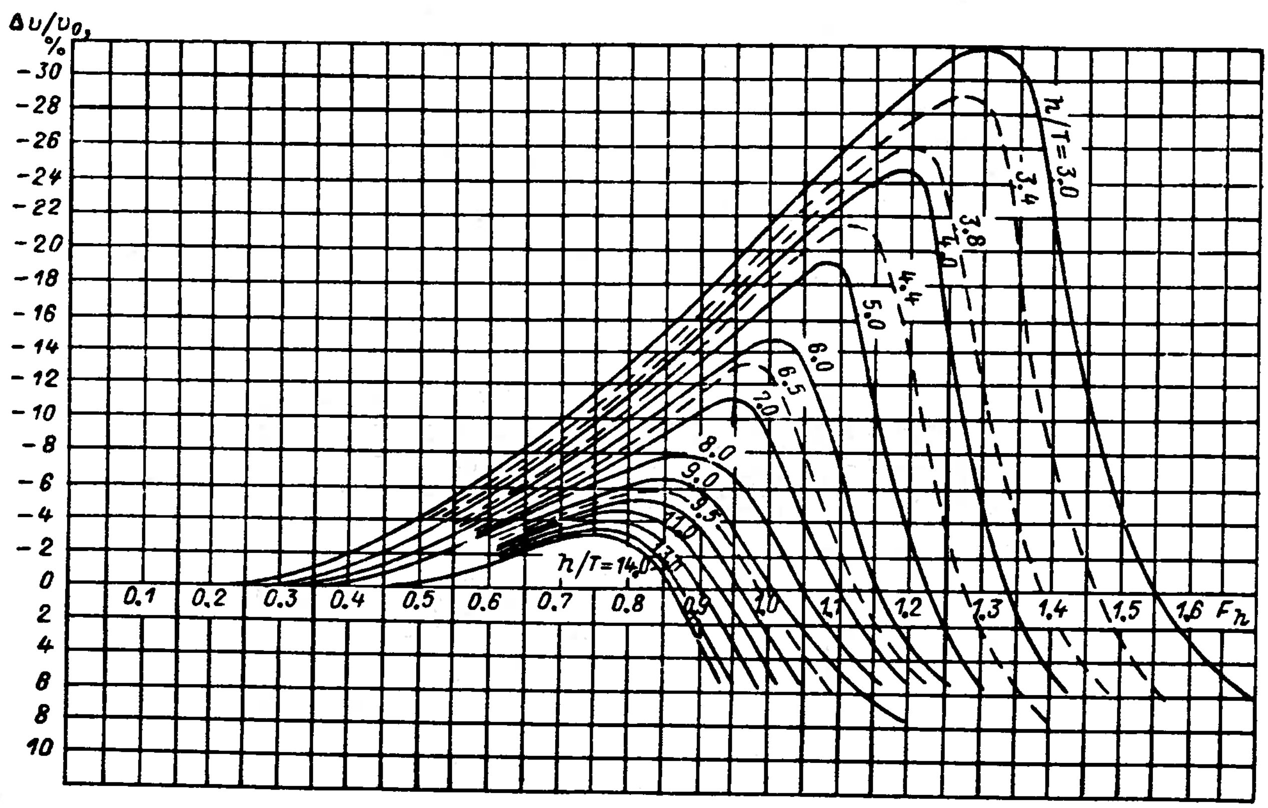

Fig. 7.4 P.A. Apukhtin's Diagram for determining change of ship speed when moving in shallow water of depth h.

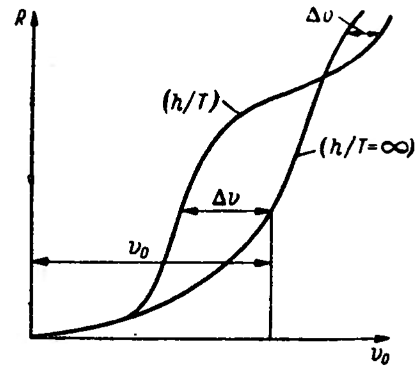

Fig. 7.5 Method of constructing resistance curve of ship moving in shallow water.

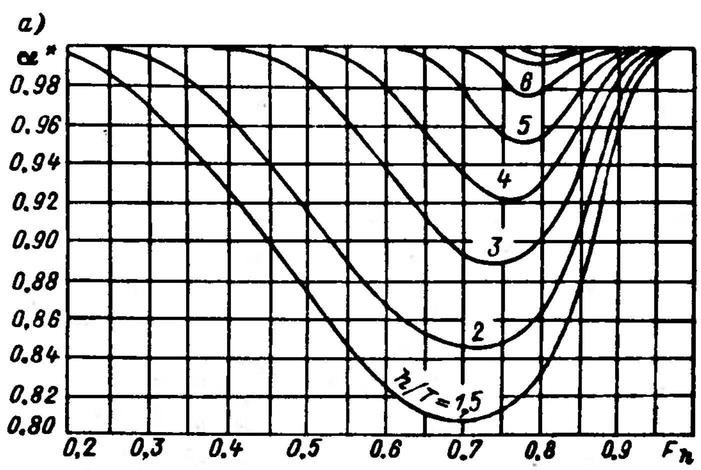

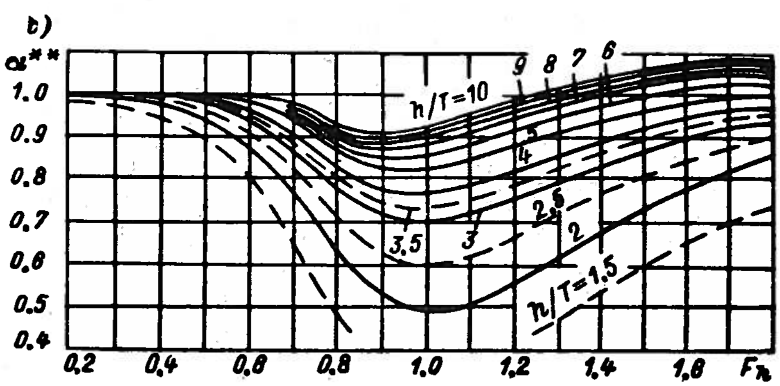

Fig. 7.6 A.B. Karpov's Graphs for determining ship resistance in shallow water.

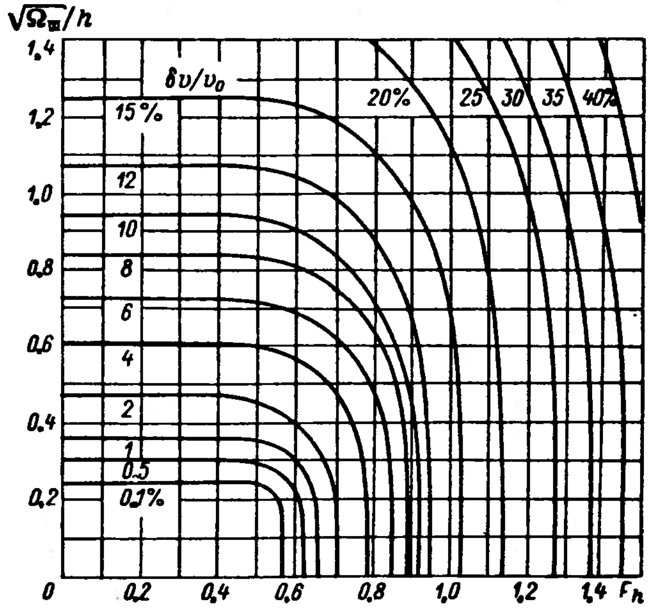

Fig. 7.7 H. Lackenby's Diagram from [204].

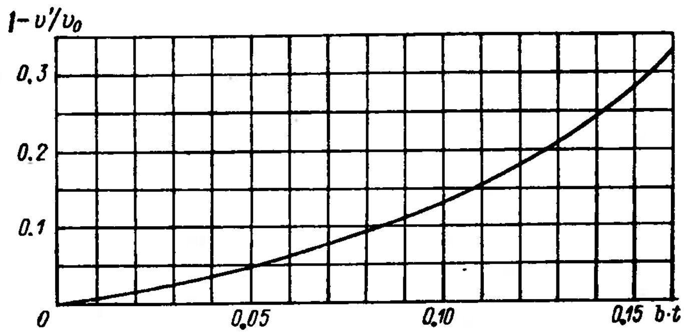

Fig. 7.8 Relationship of ship velocity to channel width and depth.

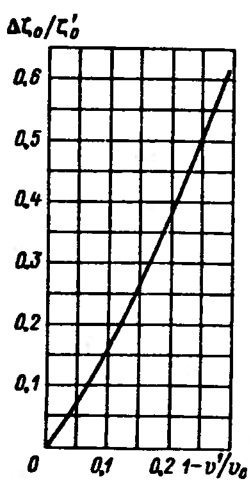

Fig. 7.9 Correction to Residual Resistance Coeff.

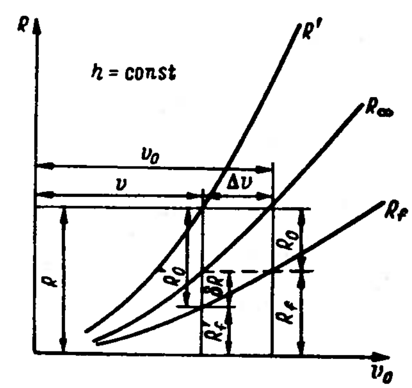

Fig. 7.10 Scaling of Residual Resistance Coefficient.

FEATURES OF THE TRIMARAN HYDRODYNAMICS AND THEIR CONSIDERATION IN THE DESIGN OF VESSELS FOR HIGH SPEED SHALLOW WATER TRANSPORT[2]

BY

A.G. LYAKHOVITSKY

ABSTRACT

This paper summarizes the results of a study of trimaran hydrodynamics conducted to develop resistance data suitable for EHP estimation. The design procedure for the EHP estimation is outlined for a trimaran with three identical hulls operating at high speeds in shallow water. Model tests indicate that the trimaran design falls between single hull and twin hull vessels at relative high speeds. $F_n > 0.40$. A design comparison for a single hull, twin hull and trimaran passenger vessel is also presented. [Translator].

TRANSLATION[2]

Conventional domestic waterways have a small depth, so high speed displacement ships are limited by the so called wave barrier, i.e., an abrupt increase in wave generation and wave resistance appearing at speeds lower than in deep water [1]. Research carried out at the Leningrad Institute of Water Transport indicated that increased speeds can be obtained by designing ships with comparatively longer hull length which decreases the role of wave resistance in the total resistance balance. One type of high-speed displacement vessel which shows great promise is the trimaran. Its hull arrangement creates a favorable wave interaction due to the longitudinal positioning of the side and center hulls [2].

Triamaran vessels show potential as displacement-type river vessels due to the following:

1. The displacement division amoung the vessel's hulls can cause a large variation between the wave and viscous resistance component ratio and in certain cases can decrease the total hydrodynamic resistance.
2. Designs of shallow draft vessels can be made with large deck surface area and fine hull forms.
3. Increased vessel stability.
4. Good seakeeping (rolling period increased and reduced rolling accelerations).
5. Reduced impact of the sea on the deck underside due to the center hull forward location which deflects the waves before they encounter the side hulls.

However, it must be taken into account that a trimaran has a complex design and larger building costs. Therefore the final selection and design chosen based on calculated economic effectiveness. To estimate this effectiveness it is necessary to estimate the trimaran resistance which is the basis for the specification of the propulsive engine power.

For evaluation of hull arrangements, main hull dimensions and the displacement division, a theoretical study of the trimaran wave resistance was made for deep and shallow water. This was accomplished using classical wave resistance theory. Theoretical formulations of the trimaran's wave resistance were obtained with each hull taken as a "slender" ship. The formulations were used with a computer to make systematic wave resistance calculations.

In Fig. 1 the calculation results are shown for the trimaran wave resistance coefficients in deep water. The trimaran has the same hulls with parabolic lines with a relative gap of $\bar{b} = \frac{b}{L} = 0.10$. Three different values of center hull position $\bar{a} = \frac{a}{L}$ (a is the distance measured from the midship of the side hulls to the center hull midship, b is the distance measured form the centerline of the side hull to the centerline of the center hull, and L is the hull length).

The nondimensional wave resistance for a trimaran is determined by the coefficient formula:

$$\zeta_w = \frac{R_w}{\frac{1}{2}\rho V^2 \sum_{i=1}^{3} \Omega_i} \qquad (1)$$

[1]Sudostroyeniye, No. 12, December, 1975, pp. 3-9.

[2]Translated by R. Latorre, Dept. of Naval Architecture and Marine Engineering, The University of Michigan.

where

V: vessel velocity
ρ: water density
R_w: ship wave resistance
Ω_i: ith hull wetted surface

As Fig. 1 indicates the center hull position has a significant effect on the trimaran wave resistance coefficient. It is especially important that a trimaran with a favorable center hull position $\bar{a}$ can be designed for operational speeds where conventional single hulls and catamarans have poor wave resistance. For example at a Froude number $Fr = \frac{v}{\sqrt{gL}} = 0.50$, and a centerhull position $\bar{a} = 0.60$, the trimaran does not exhibit the "hump" in the wave resistance coefficient. This is due to the positive interaction of the transverse wave system which is caused by the forward hull position.

The results of the theoretical calculations using linear wave theory correspond to the experimental data from model trimaran tests conducted in the model basins of the Leningrad Water Transport Institute and the Leningrad Shipbuilding Institute. These studies are used for the suggested procedure for the appropriate calculation of trimaran resistance.

The trimaran's total resistance is given by the formula:

$$R = \zeta_T \frac{\rho V^2}{2} \Omega \qquad (2)$$

where

ζ_T: total resistance coefficient

$\Omega = \sum_{i=1}^{3} \Omega_i$: wetted surface

V: velocity

The total resistance coefficient for the trimaran is determined by:

$$\zeta_T = \zeta_{f\infty} + \zeta_k + \zeta_w + \Delta\zeta \qquad (3)$$

where

$\zeta_{f\infty}$: frictional resistance coefficient of the vessel

ζ_k: hull form resistance coefficient of the vessel

ζ_w: wave resistance coefficient of the vessel

$\Delta\zeta$: added resistance from appendages hull roughness, and air.

The center hull position mainly influences the wave resistnace. The influence can be determined from the ratio K_w of the wave resistance of the trimaran R_w to the sum of the wave resistance of the individual hulls $R_{w\infty}$ (or the ratio of the nondimensional coefficients $\zeta_T/\zeta_{w\infty}$). Computer calculations were made for a trimaran with identical hulls with $\bar{b} = 0.10$ for three values of $\bar{a}$. Fig. 2 shows the results to illustrate the relation of $K_w(Fr)$ for the values of a . The trimaran wave resistance coefficient is determined by the formula

$$\zeta_w = K_w \zeta_{w\infty} \qquad (4)$$

The change in velocity and pressure around the moving trimaran hulls causes added form resistance. Assuming slender hulls so the hull surface curivature is not significant:

$$\zeta_o = \zeta_w + \zeta_k \qquad (5)$$

where

ζ_o residual resistance coefficient of trimaran

Results of model tests and theoretical calculations of trimaran resistance with identical hulls established the correction factor K_{ko} $(\bar{a},\bar{b})$ curves. This factor is determined from the formula:

$$K_{ko} = \frac{\zeta_k}{\zeta_{k\infty}} \qquad (6)$$

where

ζ_k: trimaran form resistance coefficient

$\zeta_{k\infty}$: form resistance coefficient for single hull

The K_{ko} curves are shown in Fig. 3. The asympote for $\bar{a}\to\infty$ of K_{ko} corresponds to the value for catamarans obtained by V.A. Dubrovsky [3]. In general, the correction K_k for the form resistance variation of a catamaran with identical hulls should depend on center and side hull dimensions, hull lines and displacements.

The following formula can approximate this factor:

$$K_k = (K_{ko} - 1) \frac{\nabla_1}{\nabla_2} + 1 \qquad (7)$$

where ∇_1: side hull displacement

∇_2: center hull displacement.

Thus when $\nabla_1 = \nabla_2$ it gives the correct value for a trimaran with identical hulls and when $\nabla_1 = 0$ (a single hull vessel) the value is 1.

Table 1

Basic elements and Characteristics of Vessels Compared

ITEM	Ship Type		
	single hull	catamaran	Trimaran
Length overall, m	38.20	32.00	32.00
Length on design waterline, m	36.00	28.00	28.80
Length on design waterline of center and side hulls, m			18.00
Beam on design waterline center and side hulls, m		2.30	2.30
Overall beam on Design waterline, m	5.30	7.10	8.80
Deck beam, m	5.90	7.50	9.50
Center hull position, $\bar{a}$			0.60
Side hull position, $\bar{b}$		0.086	0.180
Wetted surface, m^2	178.50	197.40	189.00
Design displacement, m^3	105.00	100.00	99.00
Total passenger accomodation	238	262	268
Speed using 2 × 300 hp diesel engines, km/hr	27.7	23.7	24.8 (25.0)*

Notes:

* $\bar{b} \neq 0.23$
$\bar{a} = 2.60$

It is especially important when designing inland waterway vessels to be able to estimate the shallow water influence on the vessel's hydrodynamic characteristics. To study the shallow water influence on the trimaran resistance model tests were made at three water depths h at the Leningrad Water Transport Institute Basin.

In Fig. 4 the residual resistance coefficient curves for $\bar{b} = 0.070$ and $\bar{a} = 0.283$ for diffferent waterway depths. From this figure it can be seen the shallow water effects typical for single hull vessels also apply to trimaran vessels.

In Fig. 5 the center hull position $\bar{a}$ effect on the residual resistance coefficient at the shallow water critical speed is shown on the basis of model tests. Although some scatter is present, the data shows that with greater a value there is a favorable effect on the vessel's residual resistance at shallow water critical speeds. There critical speed in deep water is assumed to be the speed corresponding to $F_r = 0.50$.

From data from two model with three identical hulls, the zone where trimarans can be advantegously utilized from the resistance viewpoint is shown in Fig. 6. This zone is constructed in an α-Fr coordinate system. Here the trimaran hull location is determined by the angle

$\alpha = \arctan \frac{b}{a}$. The favorable operational range of trimaran vessels $(0.20 < F_r < 0.70)$ is larger than the catamaran range and depends on the angle α. With increased speed the angle α should be decreased. It is possible that an equivalent single hull vessel may have a lower total resistance than a multi-hull vessel. While the multi-hull vessel may have a lower wave resistance coefficient, there is an increase in the wetted surface area of the vessel.

A possible trimaran design is illustrated by a passenger vessel with three identical hulls developed by the Leningrad Water Transport Institute and the MRF Design Group. A model is shown in Fig. 7 (Note: the photo in Fig. 7 is unable to be reproduced and omitted). The trimaran motor vessel will be compared with a single hull and a catamaran vessel having similar passenger space. Table 1 summarizes the designs.

In Fig. 8 the residual resistance curves are presented (Fig. 8-a). The results from the total resistance and propeller thrust calculations are presented (Fig. 8-b) for the three designs. These results are based on model tests. The single hull vessel has the highest speed followed by the trimaran design and catamaran design. At high speed $(F_r > 0.40)$ the trimaran design appears to fall between the single hull and catamaran hull vesssl in terms of speed to power ratio. Therefore the trimaran may be considered as developable for a high speed inland waterway displacement vessel when a large deck area and high values of stability are required. This type of vessel can be used for passenger vessels, car ferries, container ships etc.

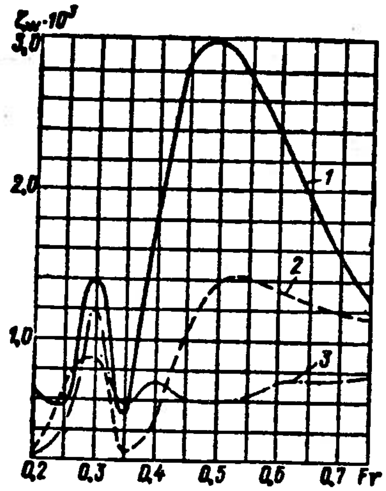

Fig. 1 Dependance of Wave Resistance Coefficient on Froude number.
Key: 1 $\bar{a} = 0$ 3 $\bar{a} = 0.6$
2 $\bar{a} = 0.4$

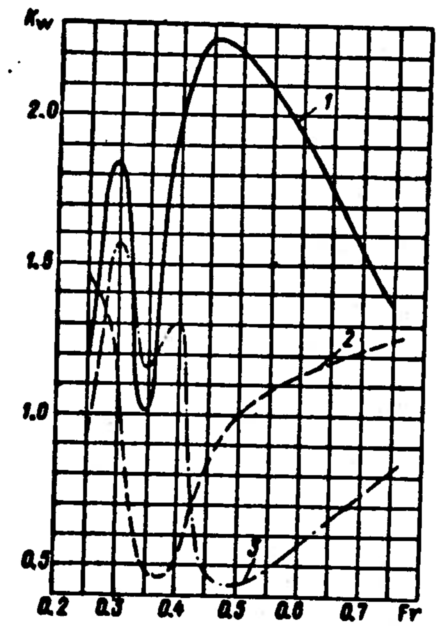

Fig. 2 Relation of K_w on Froude number.
Key: Same as in Fig. 1.

REFERENCES

1. Basin, A.M., Lyakhovitsky, A.G., "River Displacement Vessels at Critical Speeds," Sudostroyeniye, No. 7, July, 1972.

2. Basin, A.M., Lyakhovitsky, A.G., "Potential for the Development of Fast Displacement Vessels," Rechnoi Transport, No. 6, June, 1972.

3. Artyustokov, L.S., Lyakhovitsky, A.G., Yurkov, N.N., "Experimental Investigation of Trimaran Drag," Sudostroyeniye, No. 12, December, 1975.

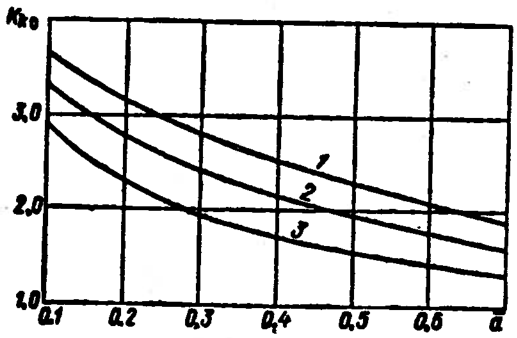

Fig. 3 Dependence of Correction Factor K_{ko} on Relative hull position of trimaran.
Key: 1 $\bar{b} = 0.05$
2 $\bar{b} = 0.10$
3 $\bar{b} = 0.15$

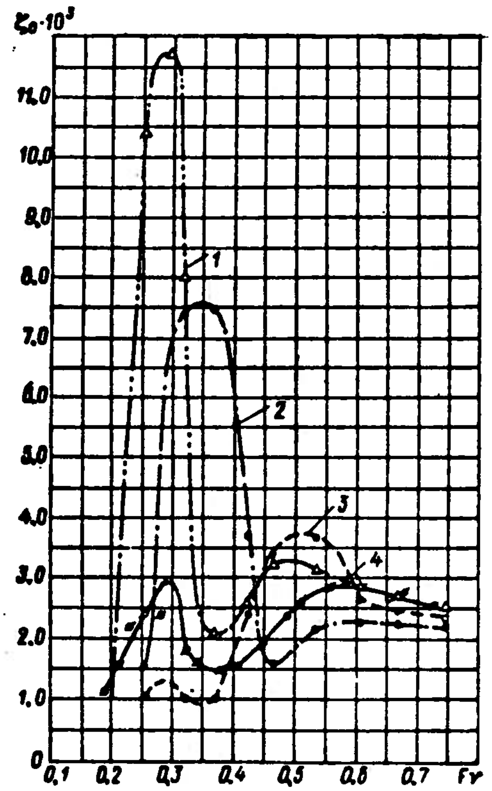

Fig. 4 Dependence of residual resistance Coefficient in Shallow Water on Froude number for model trimaran.
KEY:
1 h/L = 0.08 h: water depth,
2 h/L = 0.15 L: vessel length
3 h/L = 0.33
4 Deep water

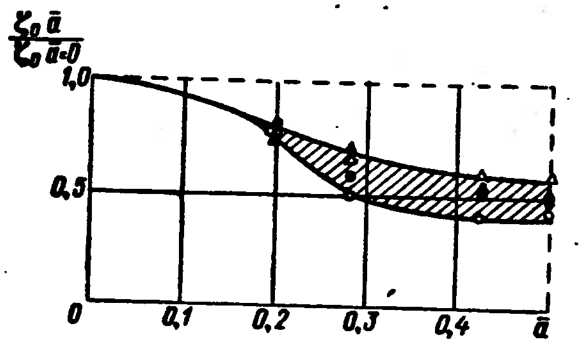

Fig. 5 Influence of position $\bar{a}$ on residual resistance coefficient for model trimaran in shallow water.

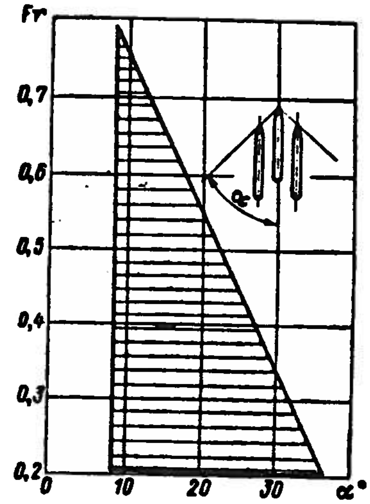

Fig. 6 Region of favorable (cancellation) of hull waves obtained from two model trimaran test data. Trimaran models have identical hulls.

Fig. 7 Photo of Model trimaran passenger vessel. (Omitted)

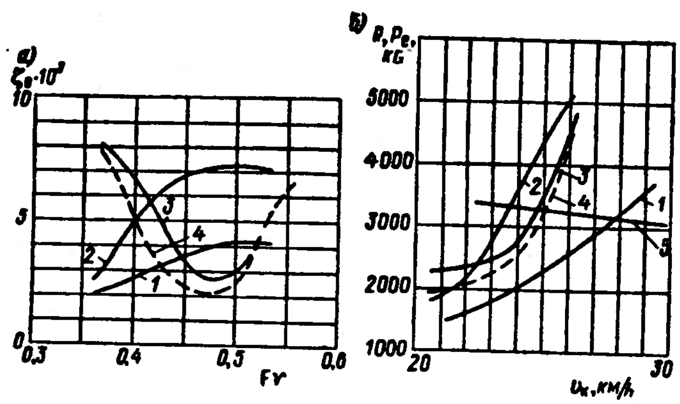

Fig. 8 Comparison of single, catamaran, and trimaran hulls for river passenger motor vessels.

a) Residual resistance coefficient

b) Total resistance and useful propeller thrust

KEY:
1 Single hull
2 Catamaran hull
3 Trimaran hull $\bar{a} = 0.6$ $\bar{b} = 0.18$
4 Trimaran hull $a = 0.6$ $b = 0.23$
5 Propeller thrust

EMPIRICAL FORMULAS FOR ESTIMATING THE WAVE FRACTION AND THRUST DEDUCTION FACTORS FOR OCEAN AND INLAND WATER WAY VESSELS[1]

BY

A.M. BASIN
I. YA. MINIOVICH

ABSTRACT

This article is taken from the Soviet book THEORY AND DESIGN OF SCREW PROPELLERS by A.M. Basin and I. Ya. Miniovich. It summarizes the empirical formulas for estimating the wake fraction w and the thrust deduction factor t for ocean and inland waterway vessels. The late Dr. Basin was active in research and design of inland waterway vessels with tunnel sterns. He has included in this article extensive material from his research. [TRANSLATOR]

TRANSLATION[2]

For the design of screw propellers from diagrams produced from the results of systematic series model propeller tests in open water, it is necessary to have data available on the hydrodynamic character of the propeller interaction with the vessel hull (sec 15). The most reliable data for the value of the factors, wake fraction w and thrust deduction t, can be obtained from comparison of self-propulsion model tests with open water propeller test data (sec. 20).

When there is a lack of data from model tests, related to the vessel, hull, its associated ship wake and thrust deduction factors, the values of these hull-propeller interaction are approximate values determined from analysis of data from numerous experiments in research laboratories and actual operation. These also draw on important conclusions of theoretical investigations. The necessary data ordinarily are presented in form of empirical formulas or graphs convenient for practical application.

The values of wake fraction and thrust deduction depend on many factors: the fullness and form of under water hull section, propeller diameter and the propeller location relative to hull, form and arrangement of protruding bow etc. It is obvious that with empirical formulas for determining the wake fraction and thrust deduction it is not possible to take into consideration the influence of all these various factors. Therefore, the thrust and wake fraction values calculated from the following formulas, should be taken as approximate.

The following are empirical formulas for obtaining the wake fraction and thrust deduction. They are applicable for the design of screw propellers for operating behind the hull when it is not possible to conduct self propelled model tests.

<u>Determination of Wake Fraction w.</u> The calculation of the velocity v_p m/s at the propeller operating behind the ship hull is related to the ship speed v by the relationship:

$$v_p = v(1-w) \tag{21.1}$$

where

w: wake fraction which approximates the resulting flow when the propeller operates behind the hull.

For lack of data, the value of w can be calculated using the following formulas which do not include corrections for the influence of the rudder. These formulas were developed from model ship data.

In preliminary calculations when it is not possible to obtain an approximate propeller diameter, the wake fraction can be estimated from the following formulas recommended by Taylor for ocean transport ships:

[1]Basin, A.M., Miniovich, I. Ya., THEORY AND DESIGN OF SCREW PROPELLERS, SUDPROMIGIZ, Leningrad, 1963, Section 23 (Empirical Data for Characterizing Propeller-Hull Interaction) pp. 143-148.

[2]Translated by R. Latorre, Dept. of Naval Architecture and Marine Engineering, The University of Michigan.

For centerline propeller:

$$w = 0.5C_B - 0.05 \qquad (21.2)$$

For twin/side propellers:

$$w = 055C_B - 0.20 \qquad (21.3)$$

where

C_B: Block coefficient = ∇/LBT

The wake fraction w can also be determined from Harvald's diagram [114] (Figs. IV 16a and b) summarizing results of numerous model basin tests of single and twin screw ocean transport ships. For single screw vessels the value of w can be obtained from Fig. IV 16-a for a specified block coefficient value (C_B = 0.50-0.77) and ratio of ship length to beam (L/B = 5.0-8.0). Correction factors $\pm\Delta w$ are for the stern form (V and U stern) and for the ratio of propeller diameter to vessel length (D/L = 0.025-0.07). The value of w for twin screw can be analogously obtained from Fig. IV 16-b (for C_B = 0.52-0.67, L/B = 6.5-7.5), but without correction for the ratio of D/L.

In domestic Soviet design practice, the wake fraction w with correction Δw is obtained from E.E. Papmel's empirical formula [72].

$$w = 0.165\, C_B^X \sqrt{\frac{\sqrt[3]{\nabla}}{D}} - \Delta w \qquad (21.4)$$

where:

- ∇: Ship volumetric displacement, m^3
- D: Propeller diameter m
- x=1: for centerline propeller
- x=2: for twin or side propellers
- Δw: Correction for vessel speed corresponding to Froude number

$$Fr = \frac{v}{\sqrt{gL}} > 0.2$$

(for F_r < 0.2 Δw=0) given by

$$\Delta w = 0.1(F_r - 0.2) \qquad (21.5)$$

Formula 21.4 is appropriate for the design of screw propellers for vessels with ordinary hull lines (without tunnel sterns). It has been used with satisfactory results. From available data of inland waterway vessels without tunnel sterns and model self-propulsion tests another relationship was developed. E.E. Papmel's modified formula for determining the wake fraction of inland waterway vessels:

$$w = 0.11 + \frac{0.16}{x} C_B^X \sqrt{\frac{\sqrt[3]{\nabla}}{D}} - \Delta w \qquad (21.6)$$

When the diameter of the propeller is not yet specified, the value of D in formulas 21.4 and 21.6 can be estimated using the value of the vessel draft T_K. From typical propeller-hull arrangements:

For single shaft (screw) vessels:

$$D = (0.7 \text{ to } 0.8)T_K \qquad (21.6\text{-a})$$

For twin shaft (screw) vessels:

$$D = (0.6 \text{ to } 0.7)T_K \qquad (21.6\text{-b})$$

The smaller value of D applies to vessels not used in towing/pushing, while the larger D value is used for tugs and pushboats.

From known characteristics of flow around the ship hull, the approximate value of D can also be determined from the horsepower N_p(H.P.) shaft rpm,n can be estimated using B_p~δ charts. The value of the wake fraction w obtained from formula (21.6) are representative when:

a) The gap between the propeller blade and the outside edges of hull is 0.12 to 0.20 the propeller diameter D.

b) For single shaft (screw) arrangements (Fig. IV 17-a) the stern post arrangement is adequately defined for rudder frame and the streamlined rudder which have proper streamlined forward section.

c) For twin shaft (screw) arrangements (Fig. IV 17-b) which have moderately sloping stern with streamlined rudders set behind the propellers, Fig. IV 17-b shows the propeller operating arrangement (each distance edge of rudder and propeller disk not less than 0.25-0.50 the value of D).

For shallow draft, flat bottomed inland waterway vessels which have beam to draft ratios B/T = 6 to 8, the wake fraction w can be determined from formulas 21.4 and 21.6 with the value of x = 1.0 irrespective of the number of propellers.

Formulas 21.4 and 21.6 can also be utilized for estimating the wake fraction for vessels whose stern end has a tunnel. In this case the value of the draft T_K is used for the value of the diameter D. For utilization of the formulas for triple shaft (screw) vessels with tunnel sterns, the next larger value of x(x=2) is used for the propeller mounted in a tunnel or half tunnel (Figs. IV 18-a and 18-b).

For high speed vessels with significant stern cut away (passenger carriers, small military vessels). There is a very small inflow disturbance so the value of w=0.

The wake fraction for ocean transport ships can be obtained from the empirical formula of Senher [93].

a) For single screw vessels;

$$w = 0.12 + 4.5 \frac{C_{vp}\, C_p\, B/L}{(7-6C_{vp})(2.8-1.8C_p)} + \frac{1}{2}\left(\frac{E}{T} - \frac{D}{B} - q_1 f_1\right) \qquad (21.7)$$

where:

- L: ship length, m
- B: ship beam, m
- T: ship draft, m
- D: propeller diameter, m
- E: height of propeller shaft above base line, m
- C_{vp}: vertical prismatic coefficient
- C_p: longitudinal prismatic coefficient
- f_1 angle of blade generatrix inclination, radians
- q_1: coefficient equal 0.3 for vessels with usual hull form and 0.5 to 0.6 for vessels with cut away dead wood

b) For twin screw vessel without ward turning propellers with propeller shaft bossings:

$$w = 2C_B^5(1-C_B) + 0.2 \cos^2\left(\frac{3f_2}{2}\right) - 0.02 \qquad (21.8)$$

with shaft brackets:

$$w = 2C_B^5(1-C_B) + 0.04 \qquad (21.9)$$

where:

- C_B: Block coefficient of vessel
- f_2: Angle of inclination of bossings to horizontal

Determination of Thrust Deduction t. The propeller horsepower P transmitted at a given ship speed must overcome the corresponding hull resistance P_e (effective horsepower) without the propeller given by the following relationship:

$$P = \frac{P_e}{1-t} \qquad (21.10)$$

where t: thrust deduction value for effect of operating propeller on ship hull.

The value of t can be determined from relations using the corresponding value of w determined by the previous formulas and related with calculation of the propellers operating behind the ship hull.

To use formulas 21.2 and 21.3, Taylor has recommended the value of t calculated from the value of w be determined.

a) For single screw vessels:

$$t = k_t w \qquad (21.11)$$

where:

k_t: Factor having a value
- 0.5-0.7 for a streamlined rudder mounted behind the propeller
- 0.9-1.05 for a non-streamlined rudder mounted behind the propeller.

b) For twin screw vessels with shaft brackets:

$$t = 0.7w + 0.06 \qquad (21.12)$$

(at center screw t=w)

In the case when the value w is obtained from formula 21.6 for hull without a tunnel stern, it is recommended that the value of t be obtained as follows:

For propeller located on centerline:

$$t = 0.6w(1 + 0.67w) \qquad (21.13)$$

For twin/wing propellers:

$$t = 0.8w\ (1 + 0.25w) \qquad (21.14)$$

When using the values of wake fraction w determined from formulas (21-7) and (21-9), Shenher [93] recommends that the thrust deduction t be determined as follows:

a) For single screw ships:

t is calculated from formula (21.11) with streamlined rudder k_t = 0.7-0.9.

b) For twin screw ships:

with bossings $t = 0.25w + 0.14$
with shaft brackets $t = 0.70w + 0.06$

(21.15)

For propellers in tunnels and completely submerged under water surface, the thrust deduction factor t can be determined from the wake fraction w for vessels with tunnel stern hull form, ie.:

$$t=w \qquad (21.16)$$

In case the propeller is only partially submerged under the water surface and the vessel has a tunnel stern, the additional influence on the thrust deduction is represented by Δt.

$$t = t_{submerged} + \Delta t \qquad (21.17)$$

The value of Δt can be obtained from graph in Fig. IV.19 for a given value of T_B/D where T_B is the depth the propeller tip is sumberged (Fig. IV.19).

For the design of high speed vessel propellers (cutter, light military craft) the thrust deduction factor can be estimated at t=0.05-0.08.

REFERENCES CITED

72. Papmel, E.E., DESIGN CALCULATIONS OF SCREW PROPELLER NIVK, 1936

92. Shahoeva, L.M., "Investigation of Thrust Deduction Factor for Single Screw Transport Vessels," Sudostroeniye, No. 8, 1958.

93. Shenher, K.E., "Screw Propellers," In BASIC NAVAL ARCHITECTURE, SUDPROMIGIZ, Leningrad, 1949.

114. Harvald, S.V., <u>Wake of Merchant Ships The Danish Technical Press</u>, Copenhagen, 1951.

114-b. Guldhammer, H.E., Harvald, S.V., <u>Ship Resistance</u>, Akademisk Forlag, Copenhagen, 1974.

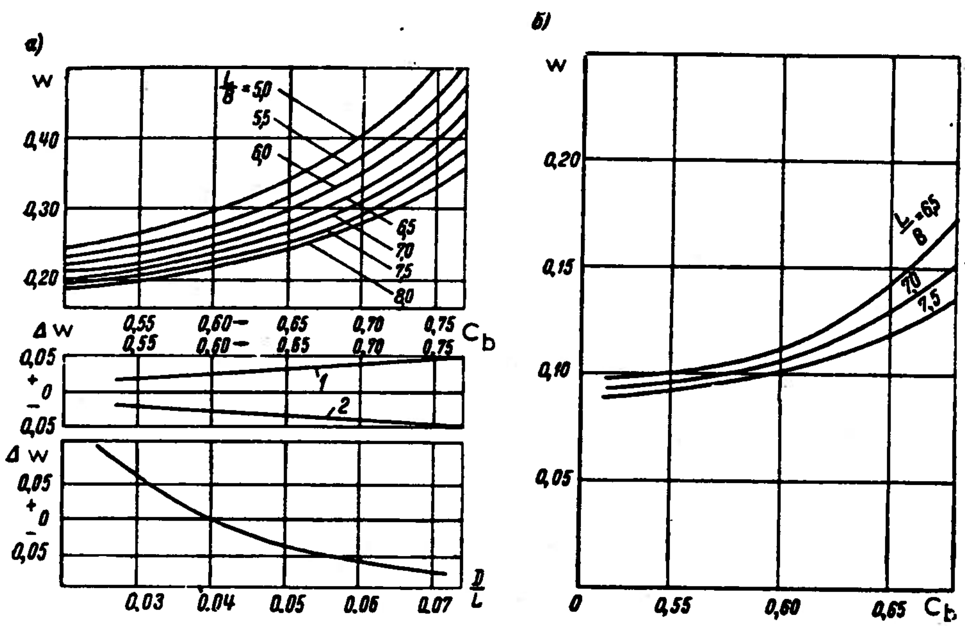

Fig. IV.16 Harvald's Diagram for determining the wake fraction w [114]

a) Single screw ocean going vessels
b) Twin screw ocean going vesssls
1 : U shaped stern
2 : V shaped stern

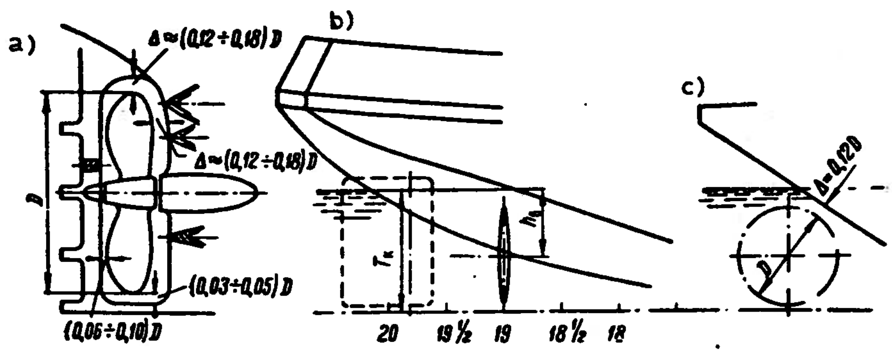

Fig. IV.17 Propeller and hull clearances

- a) Single screw vessel
- b) Twin screw vessel
- c) Section at center of propeller disc

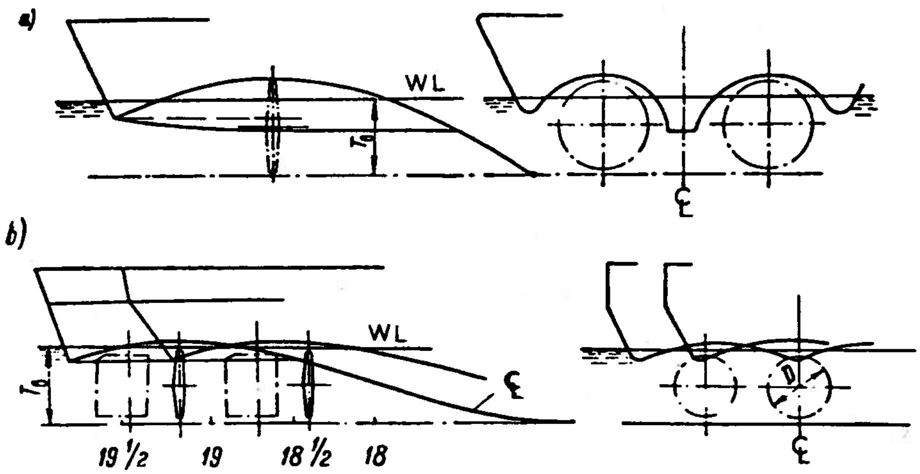

Fig. IV.18 Arrangement of propellers in tunnel stern

- a) Separated tunnels
- b) Combined tunnels

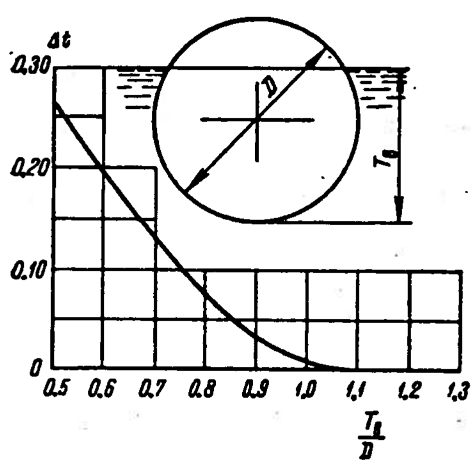

Fig. IV.19 Graph for determing $\Delta t = f(T_B/D)$

DIAGRAMS FOR PREDICTION OF EFFECT OF NOZZLES ON PROPELLER PERFORMANCE[1]

BY

YU N. MAMONTOV

ABSTRACT

Propeller design diagrams are presented to estimate the optimum propeller with and without mozzles. An example of the application of these diagrams is given for design of propellers for a twin screw inland towboat with D_{max} = 1.5m . Using reference [3], the printing errors in Pampel's expression (4) and Anfimov's expression (5) for the wake fraction w have been corrected along with several calculation errors [translator].

TRANSLATION[2]

At the time of the preliminary design it is necessary to make rapid and accurate estimates of maximum possible vessel speed, thrust, optimum diameter of propeller, and the effect of a nozzle on propeller performance to determine the ship's operation. Using the diagrams presented here these estimates can be easily made.

The diagrams are for the design calculations of a combined propeller-rudder for transport vessels. In such cases, it is necessary to estimate the operational characteristics or thrust for a given vessel and engine. The values known are: horsepower delivered to propeller, shaft rpm, and vessel speed either specified (in tugboat case) or evaluated in other designs by the method of successive approximations.

For the main parameter the following coefficient has been selected:

$$K_n'' = \frac{V_p}{\sqrt{n}} \sqrt[4]{\frac{\rho V_p}{N_p}} \qquad (1)$$

where

$V_p = V(1-\omega)$: velocity at propeller m/s

V : ship speed m/s (V=0.514 V_{knots})

n : propeller rps = rpm/60

$\rho = \frac{\gamma}{g}$: mass density kg-s²/m⁴

γ : specified weight (γ = 1000kg/m³ fresh water) (γ = 1025 kg/m³ salt water)

g : 9.81 m/s²

$N_p = N_e \eta_s$ Metric Horsepower delivered to propeller, MHP (MHP = 1.013 BHP)

η_s : Transmission efficiency (shafting, gear, bearings).

In Fig. 1 the curves are for four-bladed propellers without nozzles and an expanded area of 0.4 (B 4.40 of Troost Series). In this figure three sets of curves are given: advance coefficient $J = \lambda_p = \frac{V_p}{nD} = f_1 (K_n'')$, propeller efficiency $\eta_p = f_2 (K_n'')$ and pitch-diameter ratio $H/D = f_3 (K_n'')$.

Each set of curves include an optimum diameter curve and curves for smaller diameters, 0.95, 0.90, 0.85, 0.80 of the optimum.

Utilization of the diagram is simple:

1. Compute K_n'' coefficient and determine λ_p for the optimum propeller diameter.
2. Use $D = \frac{V_p}{n\lambda_p}$ to calculate optimum diameter. If the value of D does not exceed the maximum value, determine propeller efficiency and pitch-diameter H/D ratio, for the optimum diameter D at K_n'' .
3. In the case of the optimum diameter D exceeds the maximum allowed. The ratio of the maximum allowed diameter to optimum diatmeter is determined and from the proper curve obtain the propeller efficiency η_p , and pitch-diameter H/D ratio. For intermediate ratios linear interpolation can be utilized.

---

[1]Sudostroyeniye, No. 8, August, 1959, pp. 9-11.

[2]Translated by R. Latorre, Department of Naval Architecture and Marine Engineering, The University of Michigan.

In an anologous manner, the diagrams of Fig. 2 can be used for nozzle propeller calculations. The differences in the diagrams are:

a) a set of $\lambda_e = \frac{V_e}{nD} = f_1\ (K''_{ne})$ curves are used instead of λ_p ;

b) a set of $\eta_e = \eta(1-wf) = f_2\ (k_{\eta e}'')$ curves are used instead of η_p ; where $V_e = V(1-w_f)$ and w_f is is the frictional wake fraction.

The main parameter used in diagrams is

$$k_{ne}'' = \frac{V_e}{\sqrt{n}} \sqrt[4]{\frac{\rho V_e}{N_p}} \tag{2}$$

In Fig. 2 the curves are drawn for four bladed propellers with a 0.55 expanded area ratio in a nozzle. The nozzle has an entrance coefficient $\alpha_e = \frac{F_e}{F_d} = 1.30$ and and an exit coefficient $\beta_a = \frac{F_a}{F_d} = 1.10$ and nozzle length to propeller diameter ratio $\ell = \frac{\ell_n}{D} = 0.5$ to 0.9 , here ℓ_n : nozzle length, F_e : nozzle entrance area, F_a: nozzle exit area, and F_d : the nozzle area of the propeller. The curves in Fig. 2 were drawn following the procedure of the TsNIIRF).

For nozzle propeller calculations the frictional wake calculation is required. It can be determined by the formula:

$$w_f = C_f\ w \tag{3}$$

where w is the total wake fraction. It can be determined for a given vessel by empirical formulas. Here E.E. Papmel's relationship is used [3]

$$w = 0.165\ C_B^x \sqrt{\frac{\sqrt[3]{\nabla}}{D}} \tag{4}$$

w: Wake fraction

C_B: Block coefficient

x: Propeller number

∇: Vessel volume displacement, m^3

D: Propeller diameter, m

C_f: Vessel stern coefficient

The following C_f values are recommended:

Centerline Propellers:

$C_f = 0.7$ for vessels with U-shaped stern

$C_f = 0.5$ for vessels with V-shaped stern

wing/twin propellers

$C_f = 0.6$

PUSHER VESSEL PROPELLER CALCULATIONS

Problem: Determine nozzle influence and initial propeller design calculations at $V_s = 5$ knots to obtain maximum thrust by full utilization of available power. Specified data:

Vessel dimensions

Length on waterline	L	= 37.2 m
Beam	B	= 7.4 m
Draft at stern	T_s	= 2.0 m
Volume displacement	∇	= 319.4 m^3
Block coefficient	C_B	= 0.640
Propeller number	x	= 2
Maximum propeller diameter	D_{max}	= 1.50 m

Main Engines

Type marine spark ignition		Mk CRP 25/34
Power nominal	N_e	= 300 hp
Propeller rpm	n_m	= 300 rpm
Shafting efficiency	η_s	= 0.97

The expression of V.N. Anfimov [2], a modified version of E.E. Papmel's formula for the wake fraction, is used to calculate the total wake fraction for this inland waterway vessel:

$$w = 0.11 + \frac{0.165 C_B^x}{x} \sqrt{\frac{\sqrt[3]{\nabla}}{D}} = 0.18 \tag{5}$$

Here the maximum propeller diameter value $D = 1.50$ m is used.

Propeller Thrust Calculation Without Nozzles:

The thrust deducation factor for twin screw vessel [3] is taken as:

$$t = 0.8\ w(1 + 0.25\ w) = 0.15 \tag{6}$$

The delivered power is:

$$N_p = N_e \eta_s = 291 \text{ metric Hp} \tag{7}$$

The propeller inflow velocity is:

$$V_p = 0.514\ V_s(1 - w) = 2.107 \cong 2.11 \text{ m/s} \tag{8}$$

The K_n'' coefficient is:

$$K_n'' = \frac{V_P}{\sqrt{n}} \sqrt[4]{\frac{\rho V_P}{N_P}} = 0.875 \qquad (9)$$

The maximum advance coefficient $\lambda_{P_{opt}}$ is obtained from Fig. 1.

$$\lambda_{P_{opt}} = f_1 (K_n'') = 0.250 \qquad (10)$$

The optimum propeller diamter is then:

$$D_{opt} = \frac{V_P}{\lambda_{P_{opt}} n} = 1.69 \text{ m} \qquad (11)$$

The maximum diameter in comparison with the optimum diameter is:

$$\frac{D_{max}}{D_{opt}} = 0.892 \qquad (12)$$

From linear interpolation in Fig. 1 between 0.85 D_{opt} and 0.90 D_{opt} the efficiency and pitch-diameter ratio of the propeller are obtained:

$$\eta_P = f_2 (K_n'') = 0.350 \qquad (13)$$

$$H/D = f_3 (K_n'') = 0.85 \qquad (14)$$

The propulsive coefficient is:

$$\eta = \frac{(1-t)}{(1-\omega)} \eta_P = 0.363 \qquad (15)$$

At a speed of 5 knots the total propeller thrust equals.

$$T = 2 \cdot \frac{75\ \eta\ N_P}{0.514\ V_S} = 6162 \text{ kg} \qquad (16)$$

Propeller Thrust Calculation with Nozzles:

For wing/twin propellers the frictional wake is:

$$w_f = 0.6\ w = 0.108 \cong 0.11 \qquad (17)$$

The velocity is:

$$V_e = 0.514\ (1-\omega_f)\ V_s = 2.29 \text{ m/s} \qquad (18)$$

The K_{ne}'' coefficient is calculated:

$$K_{ne}'' = \frac{V_e}{\sqrt{n}} \sqrt[4]{\frac{\rho V_e}{N_P}} = 0.968 \qquad (19)$$

The optimum advance coefficient from Fig. 2 is:

$$\lambda_{e_{opt}} = f_1 (K_{ne}'') = 0.290 \qquad (20)$$

and the optimum propeller diameter is:

$$D_{opt} = \frac{V_e}{(\lambda_e)_{opt}\ n} = 1.58 \text{ m} \qquad (21)$$

The maximum diameter* in comparison with the optimum is:

$$\frac{D_{max}}{D_{opt}} = 0.873 \qquad (22)$$

*(With a nozzle propeller the maximum allowable propeller diameter is reduced by 8% compared to the conventional propeller diameter, so the maximum nozzle propeller diameter is D_{max} = 1.38 m .)

Linear interpolatin between the 0.90 D_{opt} and 0.85 D_{opt} the efficiency and pitch diameter ratio are determined.

$$\eta_e = f_2 (K_{ne}'') = 0.390 \qquad (23)$$

$$H/D = f_3 (K_{ne}'') = 1.16 \qquad (24)$$

At a speed of 5 knots the total nozzle propeller thrust equals:

$$T_n = 2\ \frac{75\ \eta_e\ N_P}{0.514\ V_s} = 7439 \text{ kg} . \qquad (25)$$

The results of the comparison show that using nozzles increase the thrust 20% at 5 knots.

REFERENCES

1. Basin, A.M., Anfimov, V.N., and Mamontov, Yu. N., "Calculation and Design of Inland Waterway Ship Propellers," Trans. T.NIIRF, Vol. XXXVII, 1958.

2. TRANS. T.NIIRF, Vol. XXXVII, 1958.

3. Basin, A.M., Miniovich, I. Ya, Theory and Calculation of Screw Propellers Leningrad, 1963, pp. 143-150. English Translation: "Empirical Formulas for estimating the wake fraction and thrust deduction factors for ocean and inland waterway vessels," in this report.

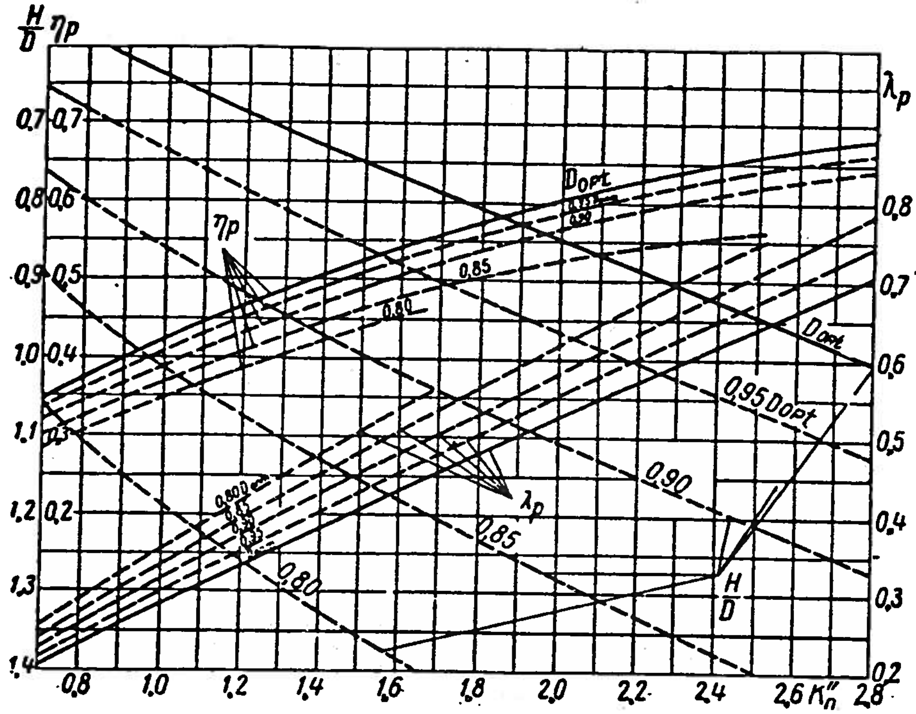

Fig. 1 Diagram for propeller without nozzle
$z = 4$, $Ae/Ao = 0.40$

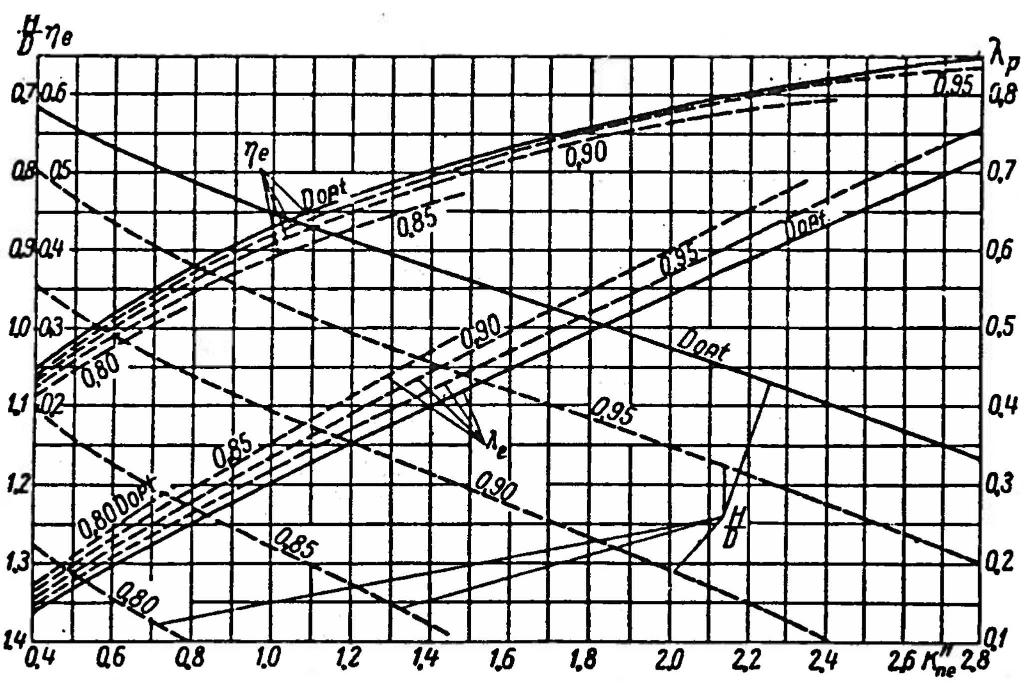

Fig. 2 Diagram for propeller in nozzle (Ducted Propeller)
$z = 4$, $Ae/Ao = 0.55$, $\alpha_e = 1.30$, $\beta_a = 1.10$
$\overline{\ell} = \frac{\ell_n}{D} = 0.5–0.9$

ON THE PROPELLER DESIGN POINT OF DIESEL-POWERED SHIPS[1]

BY

W. JIANG[2]

C. CUI[2]

ABSTRACT

This paper gives a description of power-margin, revolution margin and resistance-margin to be considered during the design of the propeller. With a single-screw cargo carrier and a twin-screw passenger-cargo ship as illustrated examples, it infers that these margins are common in nature but not equivalent in the percentages taken. The paper emphasizes the main factors to be considered when determining the margin and the relation between P-margin and R-margin. A P-n-V diagram is proposed for a further understanding of the problem of matching propeller and engine.

TRANSLATION[3]

1. Introduction

In the design of a ship we first determine the principal ship dimensions, the hull lines, and the main engine and then select a propeller to match the hull and engine. As the hull resistance changes the hull, propeller, and engine will reach a new equilibrium point which depends on the original propeller design point.

The curve A-A' in Fig. 1 (power vs. rpm) represents the theoretical propeller curve which is a cubic parabola passing through 100% power (P_0) and 100% rpm, n_0:

$$P = P_0 \left[\frac{n}{n_0}\right]^3$$

The region to the right of A-A' is the acceptable power-rpm domain for continous engine operation (region A). The design point is point A in Fig. 1 when the propeller absorbs 100% power P_0 at 100% rpm n_0 with the ship at full load condition. However, the propeller becomes "heavier" to drive when the hull resistance increases from hull fouling or a worsening sea state, so the operating point gradually moves from point A to point B (fuel rack position remaining unchanged) causing a reduction in engine power and rpm. With turbocharged diesel engines, the decreased rpm reduces the exhaust gas mass flow and pressure which reduces the exhaust gas turbine power. At the reduced turbocharger output there is a lower scavenging air pressure and a decrease in the turbocharger's scavenging effect. While the engine power and rpm are reduced, the thermal load of the engine increases because of the constant amount of fuel injected during each piston cycle. This is unacceptable from the maintenance viewpoint. For this reason some engine manufacturers permit their engines to be run only intermittently in the region on the left side of curve A-A' between the torque limit and propeller characteristic curves (region B).

If a margin is adopted so the design point is a point C, the engine operational point will move along curve C-C' at full load conditions with calm weather and clean hull and the propeller is "easier" to drive. When the propeller loading increases, the operating point moves from C to A (engine regulated by governor) or to point A_1 (without engine governor and fuel rack position fixed) so the engine is not overloaded. Consequently curve A-A' can be regarded as a full load service curve for the ship operating in high sea-states with a fouled hull.

It can be pointed out that the design point for the propellers of some ships were taken at 100% power and 100% rpm and these ships did not experience any trouble in service. The reasons for this may be:

1) A margin was added in calculating the propeller thrust power, resulting in the actual propeller operates on curve CC' below curve A-A'.

2) The diesel engine power and turbocharger pressure were moderate in the past so the thermal load was not high and the engines could run in the region B below the engine power curves.

Recently both turbocharging pressure and thermal load have increased and engine manufacturers have specified that their engines can be run only intermittenly in region B. At the same time, ship resistance estimates are more accurate, approaching the actual

---

[1] Transactions of Chinese Society of Naval Architecture and Marine Engineering, No. 74, July, 1981, pp. 23-33.

[2] The Shanghai Merchant Ship Design and Research Institute.

[3] Translated by Mr. Tang Kezhang, Associate Professor, Dalian Marine College, Visiting Scholar from P.R. China.

value, so there is a very small resistance margin (if any) in the design of propellers. Consequently if we should use 100% power and 100% rpm as the propeller design point, the engine will run along curve A-A' during the sea trials and then as the propeller load increased trouble will appear. It is known that after vessels have been operating, troubles with main engine overloading due to driving the ship with "heavier" propellers, required cutting down the propeller blade radius. Hence, the old subject of hull, propeller and engine matching is now being given increased attention by naval architects and marine engineers. This paper gives a discussion on choice of the propeller design point and presents examples using a single-screw bulk carrier and a twin-screw cargo-passenger vessel.

2. P-Margin, n-Margin and R-Margin

Following the above discussion, some degree of margin must be adopted in designing the propeller. Three margines usually adopted are described below:

a) Power Margin (P-Margin): For the propeller design point choose a certain percentage (i.e.: 90%) of the manufacturers rated power, 100% rated rpm, and hull resistance corresponding to full load trial conditions with clean hull. Point C shown in Fig. 1 .

b) RPM Margin (n-Margin): For the propeller design point choose 100% manufacturer's rated power, an increased rpm (i.e.: 103%) and hull resistance corresponding to full load trial conditions with clean hull. Point D shown in Fig. 1.

c) Resistance Margin (R-Margin): For the propeller design point choose 100% manufacturer's rated power, 100% rated rpm, and hull resistance corresponding to full load conditions in heavy seas with a fouled hull. For example, choose 120% of the hull resistance corresponding to full load trial conditions in calm weather with a clean hull. Curve A-A' in Fig. 1 represents the anticipated full load service condition. The actual curve during the sea trial with the new vessel will fall below curve A-A'.

Although these methods appear to be different, their meanings are the same, namely to ensure the propeller is "easy" to drive during the sea trials and the main diesel engine will not be overloaded in service or during operation in heavy seas. Naturally if a margin is adopted in the propeller design, the engine must overspeed to be produce the 100% rated engine power. In addition to these three methods, some designers adopt added resistance and reduce the power at 100% rated rpm when determining the propeller design; and some designers have the propeller design on a "zero margin" condition (100% rated power, 100% rated rpm, 100% hull resistance of new ship) then make empirical corrections to the propeller design based on their experience. These last two methods will not be treated in this paper.

For illustration two design examples will be used. A single-screw bulk carrier (max continuous power, MCR = 12,000 BHP at 122 rpm) and a cargo-passenger ship (max continuous power MCR = 2 x 5,200 BHP at 148.5 rpm). The propeller designs are based on the Japanese AU Propeller Charts for these vessels with three different margins described above. The propeller design results for these different design conditions are summarized in Tables 1 and 2. For comparison the results calculated with zero margin are included in the tables.

In Tables 1 and 2 100% P denotes maximum continuous power and 100% n denotes maximum continuous rpm (MCR condition). These examples give rise to the question of what would happen if the propeller design condition is taken as the normal service power and normal service rpm (NOP condition). It can be shown with either the MCR or NOP condition the propeller designs will be the same provided the ship resistance is proportioned to V^2, the propulsions factors remain within a given range, and the same margins is used. If the resistance is not proportional to V^2 there will be some difference. But it is very small as shown below:

Assume $R_1/R_2 = (V_1/V_2)^{\alpha}$

$$P_1/P_2 = (V_1/V_2)^{\alpha+1}$$

Where subcript 1 denotes the MCR condition and subscript 2 denotes the NOP condition so:

$$(n_1/n_2)^3 = P_1/P_2$$

$$B_p = \frac{n\sqrt{P}}{V_a^{2.5}}$$

and

$$\frac{B_{P_1}}{B_{P_2}} = \frac{n_1}{n_2}\sqrt{\frac{P_1}{P_2}}\left(\frac{V_2}{V_1}\right)^{2.5} = \left(\frac{P_1}{P_2}\right)^{\frac{5(\alpha-2)}{6(\alpha+1)}}$$

$$\delta = \frac{nD}{V_a}$$

$$\frac{D_2}{D_1} = \frac{\delta_2 V_2}{n_2}\Big/\frac{\delta_1 V_1}{n_1} = \frac{\delta_2}{\delta_1}\left(P_1/P_2\right)^{\frac{\alpha-2}{3(\alpha+1)}}$$

when $\alpha=2$, the hull resistance is proportional to the squre of the speed.

Then $\alpha-2=0$ but $\alpha+1\neq 0$

so $B_{P_1} = B_{P_2}$

$$\delta_1 = \delta_2$$

TABLE 1 Parameters of Propeller Design Single-Screw Bulk Carrier (12,000 BHP MCR, 122 rpm)

No.	Design Method	Design Condition Power P	rpm n	Resist. R	Dia. m	Pitch Ratio P/D	Disc Area Ratio A_e/A_0	Open Water Efficiency η_0
1	O Margin	100%	100%	100%	5.43	0.881	70%	56.5%
2	P Margin	90%	100%	100%	5.31	0.881	74.3%	55.4%
3	n Margin	100%	103.5%	100%	5.28	0.883	70%	55.1%
4	R Margin	100%	100%	110%	5.43	0.870	73%	55%
5	R Margin	100%	100%	115%	5.43	0.865	75%	54.6%
6	R Margin	100%	100%	120%	5.43	0.860	77%	54.3%

TABLE 2 Parameters of Propeller Design Twin Screw Cargo-Passenger Vessel (2 x 5200 BHP MCR at 148.5 rpm)

No.	Design Method	Design Condition Power P	rpm n	Resist. R	Dia. m	Pitch Ratio P/D	Disc Area Ratio A_e/A_0	Open Water Efficiency η_0
1	O Margin	100%	100%	100%	3.85	1.31	61%	73.6%
2	P Margin	90%	100%	100%	3.73	1.30	66%	72%
3	n Margin	100%	103.5%	100%	3.75	1.30	64%	72.3%
4	R Margin	100%	100%	110%	3.85	1.28	66%	72%
5	R Margin	100%	100%	115%	3.85	1.26	67%	71.5%
6	R Margin	100%	100%	120%	3.85	1.23	70%	71.1%

TABLE 3 Comparison of Propeller Designs

Design/Condition	Diameter D m	Pitch/Dia P/D -	Disc Area A_e/A_0 -	Open Water Eff. η_0
P Margin, MCR Base	5.31	0.881	74.3%	55.4%
P Margin, NOP Base	5.34	0.881	71.7%	56.7%

$D_1 = D_2$ H = Propeller Pitch, m

$H_1/D_1 = H_2/D_2$ D = Propeller Diameter, m

i.e. these two propellers are identical when $\alpha>2$

$B_{P_1} > B_{P_2}$ $\eta_2 > \eta_1$

$\delta_2 < \delta_1$ so $D_2 \approx D_1$

when $\alpha<2$

$B_{P_1} < B_{P_2}$ $\eta_2 < \eta_1$

$\delta_2 > \delta_k$ so $D_2 \cong D_1$

For illustration propeller No. 2 in Table 1 is taken as an example. If the NOP = 85% MCR, then the rpm at NOP is 100 x $(0.85)^{1/3}$ = 94.7% of the MCR rpm. If a 10% P margin is adopted then the design conditions are taken as 90% x 85% P - 94.7%n - 100%R. The propeller designed using these conditions is compared with the propeller designed on the MCR in Table 3. At the same time we obtained a propeller design based on the NOP condition which has an open water efficiency η=55.3% when it operates at its MCR. Also if the propeller design is based on the MCR condition, its open water efficiency η_0=56.2% when operating at the NOP. On the whole these two propellers are equivalent.

Thus it can be seen the propellers obtained from adopting the MCR or the NOP as the design base are generally the same provided the same margin is applied. Similarly if we choose the design point at 100% NOP and 100% rpm then the design will be a zero margin propeller, rather than a P margin design.

3. Equivalence of Margins

From the previous example it was shown that a propeller designed with a margin will be different from a propeller designed without margins or zero margin. However, when a margin is adopted say 10% P margin (Design Condition 90% P, 100% n, 100% R and 10% R margin (100% P, 100% h 110% R)) will result in a different design. This means that propellers designed with 10% P maraın are not equivalent to propellers designed with 10% R margin.

It is easy to determine the relation between a propeller with a margin (i.e. P margin) and the zero margin propeller. Let subscript 1 denote the zero margin and subscript 2 denote the P margin propeller for the same rpm $n_1=n_2$:

$$\frac{B_{P_1}}{B_{P_2}} = \frac{n_1}{n_2}\sqrt{\frac{P_1}{P_2}}\left(\frac{V_2}{V_1}\right)^{2.5} = \left(\frac{P_1}{P_2}\right)^{\frac{\alpha-4}{2(\alpha+1)}}$$

$$\frac{D_1}{D_2} = \frac{\delta_1}{\delta_2}\quad\frac{P_1}{P_2}\quad\frac{1}{\alpha+1}$$

a. Assuming α=4, then

$B_{P_1} \neq B_{P_2} = 1$, $\delta_2 = \delta_1$, $\eta_2 = \eta_1$ $H_2/D_2 = H_1/D_1$

But D_1D_2 $(P_1/P_2)^{1/5}$

Assume 10% P margin (P_2=0.9P), then D_1= 1.021D_2

Assume 15% P margin ($P_2 \approx 0.85P_1$), then D_1= 1.033D_2

This shows that the larger the margin adopted becomes, the greater the difference in diameter.

b. Assuming $\alpha \neq 4$

If 10% P margin is chosen, the ratio of B_P and the ratio of diameters are tabulated as a function of α in Table 4.

when $\alpha<4$ $B_{P_1} < B_{P_2}$, $\eta_2 < \eta_1$, $\delta_2 < \delta_1$, $H_1/D_1 > H_2D_2$

when $\alpha>4$, the conclusions are reversed.

No matter which value of α is selected the propeller diameter appears as $D_1 > D_2$. Similarity the large the P margin, the larger the difference between D_1 and D_2. This is related to the resistance curve form with the difference being larger when α is smaller.

The influence of the P margin, n margin, and R margin, on the propeller designs are illustrated in Tables 1 and 2. From these tables it can be understood that a propeller with 10% P margin is equivalent to a propeller with a 3.5% n margin. This is because P_1/P_2 is approximately equal to $(n_1/n_2)^3$. The following discussed the equivalent relation between the P margin and R margin.

The P margin insures that the engine will not be overloaded when the engine power increases with 10% due to hull fouling and sea conditions. While the 10% R margin insures the engine will not be overloaded when the resistance increase 10%, considering the speed, propeller and engine rpm, the increase in power will not be 10%. For example, assume the original speed is V_1 and original resistance at this speed is R_1. If the resistance increases 10% due to operation in rough weather, the speed will decrease ΔV if the rpm is kept constant while the resistance must be 110% of the resistance at $(V_1-\Delta V)$. If the open water propeller efficiency and propulsive factors are assumed constant, then the increment in power must be less than 10% the original power. The relationship between engine power, propeller rpm and torque as a function of speed have been derived in detail by R. Dien and H. Schwancke [5]. We continue our discussion about the three relationships. We assume that:

a. The speed-resistance relationship is $R \alpha V^{\alpha}$

b. The rate of change in resistance is the same as the rate of change in thrust at the same speed

$$\Delta T/T = \Delta R/R$$

c. The rate of the rpm change is equal to of the speed change i.e. wake factor is constant.

d. Higher order terms can be neglected because the resistance change is small.

Table 5 is for the single-screw bulk carrier used earlier with the no. 2 propeller design in Table 1.

I) $\Delta n=0$ Rpm Constant when Resistance Increases

With a trial speed V=16.23 knots and the resistance increase $\Delta R/R$ = 10%, the rate of change in power $\Delta P/P$, speed $\Delta V/V$ and torque $\Delta Q/Q$ as a function of the exponent α are summarized in Table 5.

Thus if there is a 10% resistance increase with the rpm remaining constant, the required power will increase about 2% and the speed will decrease about 2.5%. For the twin screw cargo-passenger ship the required power will increase 4.5% and the speed will decrease about 2.5%.

II) $\Delta V=0$ Speed Constant when Resistance Increases

Assuming that $\Delta R/R$ = 10% we obtain the following changes in percent which are independent of the value of the exponent α:

	Single Screw Bulk Carrier	Twin Screw Cargo -Passenger Ship
$\Delta P/P$	12.44	11.07
$\Delta Q/Q$	9.11	8.8
$\Delta n/n$	3.32	2.28

III) $\Delta P=0$ Engine Power Constant when Resistance Increases

The results obtained are summarized in Table 6. Table 6 shows that if the engine power is kept constant, and the resistance increases 10%, the speed decreased about 3%, the rpm decreases about 0.5% while the torque increases 0.5%. For a twin screw cargo passenger ship the speed decreases 4.5% and rpm decreases 1.7%

IV) $\Delta Q=0$ Torque Constant When Resistance Increases

The results obtained are summarized in Table 7. Table 7 shows that if the torque is kept constant and the resistance increases 10% the speed decrease is about 3% with the power and rpm decrease about 1%. For the twin screw cargo-passenger vessel the speed decrease is 5.7% with the power and rpm decrease 2.7%.

The test results from the self propulsion tests of the single screw bulk carrier model are the same as the results obtained from these calculations.

From the preceeding calculations we know that:

a. When the resistance increases while keeping the speed constant, the speed will decrease and the torque will increase. $\Delta P/P<\Delta R/R$.

b. When the resistance increases while keeping the speed constant, the rpm will increase and the torque will increase, while $\Delta P/P>\Delta R/R$.

c. When the resistance increases while keeping the torque constant, the speed and rpm decrease and $\Delta P/P<0$.

d. When the resistance increases while keeping the engine power constant, the speed and rpm will decrease while torque will decrease.

e. When either the rpm, the torque, or the power is kept constant, the speed decreases with increased resistance. The speed decrease is smallest when the rpm is constant, and the power and torque increase. When torque is kept constant, the speed decrease is largest and the power and rpm decrease.

Consequently, a 10% P margin is not equivalent to a 10% R margin. This is the reason why the propeller designs no. 2 and no. 4 in Tables 1 and 2 are not identical. It can also be proved that when the rpm is kept constant, $\Delta P/P$ is always less than $\Delta R/R$ for any type of ship.

Assume that the open-water screw characteristic curve K_J-J and K_Q-J are linearized as shown in Fig. 2.

from [5]: $\dfrac{\Delta P}{P} = \dfrac{-E_Q}{\alpha - E_T} \dfrac{\Delta R}{R}$

where $E_T = \dfrac{dK_T}{dJ} \dfrac{J}{K_T}$, $E_Q = \dfrac{dK_Q}{dJ} \dfrac{J}{K_Q}$

from Fig. 2

$$\frac{dK_T}{dJ} = \frac{-K_T}{a} , \quad \frac{dK_Q}{dJ} = \frac{-K_Q}{b}$$

$$\frac{E_T}{E_Q} = \frac{dK_T}{dJ} K_Q \Big/ \frac{dK_Q}{dJ} K_T = \frac{K_T}{a} \cdot \frac{b}{K_T} \cdot \frac{K_Q}{K_T} = \frac{b}{a}$$

since b>a (Fig. 2)

TABLE 4 Influence of α on B_P and D

α	1.5	2	2.5	3	3.5	4	4.5
B_{P_1}/B_{P_2}	0.949	0.966	0.978	0.987	0.995	1	1.005
D_1/D_2	1.043	1.036	1.031	1.027	1.024	1.021	1.019

TABLE 5 Percent Change in ΔP/P, ΔV/V and ΔQ/Q at ΔR/R = 10% (Δn=0)

α	2	2.5	3	3.5	4
ΔP/P	2.48	2.13	1.86	1.66	1.49
ΔV/V	-3.32	-2.85	-2.49	-2.22	-2.00
ΔQ/Q	2.48	2.13	1.86	1.66	1.49

TABLE 6 Percent Change in Δn/n, ΔV/V and ΔQ/Q at ΔR/R = 10% (ΔP=0)

α	2	2.5	3	3.5	4
Δn/n	-0.86	-0.69	-0.58	-0.51	-0.45
ΔV/V	-4.16	-3.44	-2.92	-2.56	-2.25
ΔQ/Q	0.86	0.69	0.58	0.51	0.45

TABLE 7 Percent Change in ΔP/P, Δn/n, ΔV/V at ΔR/R = 10% (ΔQ=0)

α	2	2.5	3	3.5	4
ΔP/P	-1.24	-1.01	-0.85	-0.74	-0.65
Δn/n	-1.24	-1.01	-0.85	-0.74	-0.65
ΔV/V	-4.85	-3.73	-3.15	-2.72	-2.39

$E_T / E_Q > 1$

$$\frac{\Delta P}{P} = \frac{-E_Q}{\alpha - E_T} \cdot \frac{\Delta R}{R} = K \frac{\Delta R}{R}$$

$$K = \frac{-E_Q}{\alpha - E_T} = \frac{E_Q}{E_T - \alpha} = \frac{1}{E_T/E_Q - \alpha/E_Q}$$

so $E_T/E_Q > 1$ and $\alpha > 0$ $E_Q < 0$

$0 < K < 1$

4. Allowable Engine Operation Range and Operation

4a. Allowable Operation of Specific Diesel Engines

As mentioned in section 1, the running of an engine in region B of Fig. 1 is related to the engine type especially the scavenging arrangement (uniflow or cross flow), turbocharger (pulse or constant pressure), turbocharger pressure ratio and the engine thermal load. In general, the operating range of diesel engines with pulse turbocharging and uniflow scavenging is larger than that of diesel engines with constant pressure turbocharging and cross flow scavenging but the operational range in region B of Fig. 1 decreases as the thermal load is increased.

The diesel engine manufacturerers set a strict limit on the engine's operation range. This gives reliable information for use in propeller design. For example, RNDM and RLA Sulzer diesels are only allowed to run in region B for 2000 hours while the K/L-GFC and K/L-GFCA B&W diesels can run continuously in the area of A'Aab in region B of Fig. 3. The allowable operating range of the KSZ-B/BL and SEMT-Pielstick is similar to the B&W K/L-GFCA's operating range.

4b. Effects of Operation Mode on the Propeller Operation

A. The case of the vessel operating in the region below the theoretical propeller curve A'A in Fig. 3 shows that if the engine is run at point 0 on the curve CC' then the engine will run along the curve EE' after the resistance is increased by bottom fouling or entering into shallow water. Then:

1. When the engine governor is used, the rpm is kept nearly constant. The regulating process is shown on line ON and the engine finally operates at point N. This is the $\Delta n=0$ regulating method.

2. When the engine governor is not used and the fuel rack position is kept constant the amount of fuel injected during each piston cycle remains constant and the torque remains constant. The regulating process is shown as 0Q and the engine operating point is Q. This is the $\Delta Q=0$ regulating method.

3. If as the rpm decreases due to increased resistance and the fuel rack is set so that the product of the rpm times the amount of fuel injected per revolution remains constant so the power constant, then the regualting process is shown as OP and the engine operates a point P. This is the $\Delta P=0$ regulating method.

B. The case of the ship operating in the region above the propulsion curve (when the ship has severe hull fouling, operating in shallow water or during an emergency turn) the engine will operate along the F-F' curve and enter region B, then:

1. For high powered diesels with an engine governor which limits the torque, fuel injection or turbocharger air pressure, their operation condition is as follows:

Assume that the original engine operating point is 0 and the rpm is nearly constant. As the resistance increases, the amount of fuel injected and the power increase ($\Delta n=0$ regulating method). When the power gradually increases as the fuel charge increases, and the oeprating point meets the fuel limiter setting for turbocharger pressure WX, but decrease along the WX curve until it intersects the FF' curve at point S_1 to reach the equilibrium point. Consequently, the operation process is OS, and the engine runs as point S_1.

If the engine governer is equipped with a torque limiter, the amount of fuel injected per revolution increases until the power increases and reaches the setting of the torque limiter AYZ, then it decreases along AYZ until it reaches its Equilibrium position at point N_1 where it intersects the FF' curve. Consequently the operating process is N_1 and the engine runs at point N_1.

If the governor controls the engine along the fuel limiter i.e. curve CM then the engine runs at point N_1."

2. If the engine is not equipped with a governor, the operating process of main-

taining a constant amount of fuel injection is $0Q_1$ and the engine runs at point Q_1. This is the $\Delta Q=0$ regulating method. The operating process of maintaining a constant value of (fuel injected x rpm) is $0P_1$ and the engine operating at point P_1. This is the $\Delta P=0$ regulating method.

In the above mentioned operating processes, the power is kept constant or decreases in the processes described by 0P, $0P_1$, 0Q, $0Q_1$ and $0S_1$. In the processes described by 0N, $0N_1$, $0N_1'$, and $0N_1''$ the power increases, but the power increment ($\Delta P/P$) is less than the resistance increment ($\Delta R/R$). Therefore, if the ship speed must be maintained when the resistance increases, the rpm must be increased so the operation process is 0V. In this case the $\Delta P/P > \Delta R/R$ the required power rapidly increases and this may lead to engine overloading so the operating process 0V is normally not used in practice.

5. Major factors influencing the margin and the P-n-V chart

The main factors influencing the margin are the type of ship, engine, ship speed and the weather conditions. The same margin cannot be adopted for different ships. If the margin adopted is too large, the engine power will not be fully developed. When the margin adopted is too small, the engine is unable to develop the power required by the increased load. Thus the required ship speed and the engine life are affected by the margin.

The P margin adopted should be different for each ship type, engine type, and ship speed even though the hull fouling and weather conditions are the same ($\Delta R/R$ are the same). The actual power margin for example of a single screw bulk carrier with a 10% P margin is larger than the actual power margin for a twin screw cargo passanger ship with a 15% P Margin. When a 10% P margin is applied, the resulting propeller margins are larger than those resulting when the 25% R margin is adopted so the bulk carrier design has a 10% P margin.

What then is a suitable value of the margin for the propeller? The answer to this question can be obtained from statistical information of the ship service. We recommend that for every vessel a P-n-V chart be prepared (Fig. 4). To construct this figure, first the range of allowable engine operating condition should be determined and a P-n curve plotted according to the engine characteristic. Then the power, rpm, and speed measured at the ship delivery trials is then plotted as P-n and P-V curves (the two curves denoted by 'a' in Fig. 4.) From these curves the engine operating point can be checked.

a. If a curve run through the design operating point already chosen, then the previous assumed conditions agree with the actual service condition.

b. If the design operating point lies below curve a the figure indicates the resistance estimated for the design is less than the actual value and the propeller is "heavier" to drive than the design estimate.

c. If the design operating point lies above curve a there is some margin in the estimation of the vessel resistance.

The power data, rpm and speed data can be plotted on this figure to obtain curves such as curve b,c, ... in Fig. 4 so that the margin adopted in $\Delta P/P$, $\Delta n/n$, and $\Delta V/V$ etc can be measured over the ship operational life.

6. Conclusions

1. In the design of propellers a margin is required either a P margin, n margin or R margin can be adopted. However, the propeller designed with a 10% P margin is not equivalent to a propeller designed with a 10% R margin. The actual margin of the 10% P is often larger than that of the 10% R.

2. The margin size adopted is not fixed but depends on ship type, engine type, and ship speed. In general a 10% P margin is sufficient. A 5% P margin could be considered adequate for coastal vessels operating in coastal waters and rivers.

3. If either the MCR or NOP condition is used for the design basis the propeller design is equivalent if the same margins are adopted.

4. It is recommended that with each ship a P-n-V chart be prepared to estimate the $\Delta R/R$, $\Delta P/P$, $\Delta n/n$ and $\Delta Q/Q$ while the ship is operating in order to select a suitable operating point for the propeller design.

5. When the ship hull, engine, and propeller are considered as system components, the adoption of P margin in the propeller design is straight forward concept compared to using the R margin.

7. References

1. Smit, J.A., "Considerations on Propeller Layout from the Engine Builder's Point of View," Proceedings TRANS IESS Vol. III No. 6, 1967-68.

2. "The Economics of Machinery and Propeller Selection," The Motor Ship Vol. 50, No. 589, 1969.

3. Yamada, T., Tanaka, T., Masuda, K., "Problem Point in the Large Bore IHI Sulzer diesels and their Prevention," Ishikawa-harima Giho, No. 4 (Shipbuilding issue) 1970 (In Japanese).

4. Sugimura, Y., "Sea Margin and Propeller Design," Bulletin of Japan Society of Marine Engineers Nos. 7, 9, 1972 (In Japanese).

5. Dien, R., Schwaneke, H., "Die Propeller bedingte Wechselwirkung Zwischen, Schiff and Maschine-Teil 1," MT7, Vol. 34, No. 11, 1973.

6. Giblon, R.P., "Service Margins and Power Plant Selection," Proceedings STAR ALPHA, SNAME 1975.

7. Yen Zikuan, "Power Matching of Marine Diesel Engines and Propellers," Scientific and Technical Reports of Shanghai Jiaotung University No. 1, 1975.

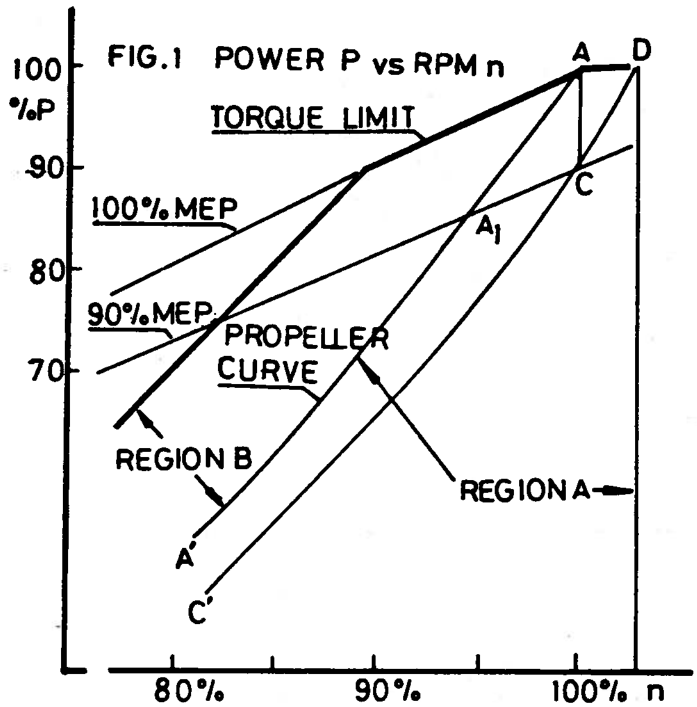

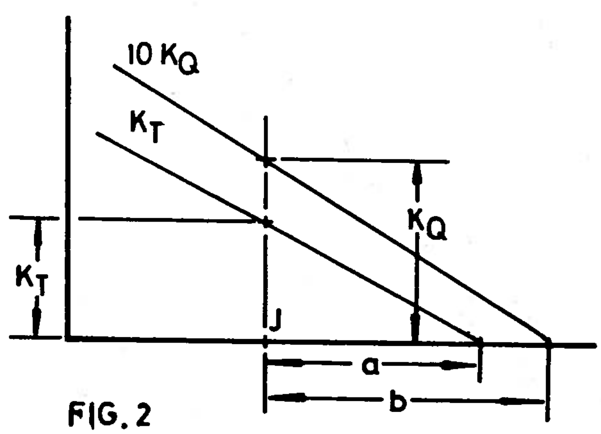

FIG. 2

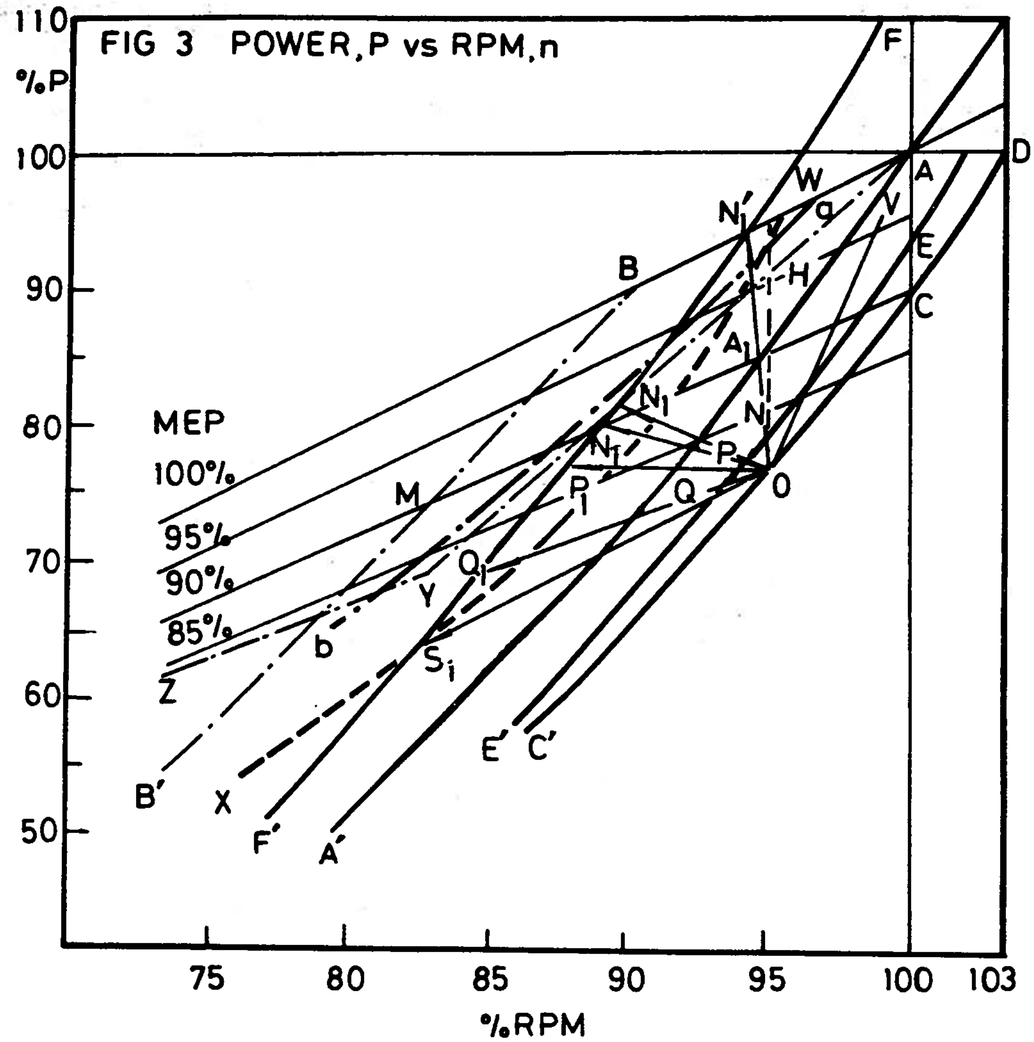
FIG 3 POWER, P vs RPM, n
110
%P
100
90
80
70
60
50
MEP
100%
95%
90%
85%
F
D
A
W
a
V
N1'
H
E
B
C
A1
N1
N1
N1
P
O
M
P1
Q
Q1
Y
b
S1
Z
E'
C'
B'
X
F'
A'
75
80
85
90
95
100
103
%RPM

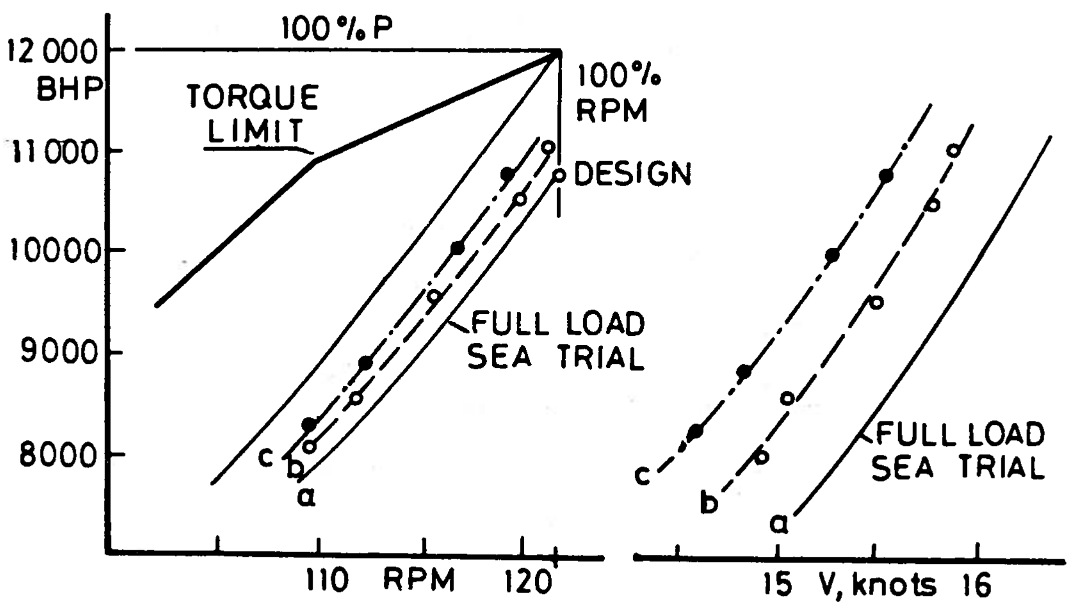
100% P
12 000
BHP
TORQUE
LIMIT
100%
RPM
11 000
DESIGN
10000
FULL LOAD
SEA TRIAL
9000
8000
c
b
a
110
RPM
120
FULL LOAD
SEA TRIAL
c
b
a
15
V, knots
16

FIG 4

STEERING EQUIPMENT OF INLAND WATERWAY VESSELS

BY

M.G. SHMAKOV

ABSTRACT

This article reviews the development of Soviet inland waterway steering units. The movable nozzle rudder has been widely adopted and found to improve the vessel's maneuverability. The applications of different types of steering machinery is discussed as well as the development of improved steering units. The article closes with a discussion of the rudder stock manufacture. [TRANSLATOR]

TRANSLATION[2]

Reliable steering gear operation ensures safe vessel maneuvering. Therefore the steering systems have strict design requirements. This article concerns steering gear problems, (nozzle rudder), steering motor, protection of rudder stock from corrosion and the casting, forging, and welding technology used in rudder stock production. Inland waterway - ocean vessels utilize steering gears with conventional rudders or movable nozzle rudders (or both combined in a steering unit). The nozzle rudders are preferred. Rudders with nozzle rudders have been used as optional equipment.

In Fig. 1 diagrams of steering systems utilized on both Soviet inland waterway and inland sea vessels. The first two types (Figs. 1-a, 1-b) are utilized on inland waterway vessels. The next type (Fig. 1-c) was tested but failed to keep the river vessel on course. The effectives of the nozzle-rudder was increased by fitting a skeg (Fig. 1-d). Operation with this system on the first of 300 HP pushboats had good results. The nozzle rudder with a turnable skeg was a failure and was used only with the KRASNOE SORMOVO-type tugboat. Consequently, the first and fourth types (Figs. 1-a, 1-d) of this five steering system are extensively used. The system in Fig. 1-d is recommended for new single-screw inland waterway vessels. One or two skegs fitted off center allow the removal of the propeller afloat. This system underwent extensive operational testing and showed itself very practical in comparison to the other types. Rudders can be used but they are less effective compared with nozzle rudders for vessel steerability.

The following steering designs may be considered for twin screw vessels. The inland waterway-ocean vessels OLEG KOSHEVOI, INZENER A. PUSTOSHKIN, INZENER BELOV, KISHINEV, TIKSI, and other vessels (Figs. 2-4) utilize a centerline rudder (Fig. 1-f). This arrangement on vessels docking at landings without facilities and vessels operating in ince protect the rudder from damage.

The next system (Fig. 1-g) using two rudders each aft of a propeller has been utilized effectively on numerous inland waterway vessels. The 1200 HP pushboat LYUBLIN utilizes the steering system in Fig. 1-h. However, in service the vessel's maneuverability was reduced by not having nozzle rudders. Therefore, the inland waterway tanker VELIKIY was fitted with the steering gear shown in Fig. 1-i. The next type (Fig. 1-j) was also fitted to inland waterway vessels yet did not become popular.

The initial 800, 1200, and 1300 HP pushboats, the initial VOLGO-DON cargo vessels, and numerous other inland waterway vessels have been fitted with the steering system shown in Fig. 1-k.

The next system (Fig. 1-l) was fitted on the inland waterway-sea cargo 50 LET SOVETSKOI VLASTI and BASKIRIYA vessels. It resulted in good maneuverability.

Two nozzle rudders with fixed skegs (Fig. 1-m) were installed on the second and subsequent series of VOLGO-DON cargo vessels, the XXIII SYEZD KPSS vessels, and other inland waterway vessels (Fig. 5). The nozzle rudders can be controlled individually or both rudders operated synchronized. To allow propeller removal afloat, it is suggested the skegs be offset. An electro-hydraulic ram type unit can replace the quadrant type steering gear. This system utilizes individual nozzle-rudder control and is designed for mass-production.

Among the twin screw steering systems considered, better ship maneuverability is obtained by the last unit (Fig. 1-m). It is utilized widely and recommended for both inland waterway and inland waterway-ocean vessels.

Inland waterway vessels operating in ice should be fitted with conventional or

---

[1] SUDOSTROENIYE, No. 5, May, 1973 pp. 21-27.

[2] Translated by Robert Latorre, Department of Naval Architecture and Marine Engineering, University of Michigan.

rudder nozzles. The efficiency of the rudder nozzles is supported by actual operation of 800 HP push boats utilized in moving vessels in frozen conditions. Nonmovable stationary nozzle rudders are not recommended because ice collects on them. The utilization of nozzle rudders rather than conventional rudders contributes to the thrust and towing characteristics of the vessel. Also the nozzle rudders contribute to a lower degree of pitching motion which allows a smoother propulsion plant operation. The individual control of the nozzle rudders improve the maneuverability in operation as well as when drifting with the engines off. Nozzle rudders are widely utilized for most inland waterway ships presently being constructed.

The L and R class of inland waterway vessels have low capacity power plants and utilize manual steering with steering cables and rigid shaft gearing. Recently constructed vessels have utilized manually operated rudders. This can be utilized only if the tiller force does not exceed 12 kg-f and the number of turns of the steering wheel from port to starboard is not more than 25. Electro-hydraulic steering units are used on the recently constructed O and M classes of inland waterway-ocean vessels.

Quadrant-type electric steering motors were installed on the 800, 1200, and 1300 HP pushboats, the cargo vessel VOLGO-DON and the river ships XXIII KPSS, the inland waterway-ocean vessels BALTIYSKY, VOLGO-BALT and the OLEG KOSHEVOY-class as well as car ferries and other series built vessels. This quadrant type electric unit was widely utilized in the 1940's-1950's because of its easy maintenance, design simplicity and and compactness. At that time, the steering systems included single quadrant type units using direct drive or reduction gearing and had an auxilary manually operated gear. These systems also included single engines without gearing (car ferries), geared auxiliary electric drivers, as well as dual systems consisting of two steering motors with an auxiliary electric motor. Their reliability is shown by their long-term serive record (10 years of operation with no repairs). The steering engine merits are of considerable importance for small vessels with small crews and of even greater importance for vessels in long term or continuous operation in tropical areas.

Improvement and development of new steering systems was delayed by the limited variety of steering gear and the (in the early 1960's) use of only electro hydraulic systems on new vessels. It is considered to be impractical to replace certain steering engines with a new type and use only a specified type of machinery, for instance, the ram-type on all vessels being built. This is supported by the fact that besides the ram type machinery only hydraulic machinery with tilting cylinders has gained acceptance.

In view of this, it is useful to continue the quadrant-type electric steering gear development and define its application. It appears that single quadrant-type electric machinery must be manufactured for torque loads of 630 to 16,000 kg-m and twin units for 2 x 1600 to 2 x 10,000 kg-m. This steering machinery is required for both electric and hydraulic systems fitted on inland waterway-ocean vessels. With quadrant type steering gear, it should be acknowledged that every case will not require such complex electrohydraulic drives. There is also a need for steering gear with operational reliability and simplicity in design. Many inland waterway-ocean vessels have been fitted with the electrohydraulic ram-type steering units. This has become the basic equipment in domestic vessel construction. Inland waterway and inland waterway-ocean vessels use a steering unit which makes it possible for the rudder to travel ±35° in less than 28 seconds with a 630-16,000 kg-m rudder stock torque. Electro-hydraulic ram type engines have greater efficiency in comparison to quadrant type electric units. With these units it is easier to adopt larger gear ratios which allow silent and smooth speed changes while producing large forces and torque relative to their small dimensions and weight. These advantages have been the determining factor for utilizing ram-type units on present vessels. Hydraulic steering units with the tilting cylinders (manually operated and with drive pumps) are widely utilized by hydrofoil and surface effect vessels. They have been operationally tested for reliability. These units design provides 100-630 kg-m rudders stock torque and a ±35° rudder angle in 15 seconds. They can be used on other small displacement vessels obtaining a ±35° rudder angle in 28 seconds. Table 1 provides steering system data for units recommended for inland waterway-ocean vessels under design and construction.

The continuing problem of steering system improvement for inland waterway and inland waterway-ocean vessels is mainly the improvement of available steering gears and the development of new types having ease in their maintenance, simple and compact design; moderate price and good arrangement. From this, these units would include electro-hydraulic vane-type steering units. These units while having merits, have drawbacks:

- The vane gear must be disassembled to its rudder stock in order to repair seals during operation.
- The engine must be mass produced to achieve moderate cost.

In regards to improvement of existing steering systems and manufacture of new types, consideration must be given to:

Time to turn rudder through a ±35° angle should be less than 28 seconds on inland waterway-ocean vessels and 30 seconds for inland waterway vessels. This time

Table 1 Recommended Steering Systems

Ship Class	Steering System	Steering Unit		
		Main	Auxiliary	Emergency
Towboats Push Tugs to 300 HP	Balanced Rudder Rotating Nozzle	Manually operated cable or geared shaft or hydraulic unit	Tiller on rudder stock	Not required
300 HP to 1200 HP	Balanced Rudders Fixed Nozzles with streamline rudders behind nozzles	Electrohydraulic unit	Steering column	Tiller
	Rotating Nozzles	Quadrant type electric unit with individually controlled nozzle rotation or electro-hydraulic unit	Steering column	Tiller
over 1200 HP	Balanced Rudders	Electrohydraulic Unit	Electrohydraulic Unit	Not required
	Rudders behind Fixed Nozzles			
	Movable Rudder-Nozzles			
Self-Propelled Inland Waterway Cargo Vessels and Tankers	Movable Rudder-Nozzles	Electrohydraulic Unit	Electrodydraulic Unit	Not required
	Balanced Rudders	Electrohydraulic Unit	Electrohydraulic Unit	Not required
Inland waterway-Ocean Cargo Vessels	Movable Rudder-Nozzles	Electrohydraulic Unit	Hydraulic cylinder with steering unit	Not required
Inland waterway passenger vessels	Balanced rudders	Electrohydraulic Unit	Hydraulic cylinder with steering unit	Not required
Non-propelled Inland	Fixed skegs	-	-	-

period is impractical for hydrofoil and surface effect vessels and must be revised.

The nominal (working) pressure of the hydraulic fluid is 100-170 kg/cm^2 in present electrohydraulic ram units. For small engines it appears that the nominal pressure should be increased to 200-230 kg/cm^2. In foreign units of this size the nominal pressure is 300 kg/cm^2. For larger units the working pressure should be increased to 160 kg/cm^2. The maximum pressure in heavy duty steering units should be at 200-300 kg/cm^2. The vane type steering units manufactured by Frydenho (Norway) use a working pressure of about 25 kg/cm^2 because their seals are not reliable at higher pressures. The pressure which activates relief value is 40 kg/cm^2.

Provision for switching from the main steering gear to an emergency unit in the wheel house should be made. In the case of vessels with two steering units, each unit must be able of turning one nozzle rudder. The steering units should permit this to be done individually as well as in synchronized motion. The period of failure free operation must correspond to the specified ship repair schedule. The failure free operational period is about

40,000 hrs. It is known that as a rule extending the service life requires increases in maintenance costs, unit size and weight. Consequently the rating of the service life of steering motors must be based on the scheduled ship repair dates.

Improvements in the steering unit structure will be based on utilization of new high-quality material and parts which can upgrade the steering gear quality and reliability along with reducing unit dimensions. It is with this approach an optimum solution can be obtained which can meet the present shipbuilding requirements. In the coming decade it is recommended the following steering equipment be used on inland waterway-ocean vessels:

Electrohydraulic steering units with tilting cylinders (manual and machine operated) for vessels utilizing new propulsion systems, hydrofoil and air cushion craft, as well as small displacement vessels. These units meet present requirements and can be designed for ±35° in under 28 seconds.

The rudder stock design should allow removal of the rudder section while the vessel is afloat without disassembly of the steering gear. This can be accomplished using a rudder stock with the fastening nut in an off center position. This rudder stock design has been utilized in systems with conventional semi or fully balanced rudders. The forging problems in the manufacture of this rudder stock has limited its use. To solve this problem by using welding resulted in the construction of a rudder stock which is partly cast, forged and welded. The rudder stock is cast of steel and the rod is forged then both are heat treated and joined by electro welding.

On inland waterway-ocean vessels cast and forged rudder stocks have become accepted. They are made from cylindrical rods with the lugs in the off center location. Figure 6 shows the stock before welding. The upper and lower cylindrical surfaces of the sections are flanged for welding. After welding small strips are removed from these flanges. Then the strips are marked and attached to the welded area before heat treatment and machining.

The method for setting the bearings eliminates the drilling of the bearings. After centering the rudder stock the bearings are fastened using bolts with thrust blocks or as shown in Fig. 3 segments are welded. This method for fastening the rudder stock bearings was tested during building trials and long term operation on inland waterway vessels and inland waterway-ocean vessels. Considerable savings in metal cutting, and reduced labor are obtained by this steering gear component manufacture. Rudder stocks with diameters of 200 mm are manufactured by casting, forging and welding. This type of manufacture is now adopted in domestic shipbuilding.

Carbon or low alloy steel rudder stocks are protected from surface corrosion by okhl8niot stainless steel jackets attached at the neck of the rudder stock. To prevent corrosion at the jacket edges, the rudder stock surface has one prime coat of VL-02 paint and three coats of EP-7 paint. The lower sections of rudder stocks on inland waterway-ocean vessels are 120 mm in diameter have similar jackets with grp and resin coatings between the necks.

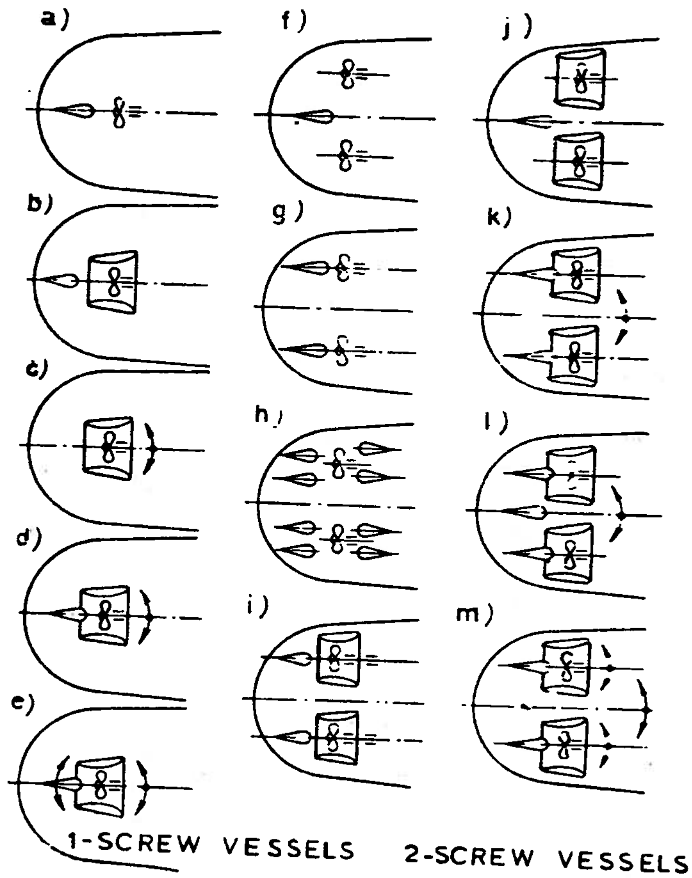

Fig. 1 Diagrams showing single screw and twin screw steering systems for inland waterway vessels and inland waterway/sea vessels.

Key:

a- centerline rudder arrangement
b- rudder with non-turning nozzle
c- turning nozzle only
d- turning nozzle with fixed fin
e- turning nozzle with turning rudder

f- centerline rudder arrangement
g- twin rudder arrangement
h- steering and flanking (backing) rudder arrangement
i- semi-balanced rudders with non-turning nozzles

j- single rudder with non-turning nozzles
k- twin turning nozzles with fixed fins (Synchronized)
l- combination of k arrangement with centerline rudder
m- arrangement k with nozzles turning separately

Arrangement m is recommended for inland waterway and inland waterway/sea vessels.

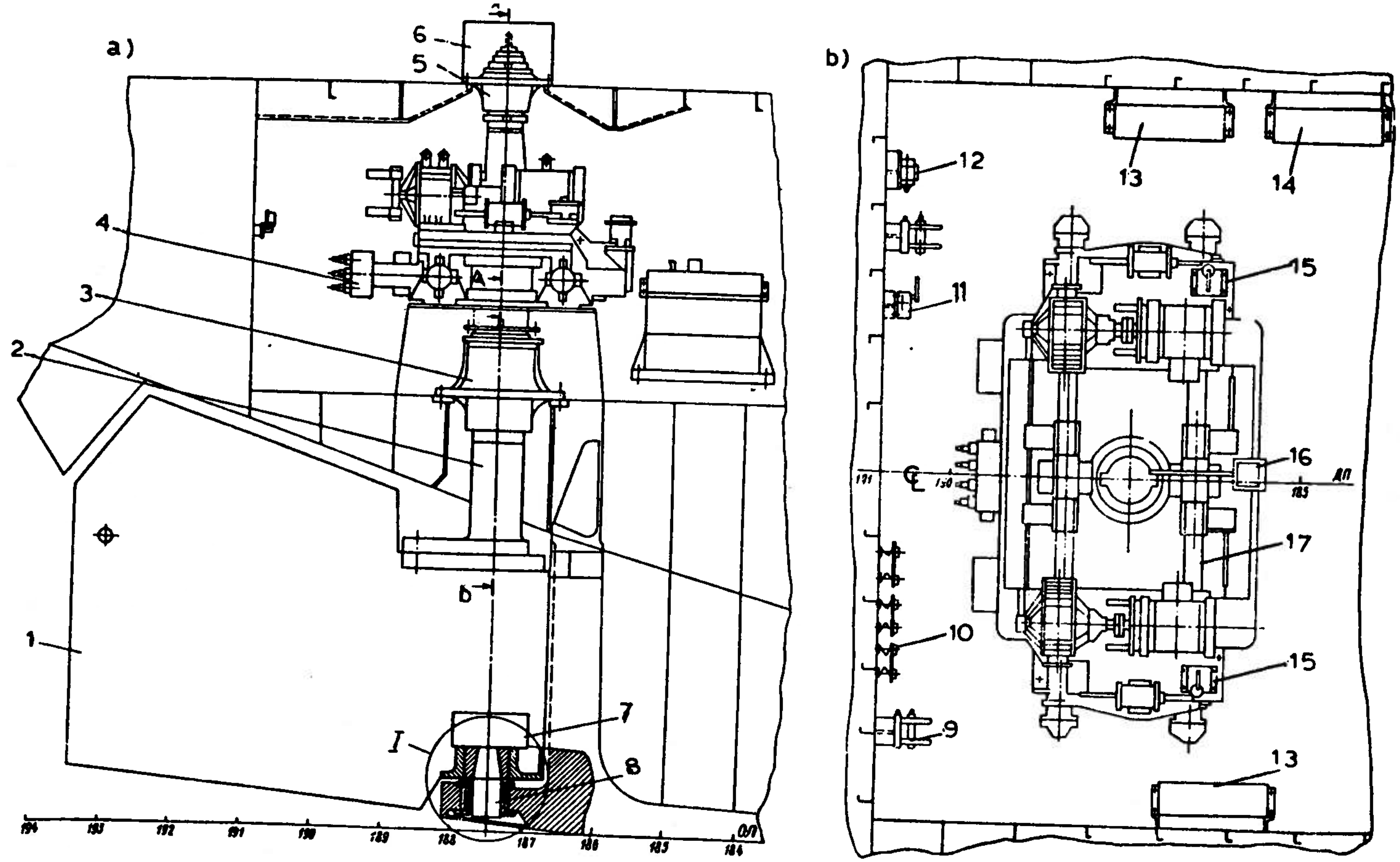

Fig. 2 TIKSI-type sea/inland waterway cargo vessel steering system.

a) Side view b) Steering layout

KEY:
1: rudder
2: rudder stock
3: lower bearing
4: electohydraulic steering gear
5: upper bearing
6: housing
7: cover
8: rudder lower bearing
9: filter
10: pressure gage
11: manual pump
12: valves
13: spare tank
14: standby tank
15: instrumentation
16: rudder position
17: electrohydraulic steering gear

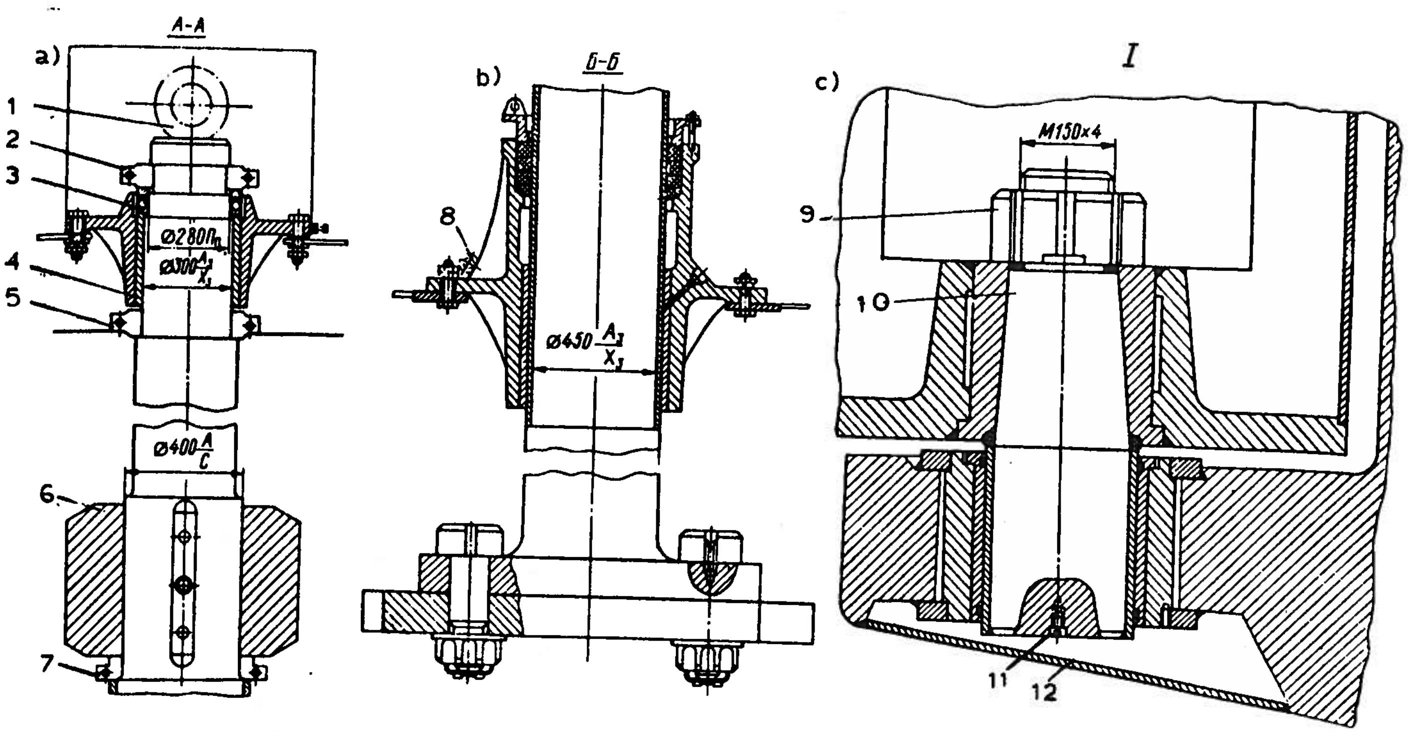

Fig. 3 Details of rudder stock and rudder mounts in Fig. 2

a) Section A-A
b) Section b-b
c) Mount detail I

KEY:			
	1: ring fastener	5: yoke	9: nut
	2: yoke	6: tiller	10: pin
	3: ball bearings	7: yoke	11: screw
	4: bushing	8: lower bearing	12: screw cap

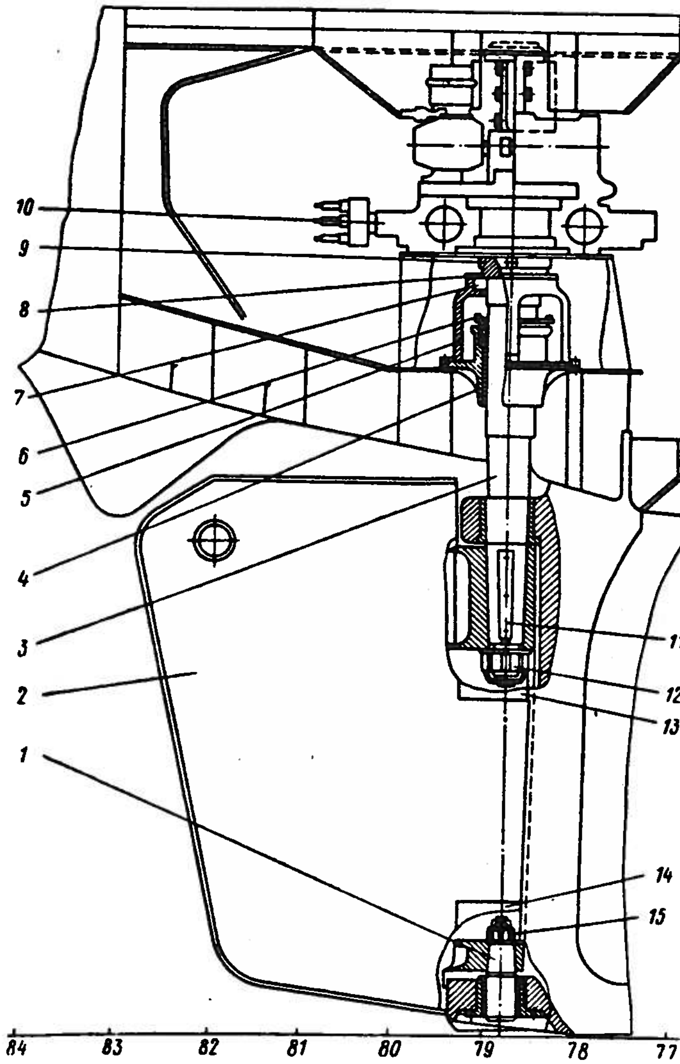

Fig. 4 4000 HP inland waterway icebeaker steering system

KEY:

1: pin
2: rudder
3: rudder stock
4: lower bearing
5: bearing housing
6: seal
7: ball bearing
8: thrust collar
9: stop
10: electrohydraulic steering gear
11: key
12: rudder stock nut
13/14: cover
15: nut

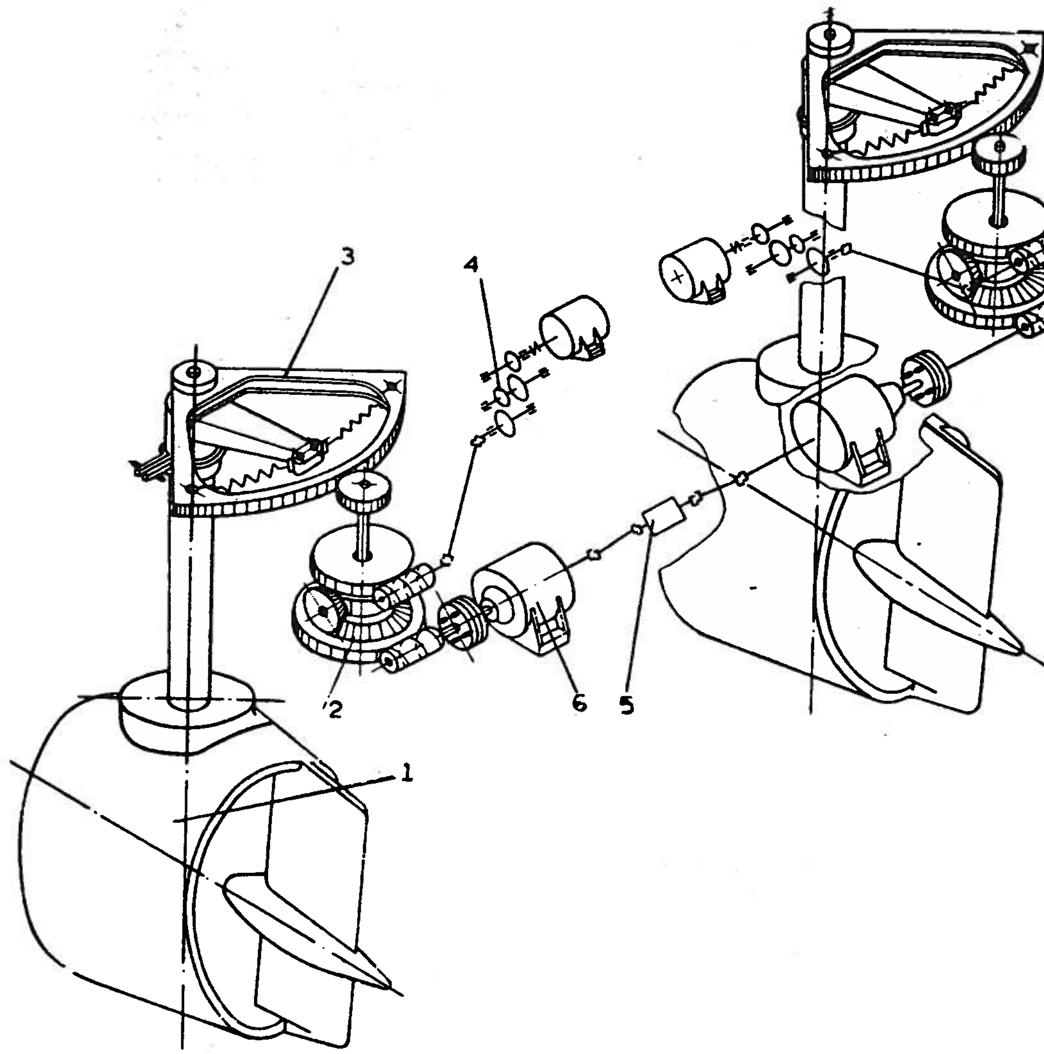

Fig. 5 Diagram of towboat (pushboat) steering system. System with both separate and synchronous nozzle turning.

KEY:

1: nozzle with fixed fin
2: reduction gear
3: steering quadrant
4: auxiliary electric drive
5: clutch, electromagnetic
6: main electric drive

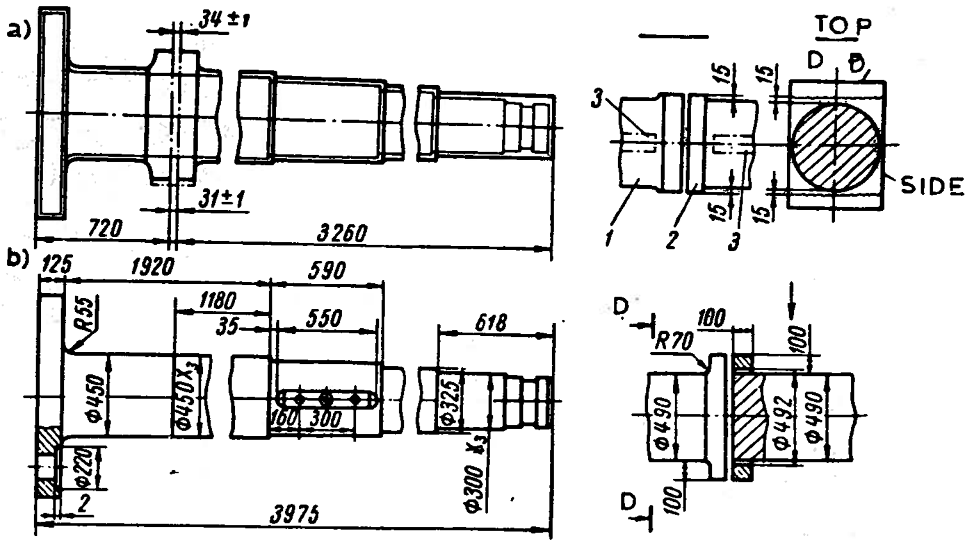

Fig. 6 Rudder stock which is cast, forged and welded.

a) View of blank
b) after heat treating
c) preparation prior to welding

KEY:

1: lower section of rudder stock
2: upper section of rudder stock
3: section used for tests

EFFECT OF PROFILE THICKNESS AND ANGLE OF ATTACK OF FLANKING RUDDERS IN PUSHER TUGS ON THRUST DEDUCTION AND PROPULSION POWER[1]

BY

G. LUTHRA[2]

SUMMARY

This paper contains an overall review of model tests described in VBD reports 884 and 911. The significant results of these tests with a twin, a triple and a quadruple-screw pusher tug with 3 different types of rudders are presented. In particular they cover comparative bollard pull and propulsive power measurements as well as investigations of the local flow conditions in the region of flanking rudders.

From bollard pull and propulsion tests specific data on thrust deduction fraction and on increment of propulsive power due to flanking rudders was determined in relationship with factors such as rudder form, pusher tug type and speed and draught of the pushed train of barges. The results are presented in the form of diagrams. They illustrate which rudder forms are favorable and together with the ascertained flow conditions supply design data to minimize the disturbance, from the flanking rudders which can have an adverse effect on the ahead operation of the tug. With the optimized arrangement of flanking rudders it can be anticipated that the propulsive efficiency will be improved and the risk of cavitation and vibration excitation reduced.

TRANSLATION[3]

1. INTRODUCTION

The following paper presents a summary of model tests described in Versuchsanstalt fur Binnenschiffbau, e.V. (VBD) reports no. 884 and 911 [1]. Report no. 884 contains comprehensive results of bollard pull and propulsive measurements from a twin screw pusher towboat with three different rudder arrangements. The influence of the rudder arrangement on the required propulsive power and thrust deduction t were determined from these tests. Report no. 911 is the continuation of this study. It describes the investigation of the influence of flanking (backing) rudders in multiple shaft arrangements on the required propulsive power and hull efficiency. This was obtained from comparative tests of triple and quadruple screw pusher tow boats.

In each test the horizontal flow was also measured in the plane of the flanking rudders. This established the flow conditions when flanking rudders are fitted on the towboat and thus enables them to be set to minimize the flow disturbance in forward operation.

While the original reports include the lines plans of the towboat models and graphs summarizing the complete test results, in the present paper they have been partly omitted to keep the number of figures small.* The test data is summarized in the next section with the principal particulars of the models presented in Table 2.1.

2. SUMMARY OF EXPERIMENTS

The experiments are summarized in Table 2 and the model-propeller data is summarized in Table 2.1.

3. MODEL TESTS

As mentioned earlier, bollard pull measurements were carried out on the twin screw model fitted with the 3 different rudder arrangements shown in Fig. 1. In these tests the propeller loading at a specified speed was varied by changes in the propeller rpm and the excess propeller thrust or pull force was measured. These tests were particularly appropriate for situations where small differences in the results were measured. The measurements were carried out with the towboat alone to determine the influence of each rudder profile on the required power and thrust deduction t.

---

[1]Shiff Und Hafen, Heft 10/1979, 6 pp.
[2]Versuchsanstalt fur Binnenschiffbau (VBD) e.V., Klocknerstraße 77, 4100 Duisburg 1. W. Germany
[3]Prepared by Dipl-Ing. G. Luthra, VBD.

*Note the lines plans of Models M-771 (twin screw), M-838 (triple screw) and M-843 (quadruple screw) along with Europa II Barge models 751-762 are shown in NA&ME Dept. Report No. 243, November, 1981, pp. 19 and 32.

TABLE 2. SUMMARY OF EXPERIMENTS

Tank	9.8 m wide × 190 m long tank of VBD, still water, water depth corresponding to h=5.0 m full scale.				
Models λ=16	Pusher Towboats 2-Screw M-771 (Ref. A p 14-24) 3-Screw M-838 (Ref. A p 25-50) 4-Screw M-843 (Ref. A p 25-50) [Ref. A: NAME Rept. 243 11/81]		Barges M 751-762 Type EUROPA II Twin row, double/triple column train (Table 2.1)		
Nozzles and Rudders	Model	Installation Description Type	Nozzles	Rudders at Each Propeller Steering	Flanking
	M-771	I. "Becker"	2 × D124	1 × R474 Flap	2 × R475 Top: Short Bottom: Long
		II. "Biesbosch"	2 × D106	1 × R465 Fixed Struct	2 × R466 Simple Profile
		III. "Schilling"	2 × D106	2 × R401 2 × R402	2 × R403 2 × R404
	M-838	I above	3 × D124	1 × R474	2 × R475
	M-843	IV Main type I Flanking III	Outer: 2 × D126 Inner: 2 ×D127	1 × R488 Flap	Outer: 2 × R489 Inner: 2 × R490

Tests	Description	M-771 Free Running	M-771 Pushing	M-838 Free Running	M-838 Pushing	M-843 Free Running	M-843 Pushing
	a) Push Force at V, Km/h	I,II,III 0.0, 4.0 8.0,12.0	III 0.0,4.0 8.0	-	I 8.0	-	IV 8.0
	b) Propulsion of Barge Train T,m	-	III 3.2,2.8 2.5	-	I 3.2,2.8	-	IV 3.2,2.8
	c) Flow Direction at Flanking Rudder		I, III		I		I

TABLE 2.1 MODEL AND PROPELLER DATA

	Long Distance Pushboat M-771 2-Screw	Long Distance Pushboat M-838 3-Screw	Long Distance Pushboat M-843 4-Screw	Barge M-751 - 762 EUROPA II	
Length L_{OA}, m	35.0	35.0	37.0	76.5	
Beam mld B m	14.0	14.95	15.0	11.33	
Draft T m	1.75	1.70	1.65	2.8	3.2
Length L_{WL} m	33.9	33.89	36.0	73.05	73.78
Displ. ∇ m^3	525.5	553.5	608.1	2195.0	2528.9
Wetted Surf. S m^2	545.2	696.3	616.7	1192.0	1257.7
Block Coeff. C_B	0.622	0.643	0.682	0.947	0.945
Lower Edge Transom				Total Displacement m^3 of Barge Train;	
above B.L. m	1.55	1.55	1.54	(Twin row, twin column)	
Propeller location					
from A.P. m	3.90	3.64	3.37	8780.0	10116.0
Distance Between Propellers					
Outer m	7.50	8.80	9.20		
Inner m	-	at CL	3.00		
Propeller shaft CL					
above B.L. m	1.12	1.11	1.08		
Rotation Direction from Aft					
Propeller	P186 r/1	P186 r/1 and P196 r/1		Outer P46 r/1	Inner P52 r/1
Diameter D m	2.10	2.10	2.10	1.92	1.92
Pitch/Dia P/D -	1.052	1.052	1.052	0.964	0.90
Area ratio Ae/Ao -	0.710	0.710	0.710	0.56	0.56
Blade Number z -	4	4	4	4	4
Chord length $c_{0.7r}$ m	0.884	0.884	0.884	0.603	0.60

Initial tests with each rudder installation were performed with only the steering rudders fitted. Then the tests were performed with both the steering and flanking rudders to enable comparison of the steering rudders and assess the deterioration in the towboat performance from fitting flanking rudders. The zero deflection angle (alignment with flow) of the flanking rudders was obtained in previous tests [2,3, and 4]. In the subsequent measurements of pull force vs. power for the triple and quadruple screw towboats these angles were adopted. In these tests however the towboat model was connected to a twin row double column barge train.

The measurements of the flow in the flanking rudder region were made using a 6 mm outer diameter, three hole cylinderical tube. Horizontal velocity vectors were measured in an imaginary vertical grid extending over the entire width and height of the rudder. This measurement plane formed an angle with the vessel centerline which was taken as the zero deflection angle.

The pressure at each of the three holes was measured separately and recorded as a pressure difference from the static pressure using a double chamber membrane type pressure gage. The reference pressure was obtained from a static pitot tube set in the undisturbed flow.

4. TEST RESULTS

4.1 PULL FORCE MEASUREMENTS

The propeller and nozzle torque K_Q coefficient and thrust K_T coefficient were obtained from the pull force measurements of the twin screw towboat fitted with the three different rudder installations. Two sets of test results are shown in Figs. 2-3 as a function of advance ratio J. In the analysis, the advance ratio was based on the vessel speed while for the open water curves the advance ratio was based on the actual speed of inflow at the propeller and nozzle. The differences between the open water and self propulsion curves were also caused by the recessed location of the nozzles in the towboat tunnel stern.

The torque absorbed by the propeller and the thrust delivered by the propeller are increased when the flanking rudders are fitted. There is an increase in the nozzle thrust with the exception of type III multiple blade rudder which exhibits a more pronounced interaction between the propeller loading and the increased propeller torque and thrust. Clearly the shorter and thinner rudder blade profiles used in the multiple rudder installation would cause minimal flow disturbance as propeller loading increases. The multiple rudders appear to effect the nozzle circulation which reduces the nozzle thrust and consequently the curves of K_T and $10K_Q$ are closer to the curves of the propeller without nozzle.

The thrust deduction t is a better index for the practical evaluation because it enables a comparison of the usable propeller thrust in each test. The values of t determined from the push measurements with each rudder type fitted are plotted in Figs. 4-6 as a function of the propeller loading coefficient C_{TH} at corresponding values of speed V and rpm N. For the towboat fitted with only steering rudders, the thrust deduction value appears independent of the rudder type with a value at $t = 0.2$. (loss in thrust amounts to 20%). This value is for the towboat operations without the barge train. In this comparison, the type III arrangement with short and thin rudder profiles does not appear to be any better for main steering rudders. They tend to exhibit a slight disadvantage which is possibly due to the fact the entire rudder blade area is in the accelerated screw race. While the type I and II single blade rudders operate behind the propeller hub outside the screwrace. This disadvantage is only small and becomes more than compensated for when the towboat is fitted with both steering and flanking rudders.

The flanking rudders increase the loss of thrust indicated by the thrust deduction t by an additional 11-15% with type I rudders, with the higher losses appearing at smaller propeller load. In comparison the type III arrangement gives the best results. Additional loss in thrust amounts to about 10% at smaller propeller loadings. This improves with increasing propeller loading so that it amounts to a loss of only 3-4% at typical values of C_{TH} and with continued propeller loading this loss disappears.

A numerical comparison of the thrust deduction is given in Table 4.0 for three values of thrust loading C_{TH}.

The thrust deduction of the triple and quadruple screw towboats is plotted in Fig. 7. The measurements were made with the towboat pushing a twin row-twin column barge train and give an indication of the influence of the barge convey. With the barge train present, the thrust deduction t is 5-10% larger than the value measured in the corresponding free running condition. The lower value represents larger propeller

TABLE 4.0 COMPARISON OF THRUST DEDUCTION t

Test Conditions		Thrust Deduction for:		
C_{TH}	Flanking Rudders	Installation I	Installation II	Installation III
3.0	without	0.20	0.24	0.22
-	with	0.33	0.27	0.29
10.0	without	0.18	0.20	0.20
	with	0.30	0.29	0.23
∞	without	0.125	0.14	0.16
(Bollard)	with	0.225	0.22	0.16

$$C_{TH} = \frac{T}{\rho/2\ V_S^2 \cdot Ao}\ ;\ \text{where}\ \ T = \text{total thrust Propeller + Duct.}$$

thrust loading. This 5-10% increase is found in both tests with and without flanking rudders fitted.

Comparison of the towboat thrust deduction values for similar tests indicates the small influence of the towboat hull form or number of propellers on the value of thrust deduction t at high propeller loadings. Due to the lower shaft horsepower for each propeller on the quadruple screw towboat, the value of t at the same total thrust value is better than that for the triple screw towboat. At higher propeller loadings there appears to be no significant differences.

When type IV, multiple blade flanking rudders were fitted there was less inflow disturbance. This supports the conclusions obtained from the twin-screw towboat tests.

4.2 POWER MEASUREMENTS

Self propulsion tests were completed for each towboat pushing a twin row, twin column barge train following the test program in Table 2.0. The results of these tests which include the propeller and nozzle thrusts are plotted in Figs. 11-13. Here, the thrust values for symmetric propellers/nozzles are given for the starboard side. Therefore with the exception of the triple screw towboat, these values must be doubled to obtain the total thrust.

Resistance measurements were made with the twin screw towboat behind the barge train for various barge train depths. The towboat was not fitted with flanking rudders in these tests. Since the other towboats have nearly the same dimensions, it was not necessary to repeat the resistance measurements for the triple and quadruple screw towboats. Also the resistance measurements were not repeated when the flanking rudders were fitted because of their negligible increase in the total resistance. Therefore in the thrust deduction fraction calculation the twin screw towboat-barge train resistance was adopted for all three towboats and used as the basis for comparing propeller and nozzle thrust measurements. The results from this analysis are plotted in Figs. 11-13.

In the low speed range there is a "stacking" of the thrust deduction t curves with higher t values corresponding to increased barge train draft. This appears for all three towboats fitted with steering rudders and no flanking rudders. This tendency is evident more or less when the flanking rudders are fitted. It is caused by the high propeller thrust loading at each speed resulting from the deeper barge train draft. At respective service speeds corresponding to a total power of P_D = 2650 kw ; the thrust deduction is independent of barge draft and is nearly the same for all three towboats. The absolute value of the thrust deduction varies between $0.27 < t < 0.29$ with flanking rudders.

It can be concluded that the increase in thrust deduction from fitting flanking rudders is mainly influenced by the rudder profile form and propeller thrust loading. The presence of a barge train ahead of the towboat or changes in their draft appears to cause no significant change to this increase within the test range covered by the present study. Type III or type IV multiple blade flanking rudders increase the thrust deduction by 3 to 5 percent points (Δt = 0.03 to 0.05), while type I flanking rudders increase the thrust deduction by 6 to 8 percentage points (Δt = 0.06 to

0.08). These values correspond to a lowering of the hull efficiency by 6 and 10% respectively. However, since the wake fraction also changes, the drop in hull efficiency or the increase in required power from fitting the flanking rudders is not completely identical with these figures. As shown in Fig. 14 it has a more pronounced relationship with the barge train draft.

The wake fraction was calculated from open-water diagrams of the respective propeller+nozzle under the assumption of the propeller thrust and torque identify the mean being plotted in Figs. 11 to 13. The thrust identity and torque identity methods while commonly used, are not completely correct for this case. This is because the nozzle fitted to the towboat hull is partially recessed in the hull and therefore it is only partially effective. Nevertheless, while the absolute wake fraction values may be erratic, the relative trends in these values should be accurate enough to indicate the effect of flanking rudders.

The changes at the center propeller in the triple screw towboat are small due to the high original wake fraction value. This is because the center propeller draws water from the restricted bottom region. This is the reason why further increases in barge train draft do not have any significant effect on the wake. In contrast the wing propellers and outer propellers in the quadruple screw towboat draw water increasingly from the sides as the barge train draft increases. This exaggerates the influence of barge draft change and its influence on the wake of both flanking rudders.

The increase in forward speed required power from fitting flanking rudders is shown in Fig. 14. Parameters used in this figure are the delivered power and barge train draft. They illustrate that the flanking rudder losses decrease with larger barge train draft for a specified power or with increasing thrust load. This confirms the results from the push force measurements in Section 4.1. The quadruple-screw towboat test results show an opposite trend with the losses increasing with larger barge train draft. The flanking rudders were fitted only on the outer propellers where the rudders and draft effects act to retard the wake the most, while the thrust deduction fraction is not increased substantially or influenced by the barge train draft change.

The increment in required power caused by fitting the flanking rudders represents about 5 to 10%.

Finally Fig. 15 shows a comparison of the propulsive efficiency for each of the three towboats. The calculations were made analogous to the thrust deduction t calculations using the resistance measurements of the twin screw towboat and barge train. These values refer to the condition of "towboat without flanking rudders fitted" which are corresponding smaller when the flanking rudders are fitted. The overall propulsive efficiency can be considered good in view of the high propeller loading. The twin screw towboat has the least favorable propeller loading which is the reason for its results are below those of the other models. Depending on the towboat type the propulsive efficiency is between 41 and 50%.

4.3 FLOW MEASUREMENTS

Because the horizontal flow inclination is of primary importance in determining the flanking rudder "zero angle" alignment for forward operation, the horizontal flow directions are plotted in Figs. 16-20. These plots show the horizontal flow direction without velocity component with the rudder profile as the background for all three towboats. The directions are shown along the rudder span at different chord positions. The rudder position during the measurements is also indicated in the diagram. The local flow inclination angle varies considerably over the rudder span and in the case of the inner rudders the angle also varies along the height of the rudder. A mean neutral or zero angle for the whole rudder blade from which the local flow inclinations do not greatly vary is easier to derive for shorter rudder profiles than for longer profiles. This would explain the reason for the better propulsive performance of the shorter rudder profiles in type III and IV multiple rudder installations compared with type I or II installations.

From the local flow measurements it is obvious that the outer flanking rudders on the side or wing propellers cause less flow disturbance than the inner flanking rudders. Table 4.1 gives the arithmetical mean value for the whole rudder. The entry in brackets gives the respective total mean deviation.

For the outer rudders the deviation of the local flow inclination from the mean value is relatively small. More ever, it appears that a relationship exists between the zero rudder angle and the lateral distance of the corresponding shaft from the vessel centerline. Without going into the validity of this assumed relationship, which requires a

TABLE 4.1 MEAN VALUES OF HORIZONTAL FLOW DIRECTION

Towboat Variant / Propeller Number / Propeller location	Flanking rudder	3 Center	4 Inner	2	3 Wing	4 Outer
C.L. Ship and Shaft (center propeller)	BB	-3.5° (4.9°)	x	x	x	x
	StB	10.5° (3.8°)	x	x	x	x
C.L. Shaft (side propellers) Starboard side	Inner	x	0 (5.4°)	-3.5° (4.0°)	5.0° (7.0°)	4.0° (7.5°)
	Outer	x	10.0° (5.8°)	13.0° (3.5°)	17.0° (3.0°)	16.0° (3.4°)
Lateral Distance of Shaft from Midships		-	1.50 m	3.75 m	4.40 m	4.60 m

closer study of additional parameters such as the barge train draft, propeller rotating direction, etc., it appears that the zero angle δ_0 becomes bigger with the lateral distance of the propeller shaft Yp in the form:

$$\delta_{0\,\text{outer rudder}} = 0.47\,Yp^2 - 1.03\,Yp + 1.05 \text{ deg} \quad (1)$$

where δ_0 = zero angle of flanking rudder
Yp = lateral distance of propeller shaft from midships.

No similar tendency can be found in the case of inner rudders. The flow inclinations from bottom to top are "stacked spiral wise" so the flow underneath the propeller shaft is more in the outboard direction while in the upper half the flow tends to follow the direction of the tunnel stern opening.

The rudders in front of the center propeller in the tirple screw towboat have an asymmetrical zero angle. The mean values here are -3.5° for part and 10.5° for starboard rudders with the rudders diverging towards the front. This displacement with an otherwise symmetrical arrangement is due to the strong influence of the propeller rotational direction. Apparently, the clock-wise turning propeller moves the zero angle of the rudders here to 3.5° towards starboard.

5. SUMMARY

This paper has presented an overall summary of model tests described in VBD reports 884 and 911. The significant results of these tests with a twin, a triple and a quadruple-screw pusher tug with 3 different types of rudders were presented. In particular they cover comparative bollard pull and populsive power measurements as well as investigations of the local flow conditions in the region of flanking rudders.

From bollard pull and propulsion tests specific data on thrust deduction fraction and the increment of propulsive power due to flanking rudders was determined for factors such as rudder form, pusher tug type and speed, as well as the pushed barge train draft and presented in the form of diagrams. The diagrams illustrate which rudder forms are favorable and taken together with the flow measurements supply design data to minimize the flanking rudder disturbance, which has an adverse effect on the ahead operation of the tug. With this optimized arrangement of flanking rudders, it can be anticipated that the propulsive efficiency will be improved and the risk of cavitation and vibration excitation reduced.

6. REFERENCES

[1] Luthra, G.: Einwirkung der Ruderprofildicke und des Anstellwinkels in Vorausfahrt der an Schubbooten anzubringenden Flankenruder auf Sogziffer und Antriebsleistungsbedarf
Teil I in VBD-Bericht 884
Teil II in VBD-Bericht 911

[2] Luthra, G.: Untersuchung der Nachstromverteilung eines im Verband schiebenden Schubboots in Pontonform
Hansa Nr 18, Sept. 1974
English translation: B-II-2 NA&ME Rept. No. 243, November 1981

[3] Heuser, H.: Optimierung der Hinterschiffsform von Schubbooten
VBD-Bericht 853

[4] Heuser, H.: Bestimmung des Maßstabseffektes von Propeller-Dusen-Ruder-Kombination bei Schubbooten durch Geosim-Versuche
VBD-Bericht 842

[5] Luthra, G.: Untersuchung uber die erreichbaren Leistungseinsparungen bei Schubverbanden durch den Einsatz von Katamaranen als Schubboot
Zeitschrift fur Binnenschiffahrt und Wasserstraßen, Heft 3/1978

[6] Lindgren, H.: The Influence of Propeller Clearance and Rudder upon the Propulsive Characteristics
Publication 33, SSPA Goteborg, 1955

[7] Dyne, G.: On the Scale Effect on Thrust Deduction, RINA, July 1973

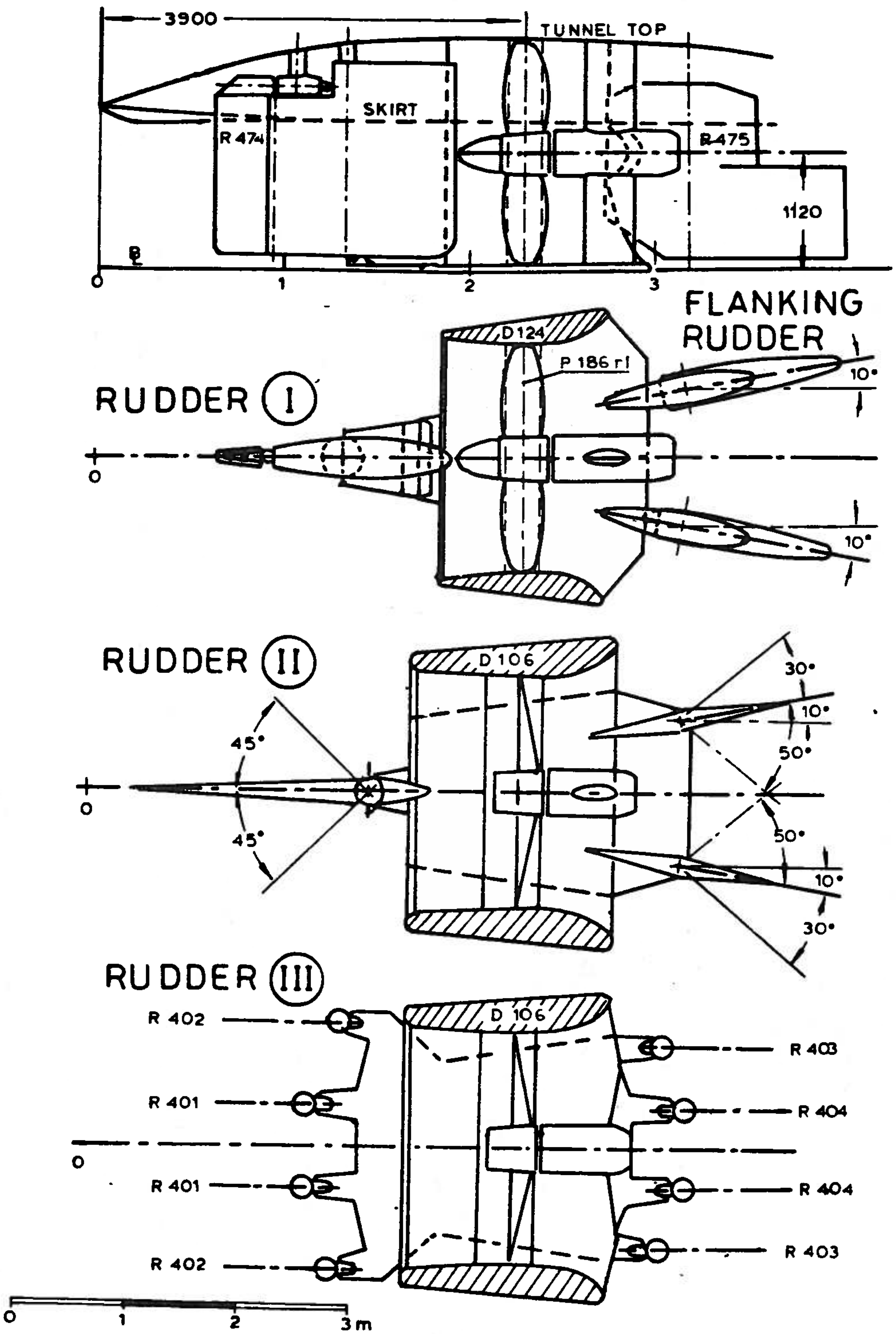

FIG.1 ARRANGEMENT 2 SCREW TOWBOAT M771

FIG.2 PULL FORCE MEASUREMENTS AHEAD MODEL 771 RUDDER (I)

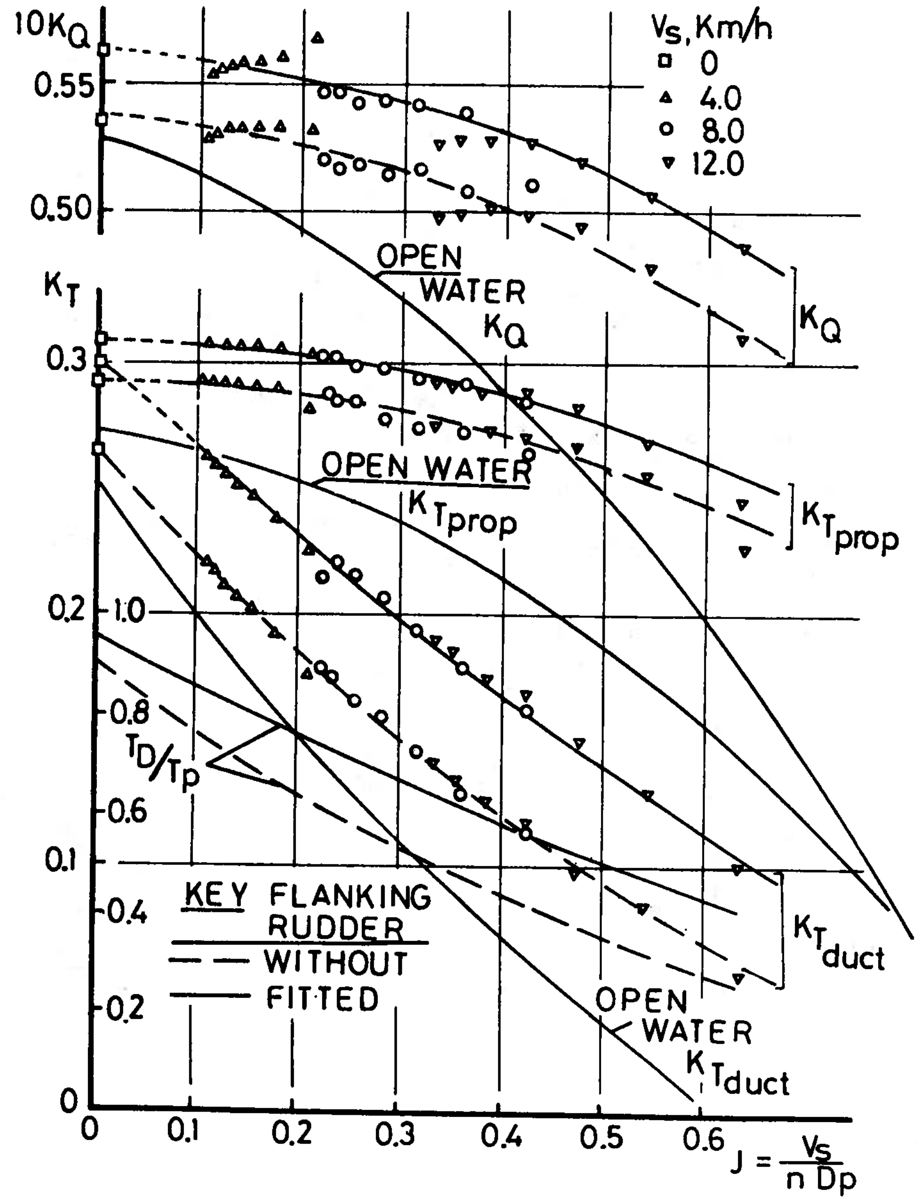

FIG.3 PULL FORCE MEASUREMENTS AHEAD MODEL 771 RUDDER (III)

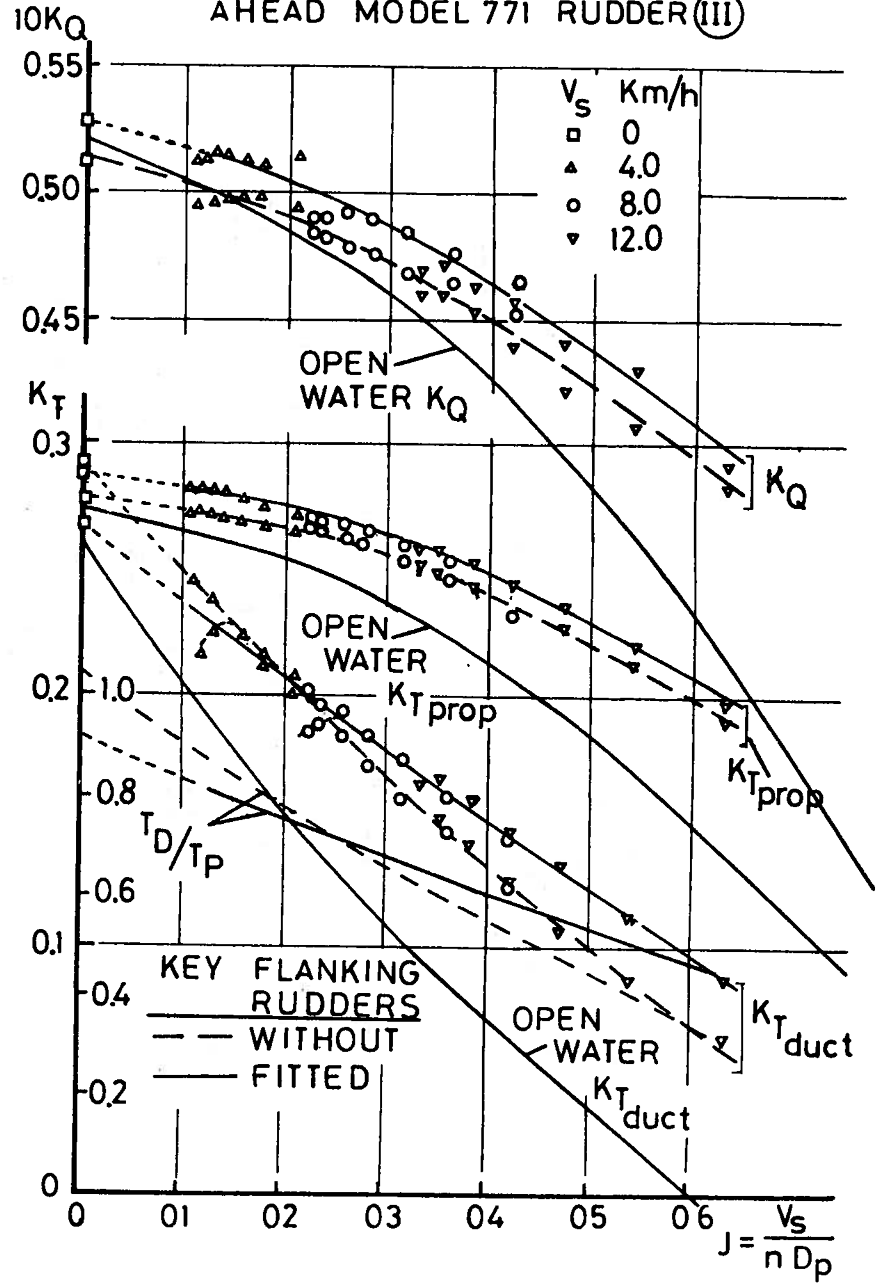

FIG. 4 THRUST DEDUCTION FROM PULL FORCE MEASUREMENTS AT CONSTANT RPM, RUDDER I

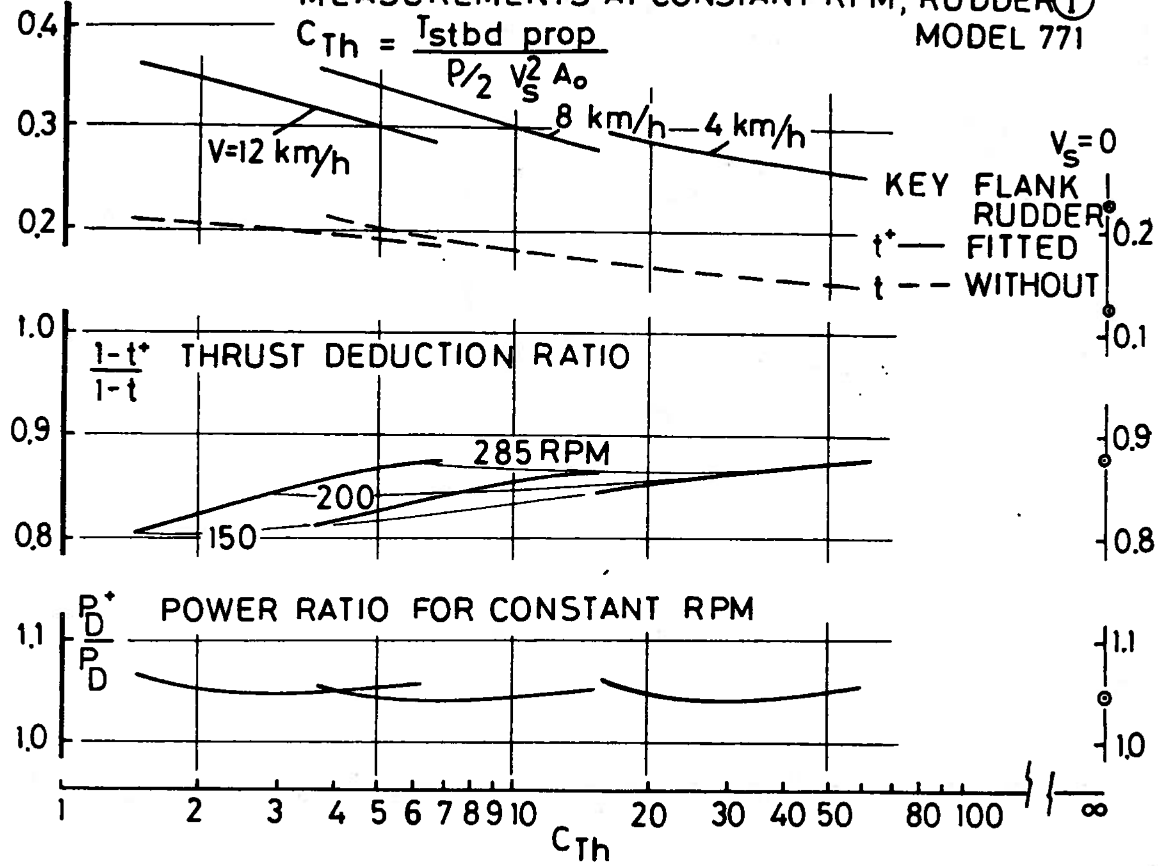

FIG. 5 THRUST DEDUCTION FROM PULL FORCE MEASUREMENTS AT CONSTANT RPM RUDDER II MODEL 771 KEY: FIG 4

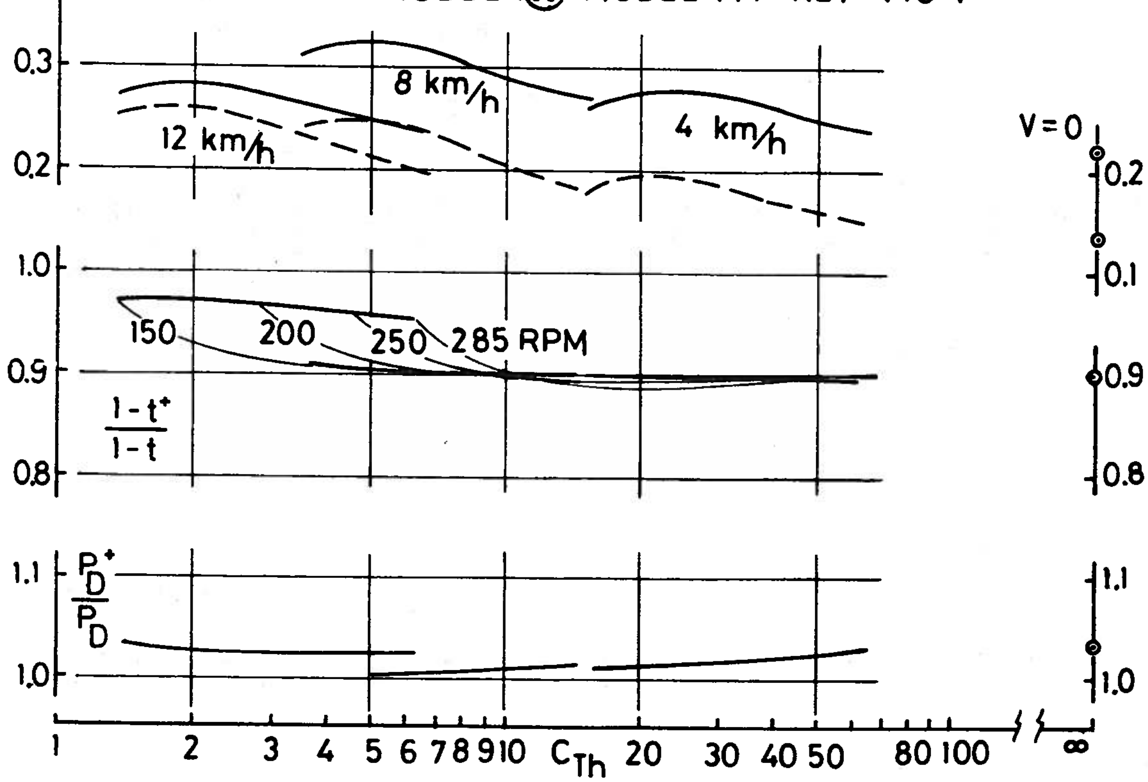

FIG. 6 THRUST DEDUCTION FROM PULL FORCE MEASUREMENTS AT CONSTANT RPM RUDDER (III) MODEL 771 KEY: FIG.4

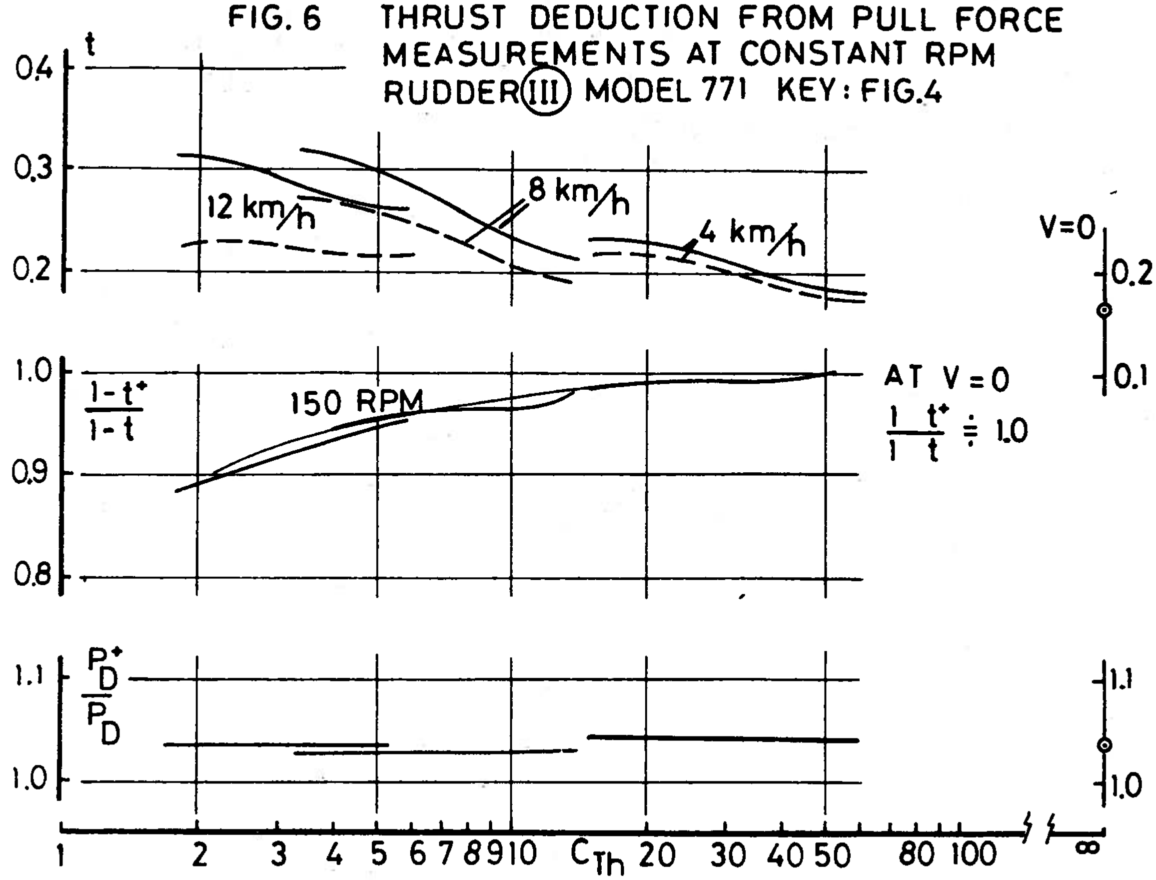

FIG. 7 THRUST DEDUCTION FROM PULL FORCE MEASUREMENTS WITH 2x2 TOW
T_{barge} = 2.8 m h = 5.0 m
KEY: FIG.4

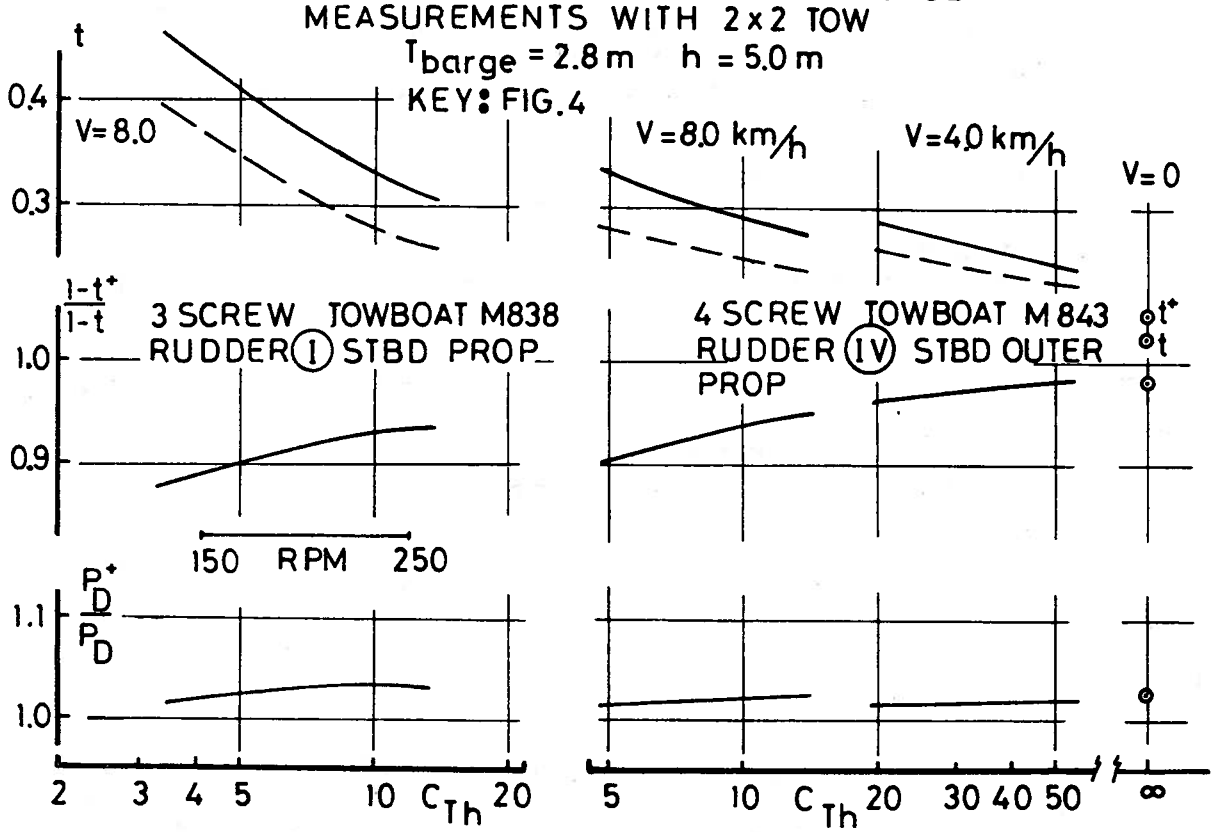

FIG.8 PROPULSION TESTS TOWBOAT M771
2 x 2 TOW, h = 5.0 m, RUDDER (III)
STBD. PROP.

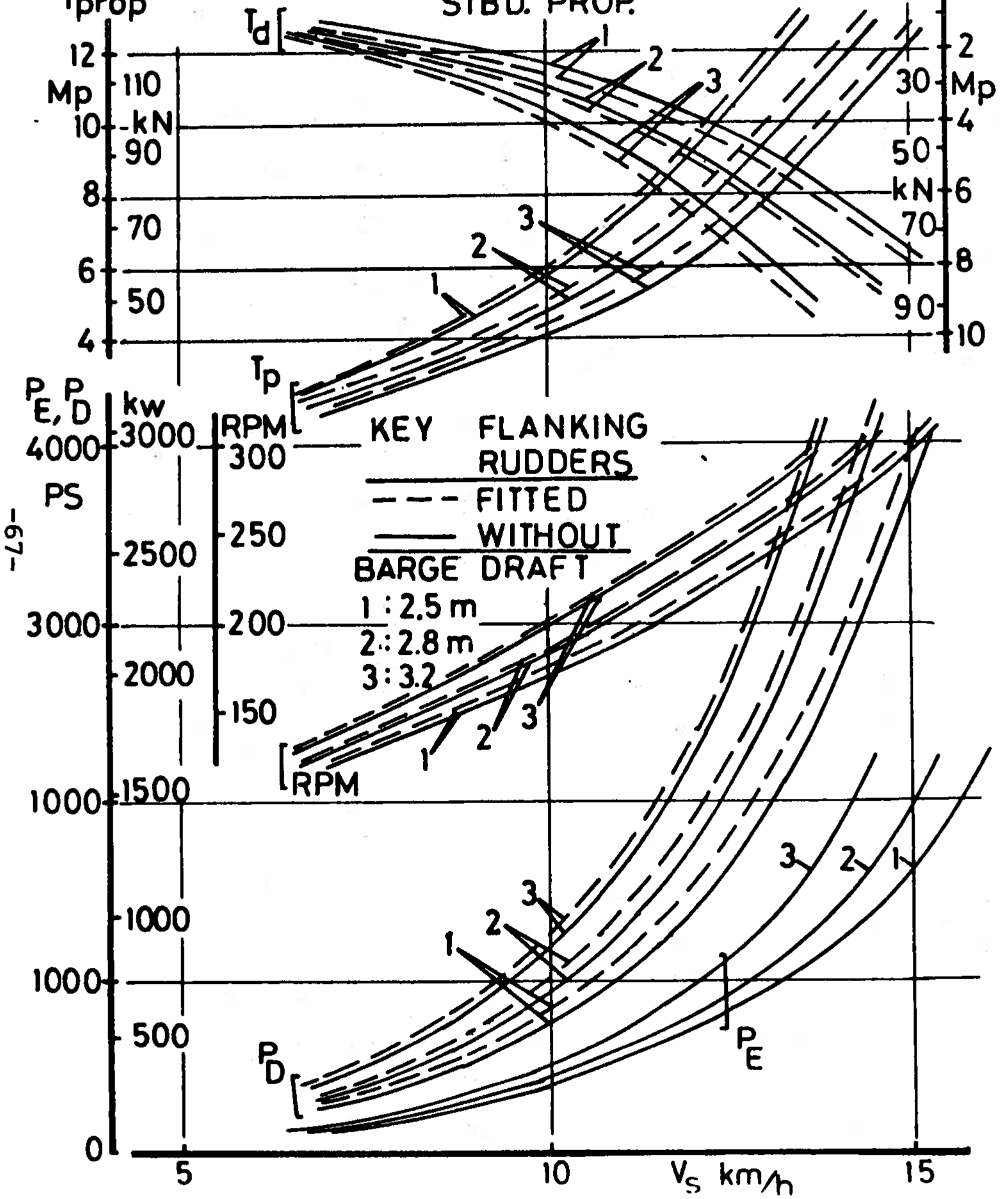

FIG.9 PROPULSION TESTS 3 SCREW TOWBOAT M838
2 x 2 TOW, h = 5.0 m, RUDDER (I)

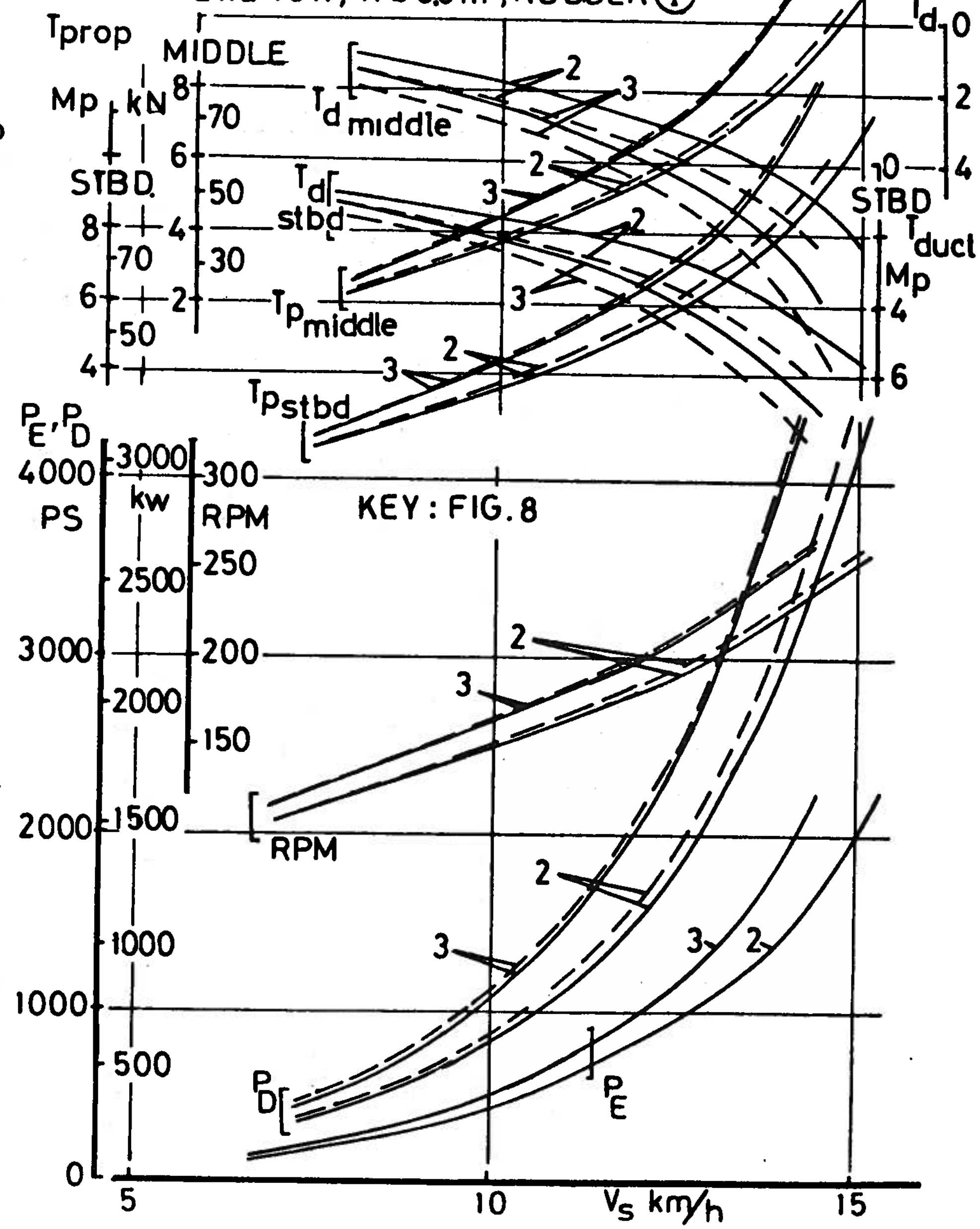

FIG. 10 PROPULSION TESTS 4 SCREW TOWBOAT
M 843 2x2 BARGE TOW RUDDER (IV)

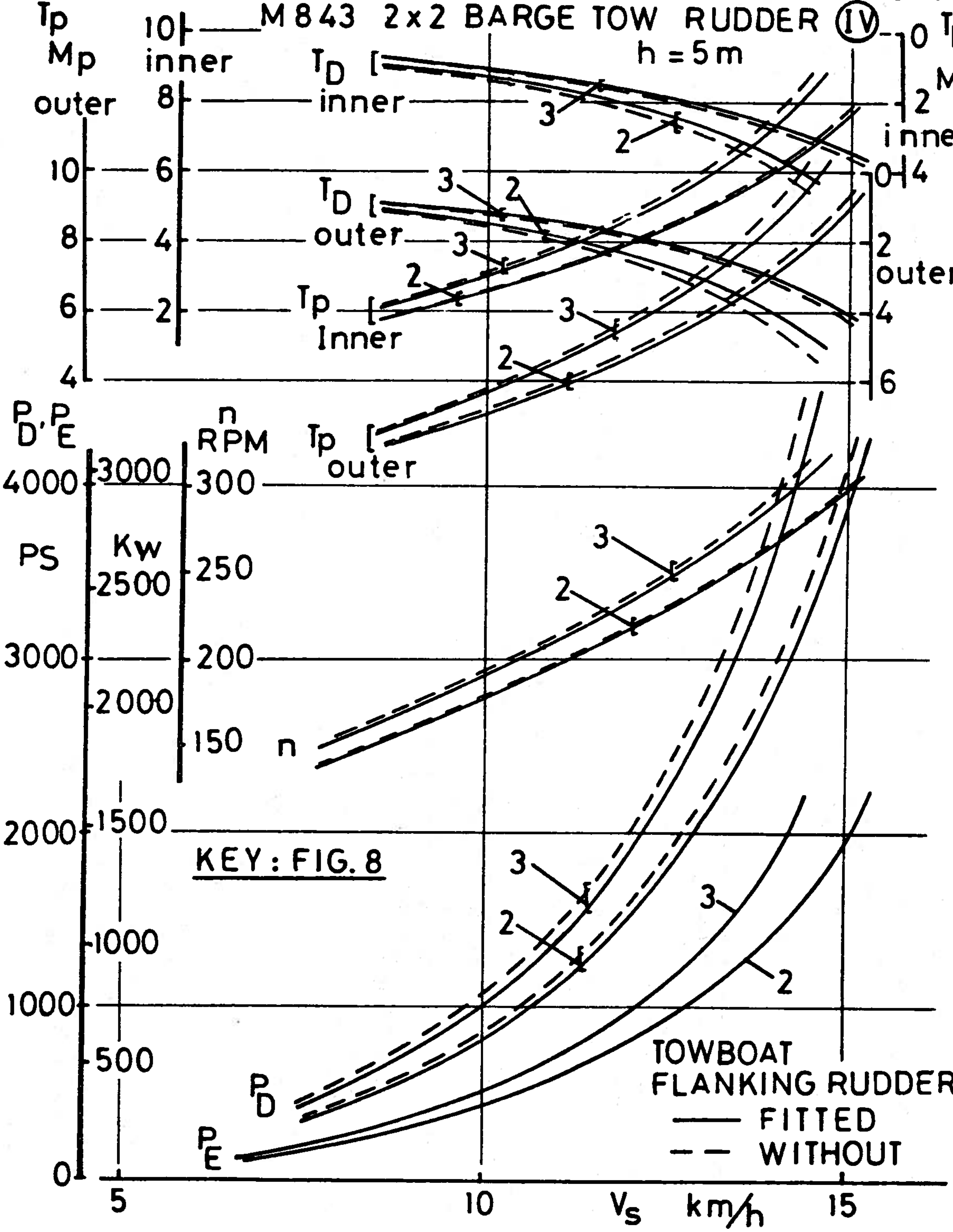

FIG. 11 THRUST DEDUCTION t AND WAKE FRACTION w
2 SCREW TOWBOAT M 771 RUDDER (III)
2 x 2 BARGE TRAIN WATER DEPTH h = 5 m

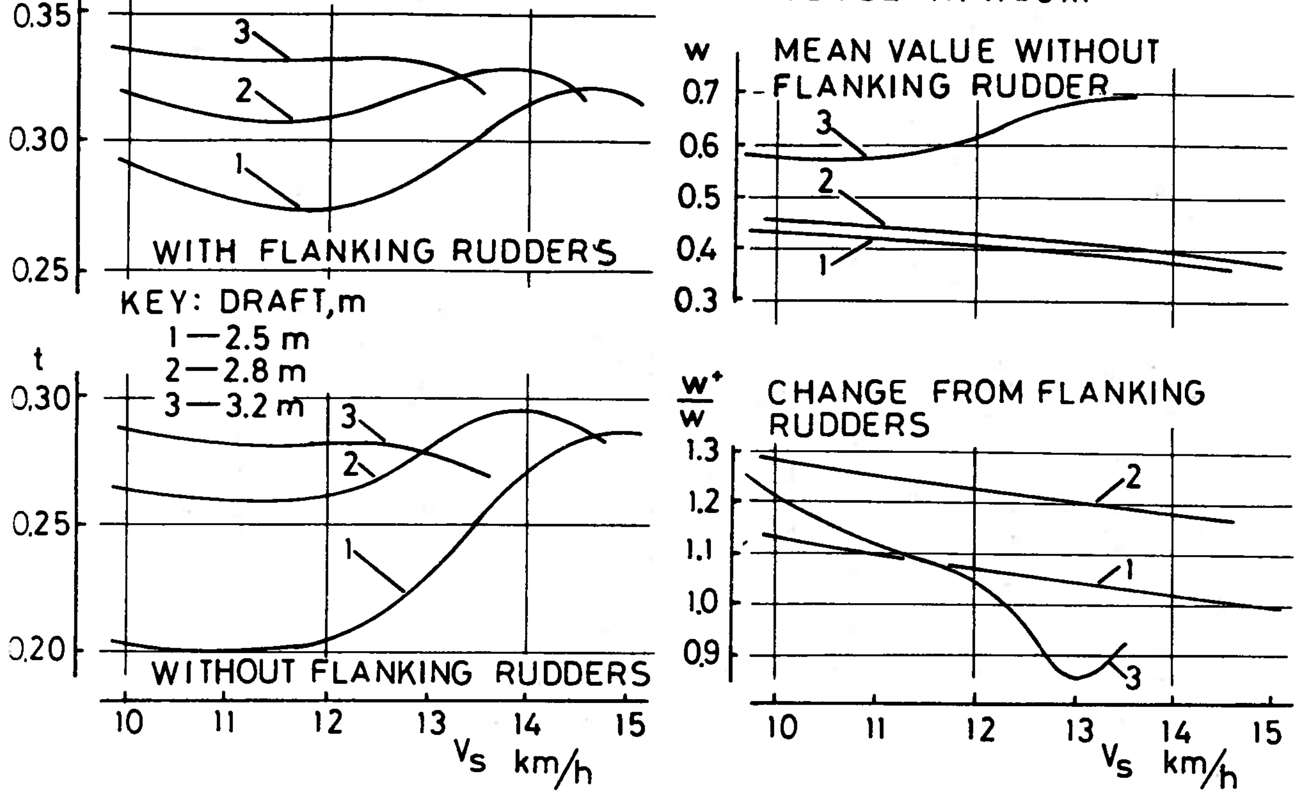

FIG. 12 THRUST DEDUCTION t AND WAKE FRACTION w
3 SCREW TOWBOAT M 838 RUDDER (I)
2 x 2 BARGE TRAIN WATER DEPTH h = 5 m

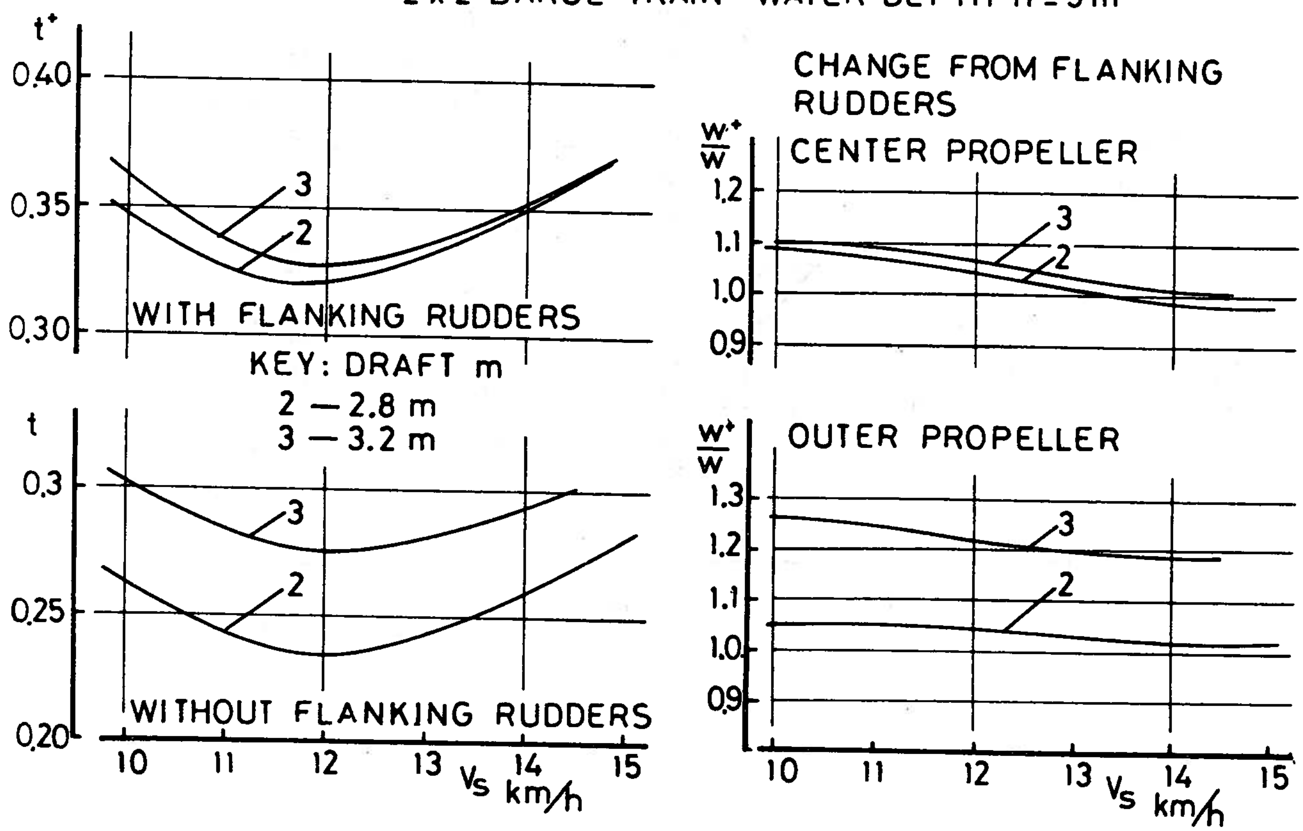

FIG. 13 THRUST DEDUCTION t AND WAKE FRACTION w
4 SCREW TOWBOAT M 843 RUDDER IV
2x2 BARGE TRAIN WATER DEPTH h = 5 m

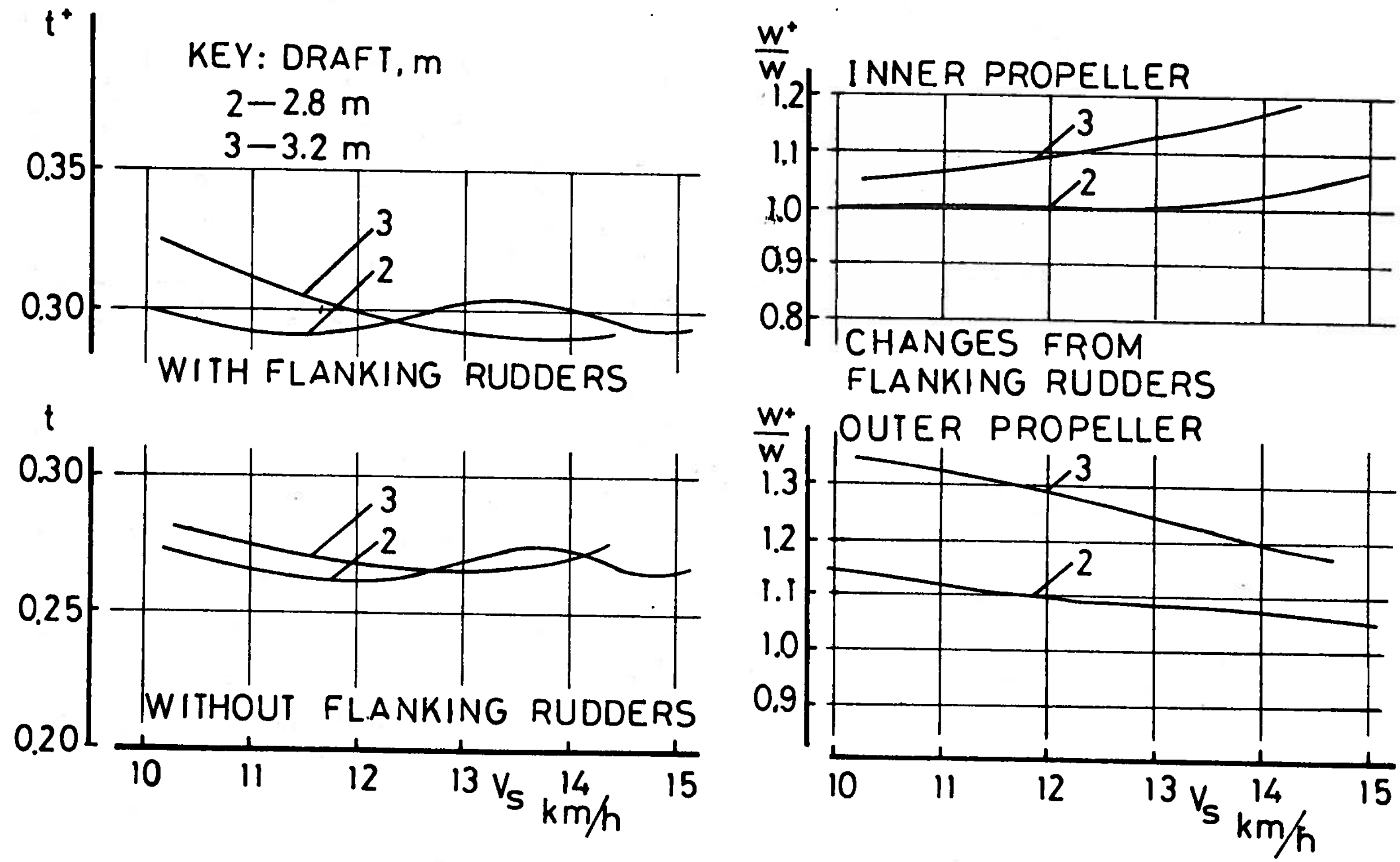

FIG.14 INCREASE IN POWER P_D FROM FLANKING RUDDERS 2x2 BARGE TRAIN WATER DEPTH h = 5.m

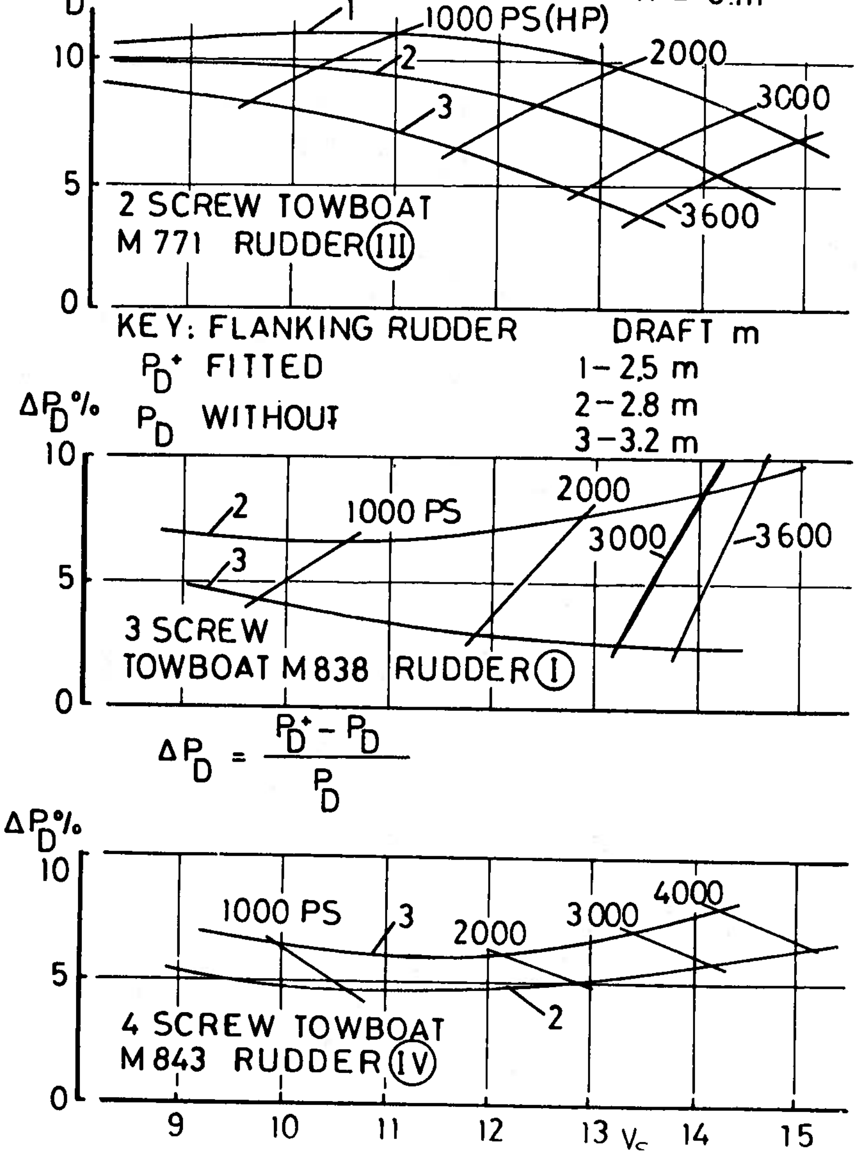

FIG.15 TOWBOAT PROPULSIVE EFFICIENCY 2 x 2 BARGE TRAIN WATER DEPTH h = 5.0 m

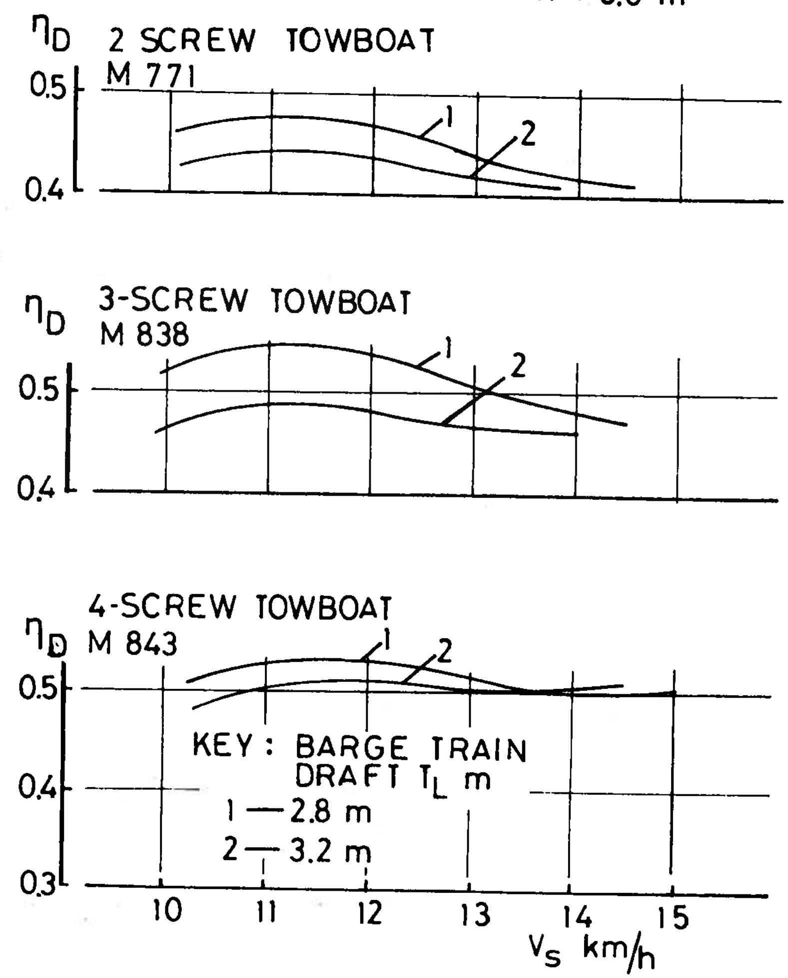

FIG. 16 FLOW DIRECTION
-A- MEASURED ALONG HORIZONTAL IN PLANE OF FLANKING RUDDERS

2-SCREW TOWBOAT M771
2x2 TOW DRAFT = 3.2 m
WATER DEPTH h = 5.0 m
SPEED V = 14.4 km/h
PROP. n = 242 rpm
FLANKING RUDDERS NOT FITTED

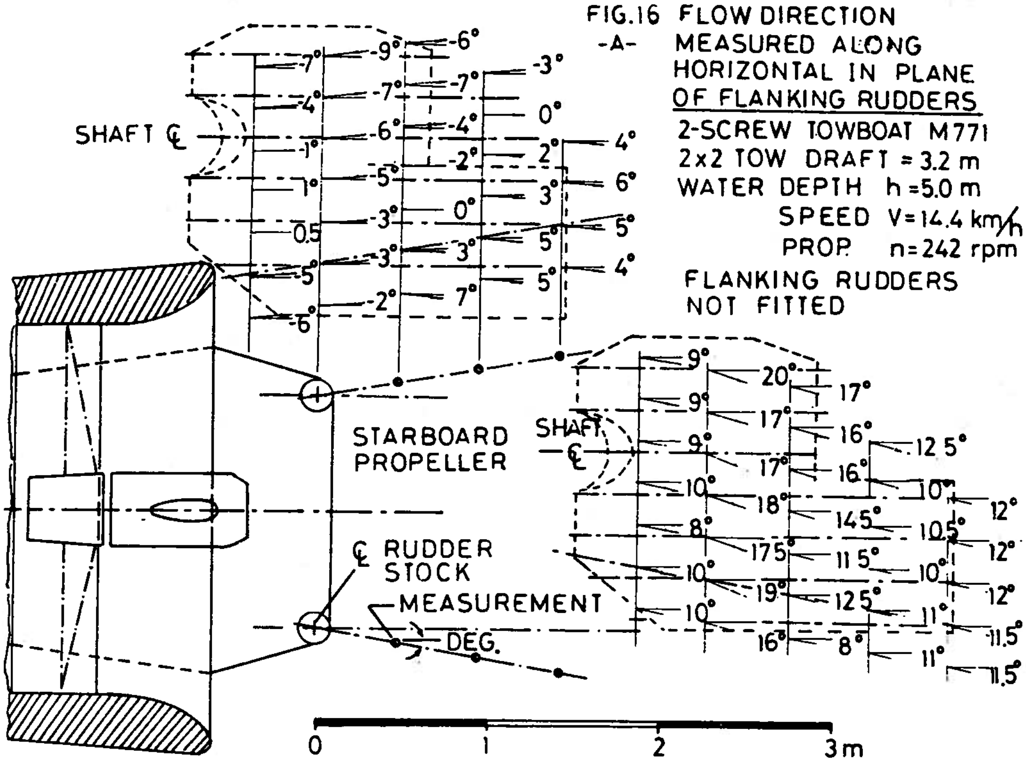

FIG. 16 FLOW DIRECTION
-B- MEASURED ALONG HORIZONTAL IN PLANE OF FLANKING RUDDERS

TEST CONDITIONS AS IN FIG. 16-A

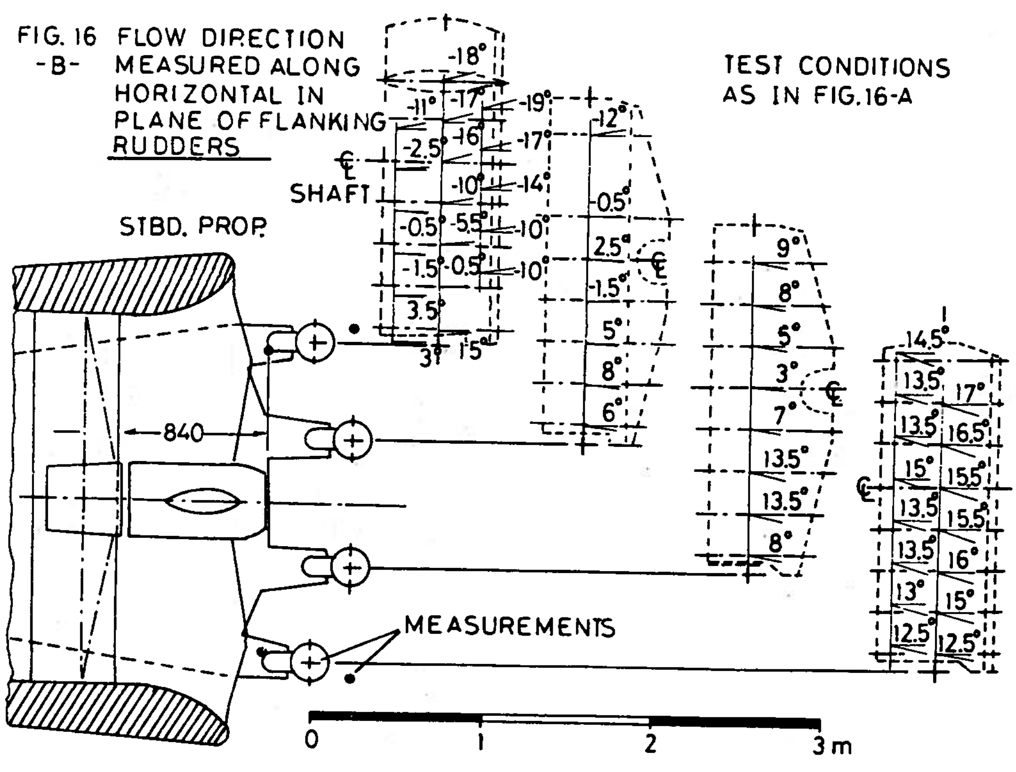

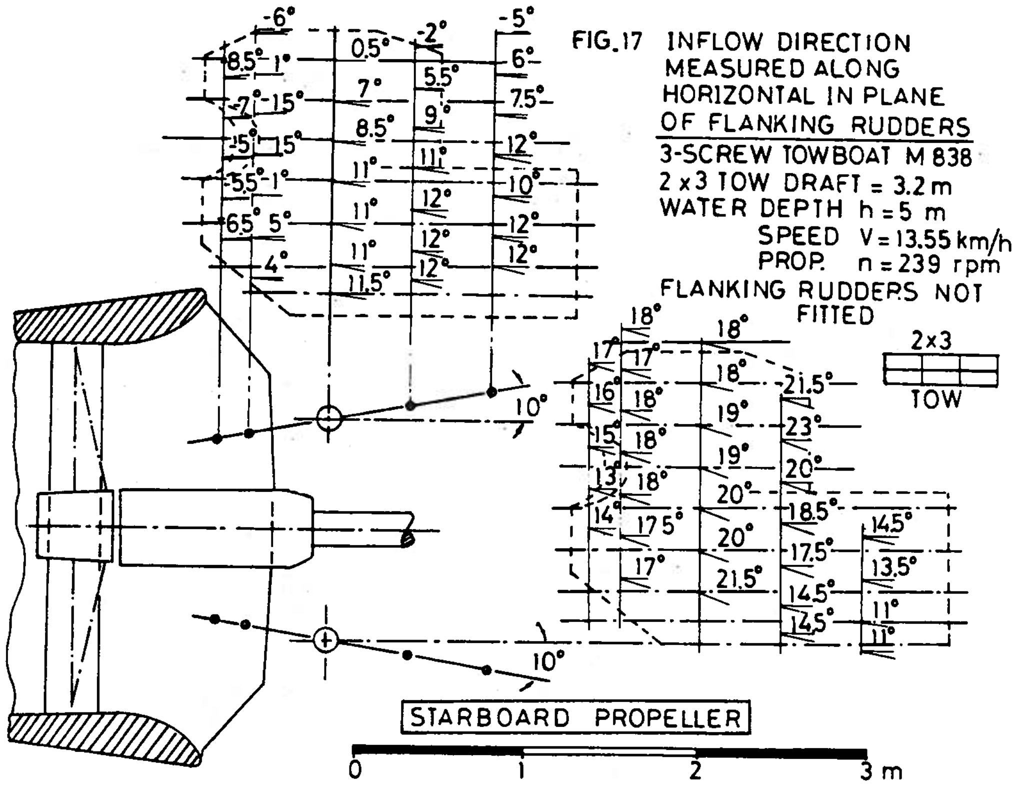

FIG.17 INFLOW DIRECTION MEASURED ALONG HORIZONTAL IN PLANE OF FLANKING RUDDERS
3-SCREW TOWBOAT M 838
2 x 3 TOW DRAFT = 3.2 m
WATER DEPTH h = 5 m
SPEED V = 13.55 km/h
PROP. n = 239 rpm
FLANKING RUDDERS NOT FITTED

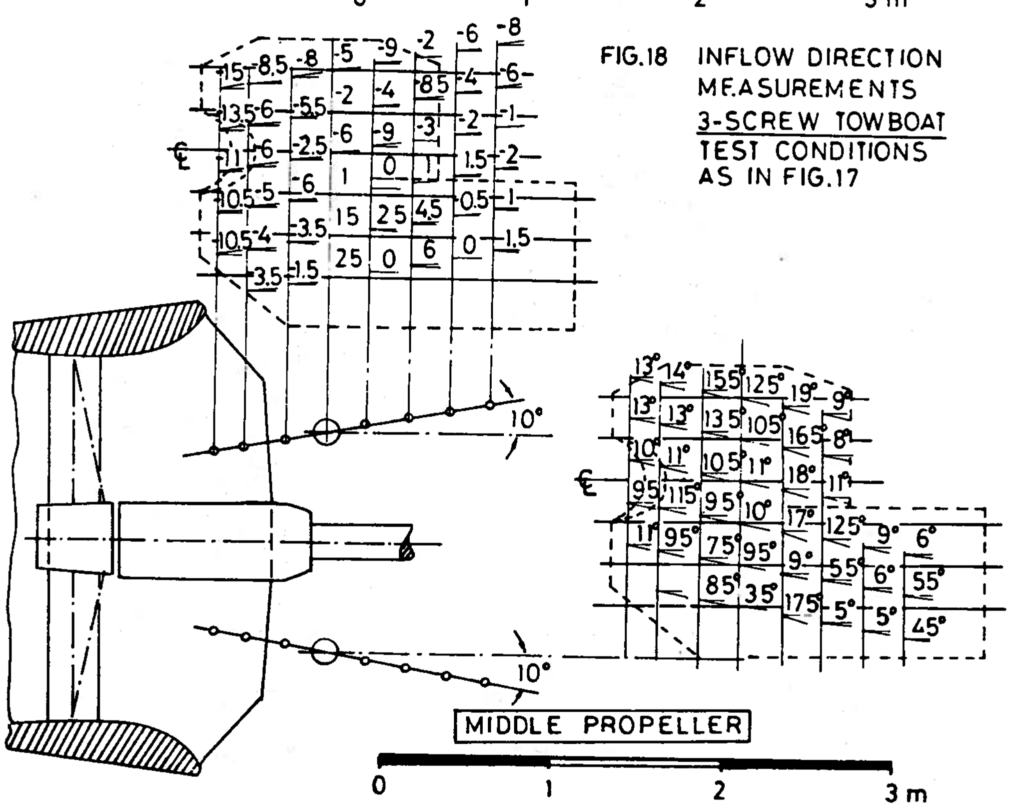

FIG.18 INFLOW DIRECTION MEASUREMENTS
3-SCREW TOWBOAT
TEST CONDITIONS AS IN FIG.17

FIG. 19 INFLOW DIRECTION MEASURED ALONG HORIZONTAL IN PLANE OF FLANKING RUDDERS
4-SCREW TOWBOAT M843
2 x 3 TOW DRAFT = 3.2 m
WATER DEPTH h = 5.0 m
SPEED V = 13.25 km/h
PROP. n = 283 RPM

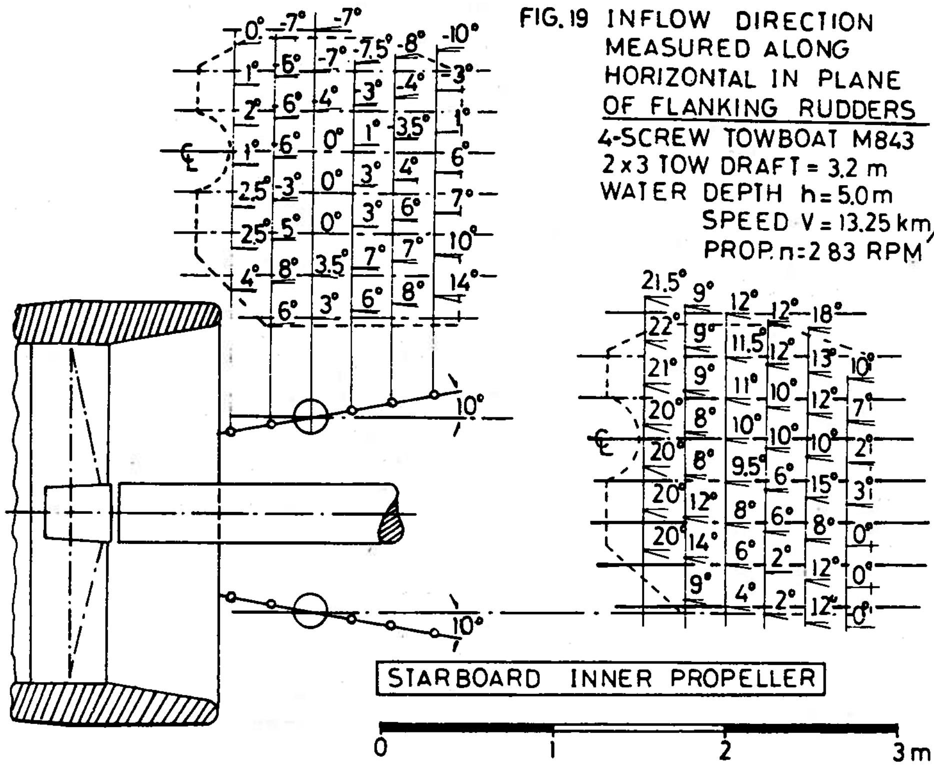

FIG. 20 INFLOW DIRECTION MEASUREMENTS
4 SCREW TOWBOAT
TEST CONDITIONS AS IN FIG. 19
FLANKING RUDDERS NOT FITTED (FIGS. 19 & 20)